

Impact of TiO₂ nanoparticles on the aquatic environment:
Investigation of cyanobacterial toxin adsorption and oxidative
stress mediated nanotoxicity towards the submerged aquatic
macrophyte *Hydrilla verticillata*

vorgelegt von
M.Sc.
Annette Spengler
geb. in Berlin

von der Fakultät III - Prozesswissenschaften
der Technischen Universität Berlin
zur Erlangung des akademischen Grades

Doktor der Naturwissenschaften
- Dr. rer. nat. -

genehmigte Dissertation

Promotionsausschuss:

Vorsitzender:	Prof. Dr. Lorenz Adrian
Gutachter:	Prof. Dr. Stephan Pflugmacher Lima
Gutachterin:	Prof. Dr. Alessandra Cincinelli
Gutachter:	Prof. Dr. Peter Neubauer

Tag der wissenschaftlichen Aussprache: 17. Juli 2018

Berlin 2019

Acknowledgements

There are numerous people behind this piece of work who have supported me in various ways during the process of my dissertation and deserve to be thanked here.

First of all, I would like to express my deepest appreciation to my supervisor Prof. Dr. Stephan Pflugmacher Lima for his guidance which helped me in all the time of research and writing this thesis. I am thankful for his believe in my potential, his continuous support of my study, his trust in my work, his support to attend international conferences, and for accepting me as a member of his research group.

I am very grateful to Dr. Valeska Contardo-Jara for her scientific advice, encouragement throughout my PhD, and thoughtful feedback on my work. I also would like to thank Sandra Kühn and Mahboobeh Behmaneshfard for their helpfulness and technical assistance in the laboratory.

My appreciation also goes to all former researchers, PhD students, and students of the chair ‘ecological impact research and ecotoxicology’ in particular Dr. Maranda Esterhuizen-Londt, Dr. Anja Peuthert, Dr. Claudia Suseth Romero Oliva, Dr. Mi-Hee Ha, Dr. Evelyn Balsano, Azam Omidi, Suhana Reddy, and Lena Wanninger for the scientific support during my PhD journey and the nice moments we had working together.

Dr. Thomas Bucheli (Agroscope Reckenholz-Tänikon Research Station, Zürich) and Ulrich Gernert (Zelmi, TU Berlin) are gratefully acknowledged for the opportunity to do nanoparticle characterization in their laboratories.

Last but not least, I would like to deeply thank my family, in particular my parents, my sister, and my dear husband for their unfailing love and unconditional faith in what I do. Your support regarding all aspects of my work and life throughout the years is the greatest gift anyone can ever give to me.

Abstract

Manufactured TiO₂-nanoparticles (TiO₂-NPs) are the most commonly employed metal oxide-based NPs. Due to the greater surface area per unit volume compared with their respective microscale counterparts, TiO₂-NPs might exhibit physicochemical properties which affect the toxicity potential of the normally inert material. Taking into account the increasing production volumes of TiO₂-NPs, they will inevitably reach the aquatic environment; thus, the normally balanced aquatic ecosystem might be disrupted as toxic effects towards aquatic organisms are conceivable. Once released in the aquatic environment, TiO₂-NPs will interact with each other as well as other environmental contaminants in water. Hereby, NPs may influence the toxicity of co-contaminants after mixture interaction. Moreover, TiO₂-NPs are considered to be potential generators of reactive oxygen species (ROS) and hence oxidative stress in aquatic organisms. As an excess ROS generation can affect cellular functioning which may ultimately result in cell death, the study of oxidative stress related parameters after TiO₂-NP exposure addresses an important mode of nano-toxicity towards aquatic organisms.

The present thesis was conducted to evaluate the impact of TiO₂-NPs on aquatic ecosystems. Therefore, the interaction of nanosized TiO₂ with cyanobacterial toxins was investigated. These toxins are potent biotoxins which are formed as secondary metabolites by most cyanobacteria and have been identified as serious stress factors and toxicological hazard in the aquatic environment. Within the diverse group of cyanobacterial toxins, microcystins account to the globally most frequently found toxins in algal blooms. To assess the potential of TiO₂-NPs to act as carriers for aquatic co-contaminants an adsorption study with microcystin-LR (MC-LR), the most common representative of microcystins, was performed. Furthermore, the oxidative-stress mediated toxicity of TiO₂-NPs towards the submerged aquatic macrophyte *Hydrilla verticillata* was investigated in a concentration- and time-dependent research trial. In respect to current studies addressing the ecotoxicity of TiO₂-NPs, macrophytes seem to be an overlooked test species, disregarding their importance for aquatic ecosystems. Hence, the analysis of oxidative stress related parameters in *H. verticillata* after TiO₂-NP exposure was conducted to identify early biological signals of stress in this essential component of the aquatic ecosystem. All experiments included TiO₂-NPs with varying crystalline structure (anatase, rutile, anatase/rutile mixed-phase) and

investigations of TiO₂-based microparticles to further assess the influence of the crystal status on nano-TiO₂ adsorption capacity and toxicity as well as the size-dependence of effects, respectively. In addition, the investigated TiO₂-NPs were characterized under study conditions as this is critical in order to correlate their specific properties to their toxicity potential.

The present study revealed MC-LR adsorption onto TiO₂-NPs at environmental relevant concentrations of both, adsorbent and adsorbate. Toxin adsorption seemed to depend on the particle size and the crystalline status of TiO₂-NPs rather than the adsorbent dosage. Moreover, the investigated adsorption kinetic data suggested a complex adsorption process with the participation of chemisorption mechanisms between MC-LR and TiO₂-NPs. The study of oxidative stress related effects in *H. verticillata* after exposure to nanosized TiO₂ showed a stimulated antioxidative stress response in such exposed macrophytes accompanied by ROS level changes. TiO₂-NPs provoked activity changes of antioxidative enzymes as well as a disruption of the homeostasis of the antioxidant glutathione in a time- and concentration-dependent manner. These adaptations in the antioxidative stress response in *H. verticillata* could be related to the nano-scaled character of TiO₂-NPs; moreover, the response did not depend on a distinct crystalline phase.

On the one hand, the results of the present thesis indicate the potential of TiO₂-NPs to act as carrier systems for MC-LR in aquatic ecosystems probably influencing its fate and toxicity towards macrophytes and other aquatic organisms. On the other hand, it is likely that nanosized TiO₂ of differing crystalline status itself provokes toxic effects in aquatic plants *via* an induction of oxidative stress. However, macrophytes exposed to currently predicted concentrations of TiO₂-NPs might be able to maintain ROS homeostasis based on compensatory ROS scavenging by their various enzymatic and non-enzymatic components of the antioxidative defense system. Overall, the thesis results confirm that the potential of TiO₂-NPs for contaminant adsorption as well as oxidative stress induction cannot be equated with their respective microscaled counterpart, even after NP aggregate formation and thus particle size increase.

Zusammenfassung

In der Gruppe der Metalloxid-basierten Nanopartikel zeichnen sich industriell gefertigte TiO₂-Nanopartikel (TiO₂-NP) durch ihren weiten Einsatz aus. Ihr im Vergleich zu mikroskaligen Gegenständen großes Oberfläche-zu-Volumen-Verhältnis verleiht TiO₂-NP besondere physikochemische Eigenschaften, auch mit möglichen Folgen für die Toxizität des sonst inerten Materials. Angesichts steigender Produktionsmengen werden TiO₂-NP zwangsläufig aquatische Lebensräume erreichen, um hier womöglich toxische Wirkungen auf aquatische Organismen zu entfalten, die diese Ökosysteme aus dem Gleichgewicht bringen. Im Gewässer werden TiO₂-NP miteinander, aber auch mit anderen Umweltkontaminanten interagieren, sodass deren toxisches Potential beeinflusst werden kann. Zudem sind TiO₂-NP als potentielle Quellen sogenannter reaktiver Sauerstoff-Spezies (ROS) bekannt und können somit oxidativen Stress in Wasserorganismen induzieren. Ein Übermaß an ROS kann die Zellfunktion nachhaltig beeinträchtigen und final im Zelltod münden. Daher spricht das Studieren verschiedener mit oxidativen Stress in Beziehung stehender Parameter nach Exposition mit TiO₂-NP einen bedeutenden Modus der Nanotoxizität gegenüber aquatischen Organismen an.

Die vorliegende Doktorarbeit sollte dazu beitragen, den Einfluss von TiO₂-NP auf aquatische Ökosysteme zu evaluieren. Zu diesem Zweck wurde ihre Interaktion mit cyanobakteriellen Toxinen untersucht. Hierbei handelt es sich um potente Biotoxine, die Sekundärmetabolite vieler Cyanobakterien darstellen und bereits als ernstzunehmende Stressfaktoren sowie toxikologische Gefahr für aquatische Lebensräume bekannt sind. Unter den verschiedenen Gruppen von Cyanotoxinen sind Microcystine diejenigen, die am häufigsten in cyanobakteriellen Blüten detektiert werden. Mit dem Ziel das Potential von TiO₂-NP abzuschätzen als Träger (engl. Carrier) für andere aquatische Kontaminanten zu fungieren, wurde die Adsorption von Microcystin-LR (MC-LR), dem häufigsten Vertreter der Microcystine, studiert. Zudem befasste sich diese Arbeit mit der auf oxidativen Stress basierenden Toxizität von TiO₂-NP auf die Makrophyte *Hydrilla verticillata* im Rahmen einer konzentrations- sowie zeitabhängigen Studie. In Anbetracht des derzeitigen Forschungsstandes bezüglich der Ökotoxizität von TiO₂-NP schienen Makrophyten als Testorganismen bisher eine weitgehend untergeordnete Rolle zu spielen, ungeachtet ihrer Bedeutung für aquatische Ökosysteme. Daher ermöglichte die Untersuchung oxidativer Stress-Parameter in *H. verticillata* nach Exposition mit TiO₂-NP einen Einblick in frühe biologische Stresssignale dieser bedeutenden aquatischen Ökosystemkomponente zu erhalten. Alle

durchgeführten Experimente beinhalteten die Untersuchung von TiO₂-NP verschiedener Kristallstruktur (Anatas, Rutil, Anatas/Rutil Mischphase) sowie von TiO₂-Mikropartikeln, um den Einfluss des Kristallstatus auf nano-TiO₂ Adsorption und Toxizität abzuschätzen, beziehungsweise die Abhängigkeit der beobachteten Effekte von der Partikelgröße zu erfassen. Des Weiteren wurden die untersuchten TiO₂-NP unter den vorherrschenden Bedingungen charakterisiert, um die spezifischen Eigenschaften der NP mit ihrer Toxizität in Beziehung zu setzen.

Die Ergebnisse zeigten die Adsorption von MC-LR an TiO₂-NPs bei umweltrelevanter Konzentration von Adsorbat und Adsorbens auf. Hierbei scheint die Adsorption des Toxins mehr von der Partikelgröße und der TiO₂ Kristallstruktur abzuhängen als von der Menge des verwendeten Adsorbens. Außerdem lassen die Daten der Adsorptionskinetik einen komplexen Adsorptionsvorgang vermuten, an dem Chemisorption zwischen MC-LR und den TiO₂-NP eine Rolle zu spielen scheint. Untersuchungen von Parametern des oxidativen Stresses in *H. verticillata* nach Behandlung mit nanopartikulären TiO₂ ergaben eine stimulierte antioxidative Stressantwort in entsprechend behandelten Makrophyten bei gleichzeitiger Konzentrationsveränderung der ROS. TiO₂-NP bewirkten einen zeit- und konzentrationsabhängigen Anstieg der Aktivität antioxidativer Enzyme sowie eine Störung der Homöostase des Antioxidans Glutathion. Die beobachteten Veränderungen der antioxidativen Stressantwort in *H. verticillata* standen in Beziehung mit der Nanoskaligkeit der TiO₂-NP und waren zudem nicht von einem bestimmten Kristallstatus abhängig.

Einerseits zeigen die Ergebnisse der vorliegenden Doktorarbeit klar auf, dass TiO₂-NP als Carrier für MC-LR in aquatischen Ökosystem fungieren können, mit möglichen Folgen für dessen Schicksal und Toxizität gegenüber Makrophyten und anderen aquatischen Organismen. Auf der anderen Seite kann nanopartikuläres TiO₂ verschiedenster Kristallstruktur, durch die Induktion von oxidativem Stress, potentiell selbst toxische Effekte in Wasserpflanzen herbeiführen. Jedoch scheinen Makrophyten durch ihr kompensatorisch agierendes System aus enzymatischen und nicht-enzymatischen Komponenten der ROS-Abwehr dazu in der Lage, die Homöostase der ROS nach Einwirkung umweltrelevanter Konzentrationen von TiO₂-NP aufrechtzuerhalten. Insgesamt untermauern die Ergebnisse, dass das Potential von TiO₂-NP andere Umweltkontaminanten zu adsorbieren oder aber auch oxidativen Stress zu induzieren nicht gleichgestellt werden kann mit dem von mikroskaligen Partikeln, auch nicht nach Aggregatbildung der NP und somit Partikelgrößenzunahme.

List of publications

The present dissertation is written as a cumulative thesis and is based on the following manuscripts, referred to in the text by their corresponding Roman numerals. All publications have been published in international peer-reviewed journals and are inserted herein as their postprint version. The manuscripts can be found in the appendix.

Publication I

Okupnik, A., Contardo-Jara, V., Pflugmacher, S., 2015. Potential role of engineered nanoparticles as contaminant carriers in aquatic ecosystems: Estimating sorption processes of the cyanobacterial toxin microcystin-LR by TiO₂ nanoparticles. *Colloids and Surfaces A* 481, 460-467. DOI: <http://dx.doi.org/10.1016/j.colsurfa.2015.06.013>

Publication II

Okupnik, A., Pflugmacher, S., 2016. Oxidative stress response of the aquatic macrophyte *Hydrilla verticillata* exposed to TiO₂ nanoparticles. *Environmental Toxicology and Chemistry* 35(11), 2859-2866. DOI: <https://doi.org/10.1002/etc.3469>

Publication III

Spengler, A., Wanninger, L., Pflugmacher, S., 2017. Oxidative stress mediated toxicity of TiO₂ nanoparticles after a concentration and time dependent exposure of the aquatic macrophyte *Hydrilla verticillata*. *Aquatic Toxicology* 190, 32-39. DOI: <http://dx.doi.org/10.1016/j.aquatox.2017.06.006>

List of presentations at international conferences

Urban Environmental Pollution 2014, Toronto (poster): Role of engineered nanoparticles as contaminant carriers in aquatic ecosystems: Estimating sorption processes of the cyanobacterial toxin microcystin-LR on nanosized TiO₂, Okupnik, A., Pflugmacher, S.

Urban Environmental Pollution 2014, Toronto (poster): Concentration dependent physiological effects of TiO₂ nanoparticles and glyphosate-based formulation Roundup Turboplus on *Lumbriculus variegatus*, Reddy, S., Okupnik, A., Pflugmacher, S.

SETAC Europe 2016, Nantes (presentation): Oxidative stress response of the aquatic macrophyte *Hydrilla verticillata* exposed to nanoparticulate and bulk TiO₂, Okupnik, A., Pflugmacher, S.

Abbreviations

APx	ascorbate peroxidase
AsA	ascorbate
BSA	bovine serum albumin
<i>C</i>	boundary layer effect
<i>C</i> ₀	initial concentration of adsorbate
<i>C</i> _{<i>e</i>}	equilibrium liquid-phase of adsorbate
CAT	catalase
Cd	cadmium
Cyanotoxins	cyanobacterial toxins
DHA	dehydroascorbate
DHAR	dehydroascorbate reductase
DLS	dynamic light scattering
DTNB	5,5-dithio-bis(2-nitrobenzoic acid)
E.C.	enzyme commission number
EDTA	ethylenediaminetetraacetic acid
FW	fresh weight
GPx	glutathione peroxidase
GR	glutathione reductase
GSH	reduced glutathione
GS-TNB	glutathione adduct of 2-nitro-5-thiobenzoic acid (TNB)
GSSG	oxidized glutathione
H ₂ O ₂	hydrogen peroxide
HPLC	high performance liquid chromatography
IEP	isoelectric point
<i>k</i> ₁	first-order rate constant of pseudo-first-order equation
<i>k</i> ₂	second-order rate constant of pseudo-second-order equation
<i>k</i> _{<i>id</i>}	intraparticle diffusion rate constant
kat	katal
LC-MS/MS	liquid chromatography tandem mass spectrometry
LPO	lipid peroxidation
m/s GST	microsomal/soluble glutathione <i>S</i> -transferase
MCs	microcystins

MC-LR	microcystin-LR
MDA	monodehydroascorbate
MDAR	monodehydroascorbate reductase
NADP ⁺	nicotinamide adenine dinucleotide phosphate
NADPH	nicotinamide adenine dinucleotide phosphate, reduced
NOM	natural organic matter
NP	nanoparticle
O ₂	di-oxygen
O ₂ ¹	singlet oxygen
O ₂ ^{•−}	superoxide radical
•OH	hydroxyl radical
PDI	polydispersity index
POD	guajacol peroxidase
q_e	adsorption capacity at equilibrium
q_t	adsorption capacity at time t
R ²	regression correlation coefficients
ROS	reactive oxygen species
SEM	scanning electron microscopy
SOD	superoxide dismutase
SPM	suspended particulate matter
TCA	Tri-chloroacetic acid
TiO ₂	titanium dioxide
TNB	2-nitro-5-thiobenzoic acid

List of content

1	Introduction	1
1.1	Titanium dioxide and its crystalline forms	1
1.2	Titanium dioxide nanoparticles – characteristics and applications	2
1.3	Titanium dioxide nanoparticles in the aquatic environment	3
1.3.1	Release of titanium dioxide nanoparticles in the aquatic environment.....	3
1.3.2	Fate of titanium dioxide nanoparticles in the aquatic environment	4
1.4	Mixture interactions of nanoparticles in the aquatic environment	6
1.5	Cyanobacterial microcystins as aquatic contaminants.....	7
1.6.	Oxidative stress.....	10
1.6.1	Reactive oxygen species.....	10
1.6.2	Antioxidative stress response	12
1.7	<i>Hydrilla verticillata</i> as a model for aquatic macrophytes.....	14
1.8.	Research objectives	15
2	Materials and Methods	17
2.1	Materials	17
2.1.1	Technical devices and software.....	17
2.1.2	Chemicals	18
2.1.3	Modified Hoagland’s nutrient solution	19
2.1.4	Cultivation of the test organisms.....	20
2.1.5	TiO ₂ -nanoparticles and bulk TiO ₂	21
2.1.5.1	Particles	21
2.1.5.2.	Preparation of TiO ₂ nanoparticle suspensions	21
2.1.6	Cyanobacterial microcystin-LR as aquatic Co-contaminant.....	21
2.1.6.1	Microcystin-LR	21
2.1.6.2	Preparation of Microcystin-LR suspensions	22
2.2	Methods	22
2.2.1	Nanoparticle characterization.....	22
2.2.2	Nanoparticle sedimentation analysis	22
2.2.3	Adsorption of microcystin-LR onto TiO ₂ -NPs	23
2.2.3.1	Batch adsorption experiments	23
2.2.3.2	Adsorption kinetic study	23

LIST OF CONTENT

2.2.3.3 Influence of adsorbent concentration and particle size.....	25
2.2.3.4 Cyanobacterial toxin determination.....	25
2.2.4 Oxidative stress response analysis in <i>Hydrilla verticillata</i>	26
2.2.4.1 Exposure design.....	26
2.2.4.2 Measurements of internal H ₂ O ₂	27
2.2.4.3 Non-enzymatic antioxidants: GSH status analysis.....	28
2.2.4.4 Enzymatic antioxidants.....	30
2.2.4.4.1 Enzyme extraction.....	30
2.2.4.4.2 Enzyme activity measurements.....	30
2.2.5 Statistics.....	34
3 Results.....	35
3.1 Nanoparticle characterization.....	35
3.2 Nanoparticle sedimentation analysis.....	36
3.3 Cyanobacterial toxin adsorption onto TiO ₂ nanoparticles.....	37
3.3.1 Adsorption kinetic study.....	37
3.3.2 Influence of the particle size and concentration on the toxin adsorption process.....	37
3.4 Oxidative stress response in <i>Hydrilla verticillata</i>	38
4 Discussion.....	45
4.1 Characteristics of the investigated TiO ₂ -nanoparticles and stability of TiO ₂ - nanoparticle suspensions.....	45
4.2 Cyanobacterial toxin adsorption onto TiO ₂ nanoparticles.....	48
4.3 Oxidative stress response in <i>Hydrilla verticillata</i>	50
5 Conclusions and Outlook.....	59
6 References.....	63
7 Figure Index.....	77
8 Table Index.....	79
Appendix I.....	81
Appendix II.....	105
Appendix III.....	129

1 Introduction

1.1 Titanium dioxide and its crystalline forms

Titanium accounts to the world's fourth most abundant metal and ninth most abundant element. It occurs as titanium dioxide (TiO_2) primarily in minerals like rutile, anatase, and brookite (Table 1). TiO_2 polymorphs distinguish themselves by their crystal structure and can be discussed in terms of octahedra (TiO_6). The distortion of each octahedral and the assembly patterns of the octahedral chains differ between the crystalline phases (Carp et al., 2004). Whereas anatase is built up from octahedra connected by their vertices, rutile and brookite exhibit corner- as well as edge sharing TiO_6 units (Carp et al., 2004; Landmann et al. 2012). Anatase and rutile exhibit a tetragonal structure, but the distortion of the TiO_6 octahedron is slightly larger in anatase than in rutile (Mo and Ching, 1995). In TiO_2 brookite, which belongs to the orthorhombic crystal system, all Ti–O bond lengths and Ti–O–Ti bond angles slightly differ from each other leading to a formal loss of symmetry of the octahedral (Landmann et al., 2012). TiO_2 is a large band semiconductor with band gaps slightly above 3 eV (Wunderlich et al. 2004). Thus, natural TiO_2 is only active in the UV region of the electromagnetic spectrum (Landmann et al., 2012). Comparing rutile and anatase polymorphs, rutile TiO_2 is the most stable form of TiO_2 , whereas anatase exhibits a higher electron mobility, lower dielectric constant, lower density, and lower deposition temperature compared to rutile (Carp et al., 2004).

Table 1. Properties of anatase TiO_2 , rutile TiO_2 , and brookite TiO_2 (Cromer and Herrington, 1954; Mo and Ching, 1995; Carp et al., 2004; Wunderlich et al., 2004; Gupta and Tripathi, 2010).

Properties	Anatase	Rutile	Brookite
Crystal structure	Tetragonal	Tetragonal	Orthorhombic
Ti–O bond length (Å)	1.937 (4) 1.964 (2)	1.946 (4) 1.984 (2)	1.87-2.04
Ti–O–Ti bond angle	77.7° 92.6°	81.2° 90.0°	77.0-105°
Band gap (eV)	3.2	3.02	2.96
Density (g/cm ³)	3.79	4.13	3.99
Refractive index	2.5688	2.9467	2.809

1.2 Titanium dioxide nanoparticles – characteristics and applications

The term ‘nanoparticle’ has not been strictly defined. Many authors refer to NPs when at least one dimension of the particle is less than 100 nm (Kaegi et al., 2008). However, nanotechnology is also defined as research and technology development using a length scale of approximately one to one hundred nanometers in all dimensions. Irrespective of the uncertainties regarding the definition of NPs, nanotechnology presents potential opportunities to create matter with unique physical properties making novel applications possible (EPA, 2007). This can be mainly due to the main difference between nano-TiO₂ and conventional bulk sized TiO₂, which is the much greater surface area of a given mass or volume of TiO₂-nanoparticles (TiO₂-NPs) compared to an equivalent mass or volume of conventional particles. TiO₂-NPs have a high particle number per unit mass and the fraction of the atoms at the surface in TiO₂-NPs is increased compared to TiO₂ microparticles, leading to increased chemical reactivity (Buzea et al., 2007). Already, TiO₂ is one of the most widely used nanoscale materials for industrial applications, as it can be readily manufactured on a large-scale (Aitken et al., 2006). Thus, it is expected that the production of TiO₂-based bulk materials will probably be exceeded by the production of TiO₂-NPs in the near future (Robichaud et al., 2009). Due to the low stability of the brookite modification, especially anatase and rutile TiO₂ play a significant role for the industry (Hadjiivanov and Klissurski, 1996). Nano-TiO₂ is advantageous in applications that require high opacity or whiteness, corrosion resistance, or photocatalytic activity (Robichaud et al., 2009). Because of the latter feature, TiO₂-NPs are used for applications of environmental remediation as well as for various consumer products such as household cleaning products, household self-cleaning coatings, household air filtration devices, electronics, and hair styling devices (Balasubramanian et al., 2004; Varner et al., 2010). Moreover, primarily TiO₂-NPs are applied as a pigment in products like paints, inks, plastics, and paper (Robichaud et al., 2009) and have found use in a variety of commercially available coatings, sunscreens or similar cosmetics, and clothes to attenuate ultraviolet radiation (Varner et al., 2010; Botta et al., 2011). In addition, food-grade TiO₂ (referred to as E 171) is widely used in e.g. dairy products, candy, gums, and baked goods and is present in concentrations varying between 0.0005% and 0.04%, also including nanosized TiO₂ (Weir et al., 2012).

1.3 Titanium dioxide nanoparticles in the aquatic environment

1.3.1 Release of titanium dioxide nanoparticles in the aquatic environment

The widespread use of TiO₂-NPs suggests that they will inevitably reach the environment. An exposure modeling study predicted the exposure of the environmental compartments air, water, and soil and revealed that TiO₂-NPs will most likely be found in natural surface waters (Müller and Nowack, 2008). Therefore, nano-TiO₂ poses a potential risk to various aquatic organisms. Sources of the TiO₂-NP release can be assumed as manifold as its range of urban applications. To date, the release of engineered NPs is largely unknown, however, may come from point sources (e.g. factories or landfills) as well as nonpoint sources (e.g. storm-water runoff, attrition from NP-containing products) (Wiesner et al., 2006). Moreover, an accidental release during the TiO₂-NP production or transport and an intentional release for remediation purposes are other possible pathways of TiO₂-NPs contamination of the aquatic environment (Nowack and Bucheli, 2007). Based on current investigations, there is evidence that TiO₂-NPs are significantly released from commercialized sunscreens (Gondikas et al., 2004; Botta et al., 2010) and can reach surface waters *via* runoff from exterior paints and plasters of facade within a concentration range of a few µg/L (Kaegi et al., 2008). Next to these nonpoint sources, waste water treatment plants have been identified as a major point source of TiO₂-NP contamination (Westerhoff et al., 2011).

As the risk assessment for TiO₂-NPs also requires quantification of the real concentrations of nano-TiO₂ in the environment, it is an important task of research. So far, measurements of engineered NPs in environmental samples is challenging due to the lack of adequate techniques for the detection and quantification of relevant concentrations in complex media (von der Kammer et al., 2012). However, Neal et al. (2011) provided information on natural TiO₂-NP concentrations in surface waters by analyzing Ti concentrations in river water in the UK. Concentrations with a range in average of 0.55 to 6.48 µg/L were measured using a 0.45 µm cellulose nitrate filter and thus including the nano-fraction but also larger colloids. Next to this estimation of an upper limit for nano-TiO₂, first modelling attempts to predict TiO₂-NP concentrations exist. Modeled concentrations of TiO₂-NPs in aquatic ecosystems strongly depend on the provided raw data and the major source of modeling error seems to lie in uncertain TiO₂-NP production and emission rates from products (Müller and Nowack, 2008; Gottschalk et al., 2013).

Moreover, the modelling studies differ in the way they include natural processes like NP aggregation (see chapter 1.3.2). Thus, the concentration modeling for nano-TiO₂ in the surface water revealed a broad spread of concentrations varying approximately by a factor of 10⁴. Despite this evident uncertainty, low concentrations of TiO₂-NPs in the range of 10⁻³ to 10 µg/L are currently predicted for surface waters (Gottschalk et al., 2013).

1.3.2 Fate of titanium dioxide nanoparticles in the aquatic environment

Aggregation and disaggregation of NPs are two of the key processes particularly affecting the NP size and mobility and thus their fate in the aquatic environment. Aggregation can be either between the same NPs (homoaggregation) or between NPs and natural colloidal materials (heteroaggregation) (Peijnenburg et al., 2015). It is already evident that the water chemistry (e.g. pH, natural organic matter (NOM), the ionic strength, ionic composition) is highly influential on the NP aggregation status and NP suspension stability (Keller et al., 2010; Ottofuelling et al., 2011). Therefore, NP characteristics need to be evaluated individually for the different natural aquatic matrices, especially when comparing NP ecotoxicity in freshwaters and marine waters.

For instance, the degree of NP repulsion is highly determined by the difference between the pH of the solution and the pH_{IEP} (pH of isoelectric point) of the respective NP, which is defined as pH at which NPs have a neutral surface charge. As one approaches the pH_{IEP} the repulsion decreases, leading to the formation of NP aggregates of increasing size and thus increased sedimentation. Moreover, the ionic strength of the water the TiO₂-NPs are suspended in affects NP aggregation (Keller et al., 2010). In waters at high ionic strength the repulsive forces between the NPs are decreased. Hence, the mean aggregate size is larger and the size distribution is broader than in waters with a lower electrolyte background (Hotze et al., 2010; Keller et al., 2010).

The importance of NOM in controlling TiO₂-NP aggregation in natural aquatic systems is already well studied (Yang et al., 2009; Keller et al., 2010; Duster and Fein, 2014). Due to the ubiquitous presence of NOM and its reactivity, it is considered unlikely to find ‘bare’ NPs in the environment (Yang et al., 2009). Moreover, NPs have significant adsorption capacities because of their relatively large surface area. Thus, they are able to bind or carry other molecules in the water like NOM (Peijnenburg et al., 2015). The adsorption of NOM, mainly fulvic and humic substances, by TiO₂-NPs is induced by electrostatic attraction and

ligand exchange between the NOM and NP surfaces and leads to more stable NP solutions driven by electrosteric stabilization mechanisms (Yang et al., 2009; Hotze et al., 2010).

In consequence, once released in the aquatic environment, TiO₂-NPs will interact with each other and with the surrounding water (Praetorius et al., 2012). Thus, the above mentioned multiple effects may take place together, influencing NP aggregation and inevitably affecting the fate and transport of TiO₂-NPs. Bare NPs occur only in well-controlled laboratory experiments (Peijnenburg et al., 2015). Already on their way from the industrial product or application through the water, NPs undergo transformations which probably result in the formation of larger particle assemblies (Praetorius et al., 2012). Moreover, after being hydrated the formation of large-scale NP homoaggregates with diameters of several hundred nanometers to several micrometers is the rule rather than the exception (Guzman et al., 2006; French et al., 2009). As an increase in size after particle aggregation impacts the particle mobility, NP sedimentation will occur when the aggregate size (mass) becomes significant enough for the gravitational forces to overcome buoyancy forces (Guzman et al., 2006). Therefore, TiO₂-NPs with a low dispersion stability will rapidly sediment out of the water column and tend to accumulate in the sediment near their emission source.

Also, heteroaggregation is an important fate process of NPs in the aquatic environment and even more likely due to the by far greater number of natural particles compared to the number of NPs (Hotze et al., 2010). Next to NOM, heteroaggregation with suspended particulate matter (SPM) is expected to have a strong influence on the fate and transport behavior of NPs (Praetorius et al., 2012). Depending on several factors (e.g. type, concentration, and density of NOM and SPM), NPs emitted to freshwater systems can be removed quickly from the water column after heteroaggregation and sedimentation or may be transported hundreds of kilometers away from their source; thus, increasing their residence time in the water body (Hotze et al., 2010; Praetorius et al., 2012).

1.4 Mixture interactions of nanoparticles in the aquatic environment

After being released, NPs will be part of a complex mixture rather than existing as single contaminants. Hence, NPs will interact with other co-existing contaminants in the aquatic environment. The potential of NPs to act as ‘Trojan horse’ like carriers is obvious due to their increased surface-to-volume ratio which enhances their reactivity; thus, NPs specific size related properties facilitate the interaction with other aquatic contaminants *via* sorption (Hartmann and Baun, 2010). In respect to environmental remediation purposes, nanoscale materials like carbon nanotubes, nanofibers, and nanoscale metal oxides have proven their applicability to target contaminants such as heavy metals in water and waste water treatment due to its adsorptive properties (Qu et al., 2013; Ray and Shipley, 2015). In particular, TiO₂-NPs may be a potential remediation tool for heavy metal removal from contaminated waters as Engates and Shipley (2011) investigated strong adsorption rates compared to the respective bulk particles, other metal oxide nanoparticles, and a commercial activated carbon. Thus, the use of nano-adsorbents for current and potential applications for water and wastewater treatment has attracted much attention (Qu et al., 2013).

Despite the research interest for interactions of NPs and environmental contaminants for remediation purposes, little is known about mixture interactions in aquatic ecosystems. Hereby, NPs may influence the bioavailability, as well as bioconcentration of co-contaminants and hence the toxicity of the individual compounds (Canesi et al., 2015). In some cases, the physicochemical properties of the NPs and the existing aquatic contaminant may prevent their interaction and thus both will independently cause their effect (Hartmann and Baun, 2010). Supporting this assumption, toxicity testing of atrazine and methyl parathion towards algae and crustaceans revealed unaffected toxicity in presence of C₆₀-NPs, which was explained by limited sorption of these common environmental contaminants onto C₆₀ fullerenes (Baun et al., 2008). However, assuming interaction between NPs, coexisting contaminants, and aquatic organisms, increased or decreased toxicity of co-contaminants are two possible scenarios (Hartmann and Baun, 2010). As the application of metal-based NPs as adsorbents appears to be an efficient method for the remediation of heavy metal contaminated waters, such NPs may further modify heavy metal bioavailability and toxicity in the aquatic environment. In this regard, current research revealed the potential of TiO₂-NPs to act as carriers for cadmium (Cd) as enhanced Cd accumulation in carp and daphnia was observed (Zhang et al., 2007; Hartmann et al., 2012).

However, the facilitated uptake of Cd by TiO₂-NPs in daphnia did not alter its toxicity towards water fleas (Hartmann et al., 2012). In contrast, algal growth inhibition tests of Cd revealed increased toxicity in the presence of TiO₂-NPs, which suggest a synergistic effect of both contaminants or increased bioavailability of Cd for the algae due to its interaction with NPs (Hartmann et al., 2010). Accordingly, increased toxicity of the xenobiotic organic contaminant phenanthrene to algae and daphnids became apparent after 85% sorption of phenanthrene onto C₆₀-aggregates which was attributed to the carrier effect of C₆₀ (Baun et al., 2008). Next to study results implying increased bioavailability and toxicity of aquatic contaminants co-existing with NPs, other study results suggest that such interactions can also be beneficial for aquatic organisms due to decreased bioavailability of the contaminant after sorption. In that respect, Knauer et al. (2007) deduced from their study results that the toxicity of the widely-used herbicide diuron towards algae in the presence of black carbon in surface waters was reduced by 20%. In contrast to previously mentioned results of studies concerning interactive effects of TiO₂-NPs and heavy metal species, the study by Yang et al. (2012) observed reduced free Cd concentration after sorption onto TiO₂-NPs in the toxicity media which further lowered the bioavailability and toxicity of Cd to freshwater algae.

Overall, the limited research results on mixture interactions of NPs and environmental relevant co-contaminants implies that these are highly dependent on the NP properties, the investigated pollutant, and aquatic species (Baun et al., 2008; Hartmann et al., 2012; Canesi et al., 2015). This could probably explain the conflicting study results. Notwithstanding the above, to assess the impact of NPs in aquatic environments, it seems indispensable to not only focus their inherent toxicity, but also their possible interactions with other aquatic compounds.

1.5 Cyanobacterial microcystins as aquatic contaminants

Cyanobacteria have a long evolutionary history and became the first microbes to produce free molecular oxygen in the atmosphere as byproduct of oxygenic photosynthesis at least 2.4 billion years ago. Thus, they played a pivotal role in the development of aerobic life on Earth (Blankenship et al., 2007). The planktonic, photoautotroph cyanobacteria are prokaryotes but have both algal and bacterial characteristics (Cole, 1982). Therefore, they have historically been grouped with eukaryotic “algae” and even today are often referred to as blue–green algae (Chorus and Bartram, 1999; Gerardi and Lytle, 2015). Cyanobacteria

are common members of the plankton community of marine, brakish, and freshwater environments and can exist as single-cells or colonies, which may form filaments, sheets or hallow balls (Wiegand and Pflugmacher, 2005; Gerardi and Lytle, 2015). When environmental conditions are favorable, buoyant cyanobacteria “bloom” and float to the water surface to form a scum layer or floating mat (Gerardi and Lytle, 2015). The occurrence of such phytoplanktonic blooms is becoming more frequent worldwide due to the prevailing environmental conditions like higher temperatures and pH values, low turbulence, and high, mainly anthropogenic, nutrient input (particularly phosphorus and nitrogen) (Bartram et al., 1999; de Figueiredo et al., 2004). Moreover, the future climate change is likely to enhance the magnitude and frequency of these blooming events (O’Neil et al., 2012). The greatest threat for aquatic ecosystems suffering from cyanobacterial bloom formation is the generation of cyanobacterial toxins (cyanotoxins) (Carmichael, 1992). Cyanotoxins are potent biotoxins which are formed as secondary metabolites at all growth stages of most cyanobacteria and generally remain inside the cell until senescence or stress causes their release. The wide range of chemical structures and mechanisms of toxicity characterize cyanotoxins which comprise of cyclic, chiefly hepatotoxins (microcystins and nodularines), alkaloids and organophosphates with strong neurotoxic effects (anatoxins, anataoxin-a(s) and saxitoxins), a guanidine alkaloid which inhibits protein synthesis (cylindrospermopsin), as well as lipopolysaccharides with pyrogenic properties (Chorus, 2011).

Microcystins (MCs) globally account to the most frequently found cyanotoxins in algal blooms. MCs contain seven amino acids, with the two terminal amino acids of the linear peptide chain being condensed to a cyclic structure. The basic structure of MCs is composed of d-alanine at position 1, two variable L-amino acids at positions 2 and 4, γ -linked d-glutamic acid at position 6, and 3 unusual amino acids: β -linked d-erythro- β -methylaspartic acid (MeAsp) at position 3; (2S,3S,8S,9S)-3-amino-9-methoxy-2,6,8-trimethyl-10-phenyldeca-4,6-dienoic acid (Adda) at position 5, and *N*-methyl dehydroalanine (MDha) at position 7 (Dawson, 1998). By derogation from this general structure, around 90 MC isoforms arise by the substitution and modification of amino acids at several positions in the heptapeptide ring (Codd et al., 1999).

This variety in toxin structure can be ascribed to the multiple genera of freshwater cyanobacteria which can produce MCs. As with many cyanotoxins, MCs were named after the first organism they were found, *Microcystis aeruginosa* (Bartram et al., 1999). Meanwhile, next to *Microcystis*, the main bloom-forming genus found world-wide, MCs have been characterized from different species including *Anabaena*, *Oscillatoria*, *Anabaenopsis*, *Hapalosiphon*, and *Nostoc* (Sivonen and Jones, 1999). The most common representative of MCs is microcystin-LR (MC-LR) (Figure 1), where the variable L-amino acids are leucine (L) and arginine (R) (Rinehart, 1994).

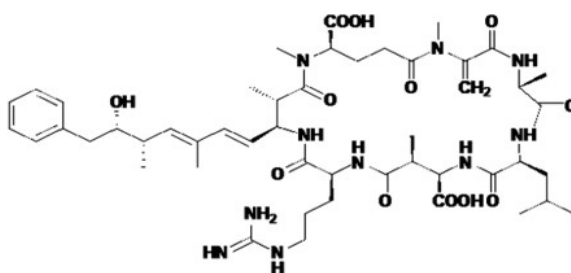


Figure 1. Molecular structure of the cyanobacterial heptapeptide microcystin-LR.

The mechanisms by which MC-LR exerts its toxicity is a highly specific inhibition of protein phosphatases type 1 and 2A (MacKintosh, 1990). This disruption of the dynamic equilibrium of protein phosphorylation/dephosphorylation results in the damage of numerous cellular processes like cytoskeleton organization, cellular proliferation, and apoptosis; moreover, it is a general mechanism of tumor promotion in various organs (Nishiwaki-Matsushima et al., 1992; Zeng et al., 2014; Chen et al., 2016). With respect to human health protection, the WHO established a provisional guideline value of 1 µg/L of MC-LR for drinking water (WHO, 1998). Fastner et al. (1999) demonstrated the overall presence of MC-producing cyanobacteria in German freshwater bodies as 72% of the cyanobacterial samples contained MCs, mainly at concentrations below 10 µg/L.

Scientific literature has recognized MCs as a potent stress factor and health hazard to organisms of varying trophic statuses. In a study conducted by Ibelings et al. (2005), MCs were found in 80% of all zooplankton and 89% of mussel samples, which are the main grazers of phytoplankton. Thus, study results indicated the entrance of MCs into the aquatic foodweb. Detrimental effects like feeding inhibition, reduced growth rate, reproductive potential, and mortality have been observed in zooplankton after MC exposure

(Nizan et al., 1986; DeMott et al., 1999; Rohrlack et al., 2005; Hansson et al., 2007). Moreover, fish can ingest MCs *via* the foodweb with the potential to cause severe toxicity (Ibelings et al., 2005). Studies regarding the effects of MCs on macrophytes are of particular environmental relevance, since they naturally come into direct contact with toxin-producing cyanobacteria and their toxins in eutrophic freshwaters (Pflugmacher et al., 2001). Several studies documented the uptake of MCs by submerged and emerged aquatic macrophytes (Pflugmacher et al., 1999 a, b; Pflugmacher et al., 2001; Romero-Oliva et al., 2014, 2015a). Moreover, there is evidence that MCs affect macrophyte growth, photosynthetic oxygen production, as well as the photosynthetic pigment pattern after exposure to environmentally relevant concentrations of MC-LR (Pflugmacher, 2002; Romero-Oliva et al., 2015b). Some of these effects could potentially be initiated after formation of reactive oxygen species (ROS) (Pflugmacher, 2004). The induction of oxidative stress (see chapter 1.6) after uptake and during biotransformation of MCs in macrophytes has been demonstrated by several authors (Pflugmacher, 2004; Romero-Oliva et al., 2015a, b). Thus, the potential role of MCs, or cyanotoxins in general, to act as allelopathic infochemicals influencing the competition for light, nutrients, and space between cyanobacteria and other photoautotrophs like macrophytes seems obvious (Pflugmacher, 2002; Holland and Kinnear, 2013).

1.6. Oxidative stress

1.6.1 Reactive oxygen species

ROS are partially reduced radical and non-radical forms of atmospheric oxygen. ROS result from the excitation of O_2 to form singlet oxygen (O_2^1) or from the transfer of one, two, or three electrons to O_2 to form a superoxide radical ($O_2^{\bullet-}$), hydrogen peroxide (H_2O_2) or the hydroxyl radical ($\bullet OH$), respectively (Figure 2) (Mittler, 2002). In this regard, $O_2^{\bullet-}$ is the initiator of a chain reaction which generates the other highly reactive free radical species (Alscher, 1989). Moreover, next to a direct electron transfer, the production of ROS can be inter-related. Dismutation of $O_2^{\bullet-}$ leads to the formation of H_2O_2 and together with $O_2^{\bullet-}$ the highly damaging $\bullet OH$ can be generated *via* metal-catalyzed Haber-Weiss reaction (Livingstone, 2003).

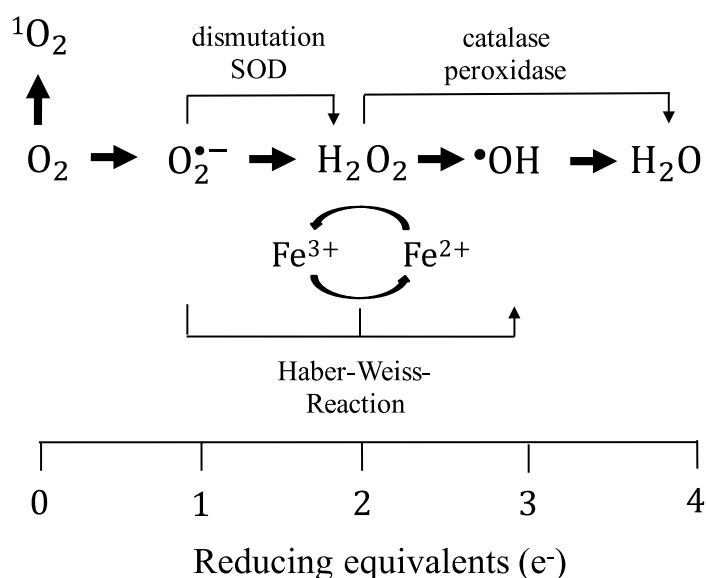


Figure 2. Generation of reactive oxygen species (ROS) from molecular oxygen and likely inter-conversion pathways. Singlet oxygen ($^1\text{O}_2$) is a highly reactive form of di-oxygen (O_2). The superoxide radical ($\text{O}_2^{\bullet-}$), hydrogen peroxide (H_2O_2) and hydroxyl radical ($\bullet\text{OH}$) are formed by one-electron reductions of O_2 . Cellular defenses like superoxide dismutase (SOD), catalase, and peroxidase serve to scavenge ROS, and thereby prevent the formation of $\bullet\text{OH}$ *via* the iron catalyzed Haber-Weiss reaction (Reilly et al., 2004).

ROS are unavoidable byproducts of normal cell metabolism due to electron transport activities of chloroplasts, mitochondria, and plasma membrane or various metabolic pathways localized in different cellular compartments (Sharma et al., 2012). Thus, the possibility of ROS formation exists at all times in aerobic cells (Alscher, 1989). Under non-stressed conditions, an equilibrium between the production and the scavenging of ROS ensures low levels of ROS in the cell (Mittler, 2002; Gill and Tuteja, 2010). However, interactions with exogenous sources like xenobiotics may disrupt this homeostasis and cause an imbalance due to excess ROS (Ray et al., 2012). Whether through an increase in ROS levels or a decrease in the cellular antioxidant capacity, when ROS overwhelm the cellular antioxidant defense system (see chapter 1.6.2) so called oxidative stress occurs with the potential to cause oxidative damage to macromolecules and induce alterations in critical cellular processes (Livingstone, 2003; Ray et al., 2012). As ROS possess a greater chemical reactivity compared to oxygen, they are thought to mediate the toxicity of oxygen during

oxidative stress (D'Autreaux and Toledano, 2007). In the environment of membranes, the highly potent $\bullet\text{OH}$ reacts instantly and indiscriminately with virtually all organic molecules and can bring about lipid peroxidation (LPO), the autocatalytic oxidative degradation of lipids (Alscher, 1989; Livingstone, 2003; Sharma et al., 2004). Products of LPO, such as malondialdehyde and 4-hydroxy-2-nonenal, may further damage proteins, DNA, and pigments (Alscher, 1989; Noctor et al., 2015). Either as direct consequence of excess ROS or LPO, altered intrinsic cell properties like loss of enzyme activity, protein cross-linking, inhibited protein synthesis, and DNA damage can significantly affect cellular functioning which may ultimately result in cell death (Sharma et al., 2012). Paradoxically, there is a growing body of evidence that ROS possess a “two-faced” character as low or transient concentrations of ROS might play an important role as secondary messengers in intracellular signaling cascades (Valko et al., 2006).

1.6.2 Antioxidative stress response

As ROS can be toxic but also participate in signaling events, two different mechanisms to regulate intracellular ROS concentrations by scavenging are required: One for the modulation of low level ROS and one that enables detoxification of excess ROS (Mittler, 2002). Therefore, the level of ROS is kept under tight control and enhanced levels of ROS can be combated by several antioxidant systems including antioxidative enzymes as well as non-enzymatic antioxidants (Figure 3) (Gill and Tuteja, 2010). The antioxidants ascorbate (AsA) and reduced glutathione (γ -glutamyl-cysteinyl-glycine, GSH) protect cells from ROS-induced oxidative damage either by directly reacting with ROS or as cofactors of antioxidative enzymes (Sharma et al., 2012). As key redox buffers, they ensure the reduction of ROS while being reversibly oxidized to relatively stable forms, not propagating stress (Noctor et al., 2015). Whereas GSH is oxidized by ROS to oxidized glutathione (GSSG), an oxidation of AsA leads to the generation of monodehydroascorbate (MDHA) and dehydroascorbate (DHA). High ratios of reduced to oxidized AsA and GSH are essential for ROS scavenging in cells and are ensured by the enzymes glutathione reductase (GR), monodehydroascorbate reductase (MDAR), and dehydroascorbate reductase (DHAR) which are key enzymes present in the AsA-GSH cycle. In respect to enzymatic ROS scavenging mechanisms, superoxide dismutase (SOD) plays a central role in the first line defense against oxidative stress, as it catalyzes the dismutation of $\text{O}_2^{\bullet-}$ to O_2 and H_2O_2 (Apel and Hirt, 2004). Subsequently, the AsA-GSH cycle is crucial for H_2O_2

degradation, which is mostly due to the high affinity of the antioxidative enzyme ascorbate peroxidase (APx) to detoxify H_2O_2 and its ubiquitous presence in various cellular compartments (Mittler, 2002). However, next to APx, glutathione peroxidase (GPx), guaiacol peroxidase (POD) as well as catalase (CAT) detoxify H_2O_2 , the latter both without the requirement of reducing equivalents (Sharma et al., 2012). The enzyme glutathione *S*-transferase (GST), a multifunctional family of phase II biotransformation enzyme, constitutes the second line of defense against ROS. Next to its primary function to catalyze the conjugation of electrophilic xenobiotics (or their metabolites) to GSH, they fulfil an antioxidant role as GST provides protection against LPO by detoxification of LPO products.

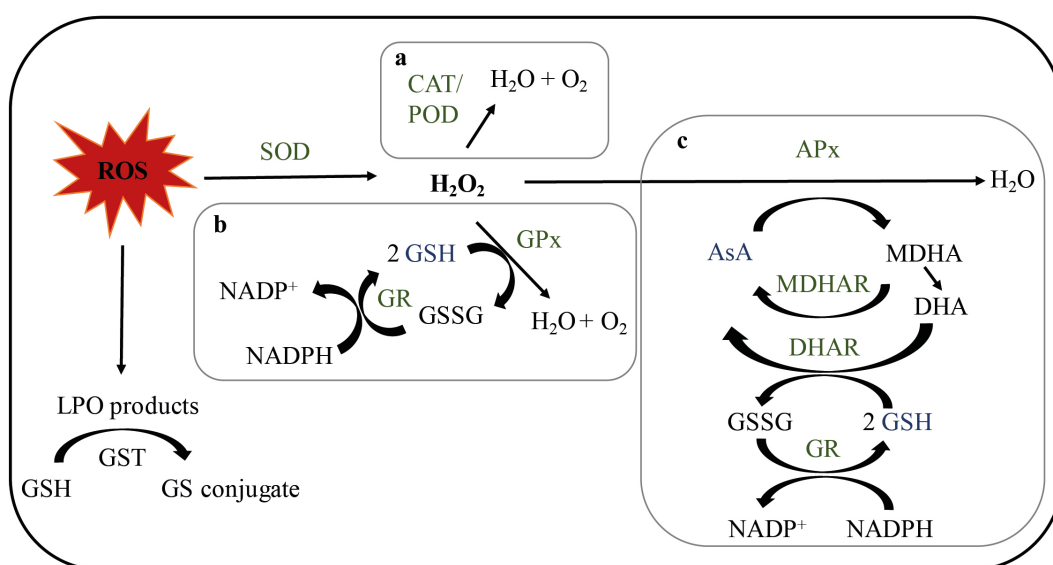


Figure 3. Antioxidative pathway. Superoxide dismutase (SOD) acts as first line defense against $\text{O}_2^{\bullet-}$ by dismutation to H_2O_2 . Possible ways of H_2O_2 detoxification can be *via* (a) catalase (CAT) and peroxidase (POD); (b) the glutathione peroxidase (GPx) cycle; (c) the ascorbate-glutathione cycle. The antioxidative enzymes are indicated in green and antioxidants in blue. Abbreviations: AsA, ascorbate; APx, ascorbate peroxidase; CAT, catalase; DHA(R), dehydroascorbate (-reductase); GSH, reduced glutathione; GSSG, oxidized glutathione; GST, glutathione *S*-transferase; LPO, lipidperoxidation; POD, peroxidase; MDHA(R), monodehydroascorbate (-reductase); NADPH, nicotinamide adenine dinucleotide phosphate; SOD, superoxide dismutase (compiled from Mittler, 2002; Pflugmacher et al., 2006).

Thus, to combat enhanced accumulation of ROS during oxidative stress events, aerobic organisms have a multitier defense system of enzymatic and non-enzymatic compounds, which also functions to detoxify electrophilic species generated by the interaction of ROS with cellular constituents, particularly LPO products (Sharma et al., 2004). Investigations of the antioxidative stress response in test organisms offer the possibility to identify early biological signals of stress, before deleterious effects progress on the physiological, individual, or population level (Bayne et al., 1985).

1.7 *Hydrilla verticillata* as a model for aquatic macrophytes

Current investigations of nanotoxicity mostly do not consider aquatic plants as test organisms and thus ignore the value of macrophytes for aquatic ecosystems. As primary producers in the aquatic food chain, they influence the biochemistry of aquatic ecosystems while influencing statuses of oxygen, nutrients, and inorganic and organic carbon through their metabolic activity (Carpenter and Lodge, 1986; Madsen et al., 2001). Moreover, they have an impact on the physical environment, are highly influential on the composition of the associated fauna, and influence interspecific relationships (Carpenter and Lodge, 1986; Thomaz and Cunha, 2010). Hence, variations in macrophytes biomass will sustainable affect aquatic ecosystems as a whole. The investigated aquatic macrophyte *Hydrilla verticillata* (L.f.) Royle, also commonly known as Eastwaite Waterweed or water thyme, is a completely submerged, rooted, monoecious, or perhaps occasionally dioecious freshwater angiosperm of the family Hydrocharitaceae. These macrophytes have erect stems which are rooted in the sediment and serrated leaves typically 2-4 mm wide by 6-20 mm long and arranged in whorls (Figure 4). Most likely native to the warmer regions of Asia, the distribution of *H. verticillata* is meanwhile worldwide, as it dominates aquatic communities in all continents, except Antarctica (Cook and Luond, 1982). *H. verticillata* is referred to as aquatic weed as it outcompetes and displaces other aquatic plants due to its biology (Langeland, 1996). Firstly, competitiveness is encouraged by its growth habitat which is characterized by a very quick growth followed by branching near the water surface which results in shading of preexisting macrophytes (Cook and Luond, 1982; Langeland, 1996). It further possesses various mechanisms of vegetative reproduction (seeds, fragmentation, and turions) that enable *H. verticillata* to spread very rapidly (Langeland, 1996). Regarding the demands on freshwater quality, the macrophyte is rarely modest as it is able to grow in water with a wide range of pH and trophic states, also including eutrophic waters (Cook and

Luond, 1982). Together with its low light requirement for photosynthesis (Van et al., 1976), it has a competitive advantage in areas of dense aquatic vegetation. Thus, as *H. verticillata* is a widely distributed macrophyte which grows in a great variety of fresh water habitats it was selected as model aquatic plant in the present study.

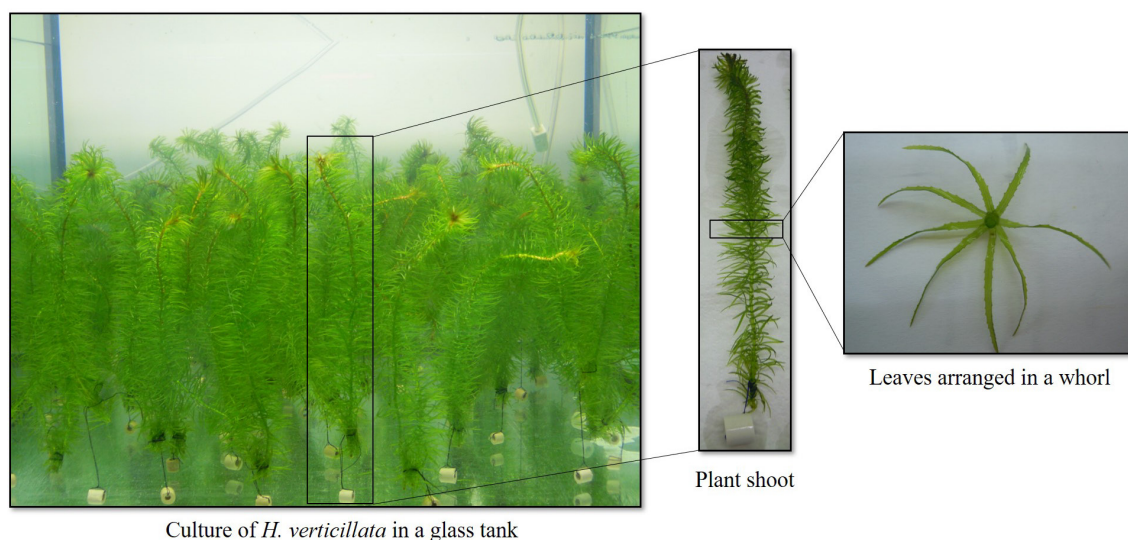


Figure 4. *Hydrilla verticillata* (photographed by Annette Spengler).

1.8. Research objectives

This thesis was conducted to evaluate the impact of TiO₂-based NPs on aquatic ecosystems either after its interaction with other environmental relevant contaminants in surface waters like cyanotoxins or directly after TiO₂-NP exposure. In this respect, the oxidative-stress mediated toxicity of nano-TiO₂ towards *H. verticillata* was investigated in a concentration- and time-dependent research trial. To estimate the potential of TiO₂-NPs to act as contaminant carriers for aquatic co-contaminants, an adsorption study with MC-LR was performed. All experiments included TiO₂-NPs with varying crystalline structure to further assess the influence of the crystal status on nano-TiO₂ toxicity and adsorption capacity.

In respect to the main objectives the following hypotheses were set for the study and tested with the stated methods:

1. TiO₂-NPs have the potential to act as ‘Trojan horse’ like carriers for MC-LR (Paper I).

→ Batch adsorption experiments with TiO₂-NPs, a bulk sized control, and MC-LR at a concentration level of environmental relevance for German freshwater bodies

2. Both, the concentration and the particle size influences TiO₂-NPs adsorption capacity for MC-LR (Paper I).

→ Study performance with different TiO₂-NP concentrations

→ Characterization of the investigated TiO₂-NPs and adsorption behavior analysis with a bulk sized counterpart in batch adsorption experiments

3. The crystallinity status of TiO₂-NPs influences MC-LR adsorption and the oxidative stress response in macrophytes (Paper I, II, III).

→ Investigations performed with TiO₂-NPs of different crystalline status

4. TiO₂-NPs stimulate the oxidative stress response in aquatic organisms (Paper II, III).

→ Examining changes in the activity of antioxidative enzymes, antioxidant status, and ROS production after nano-TiO₂ exposure of the aquatic macrophyte *H. verticillata*

5. Effects on oxidative stress related parameters are related to the nano-size and not the chemical composition of the particles (Paper I, II, III).

→ A bulk- and a nanoform of the same chemical composition (TiO₂) were investigated in regard to their impact on oxidative stress related effects in macrophytes

2 Materials and Methods

2.1 Materials

2.1.1 Technical devices and software

Following technical equipment was used for analytical chemistry and biological experiments in the present thesis.

Table 2. List of technical devices used for analytical chemistry and biological experiments.

Technical devices	Description and Company
Centrifuges	Minispin centrifuge 5417 R, Eppendorf, Germany Optima MAX-XP, Beckman Coulter, Germany
Concentrator	Concentrator plus/Vacufoqe® plus, Eppendorf AG, Germany
Deep freezer	Tenak, Denmark ProfiLine Pegasus, National Lab, Germany
Homogenizer	TissueLyser LT Quiagen, Germany Potter homogenizer, Glas-Col, Terre Haute, USA
Horizontal motion shaker	Edmund Bühler SM25, Hechingen, Germany
LC-MS/MS	Alliance 2695 UHPLC combined with a Quattro micro™ triple quadrupole mass spectrometer, Waters, USA
HPLC/UHPLC column	Kinetex™ C18, reverse phase, Phenomenex, USA
pH meter	526 MultiCal®, WTW, Germany pH 330 i, WTW, Germany
Spectrophotometer	UVIKON 922, Kontron Instrument, France Infinite M200 plate reader, Tecan, USA
Ultra-high resolution scanning electron microscope	Hitachi SU8030, Japan
Magnetic stirrer	Variomag Poly 15, Thermo Fisher Scientific, USA
Ultrasonic bath	Allpax Palsson, Germany
Vacuum manifold processor	JT Baker, Germany
Zetasizer Nano ZS	Malvern Instruments, Germany
SPE column	Sep-Pak tC18 Plus Short Cartridge, 400 mg sorbent Waters, Ireland
NAP-10 column	Sephadex G-25 DNA Grade, GE Healthcare, UK

In table 3 the commercial software for literature administration, data and text edition, and statistical analysis is summarized.

Table 3. List of software.

Software	Producer
Endnote X5	Thomson Reuters, USA
Microsoft office professional edition 2010	Microsoft Corporation, USA
SPSS 21.0	SPSS Inc., USA

2.1.2 Chemicals

The chemicals used for the cultivation of *H. verticillata*, toxin measurement, and analysis of the antioxidative stress response are summarized in table 4.

Table 4. List of chemicals.

Chemical	Description	Supplier
(NH ₄) ₂ SO ₄	Ammonium sulfate, ≥ 99%	Sigma
(NH ₄) ₆ Mo ₇ O ₂₄ *4H ₂ O	Ammoniumheptamolybdate tetrahydrate, ≥ 99%	Roth
Acetonitril	HPLC-gradient grade	Roth
Albumin fraction	Powdered, ≥ 98%	Roth
Bradford	Potein dye reagent	Sigma Aldrich
Ca(NO ₃) ₂ *4H ₂ O	Calcium nitrate tetrahydrate, ≥ 99%	Roth
CuSO ₄ *5H ₂ O	Copper sulfate pentahydrate, ≥ 99%	Merck
DMSO	Dimethyl sulfoxide, ≥ 99.5%	Sigma Aldrich
DTE	1,4-dithioerythritol, ≥ 99%	Sigma Aldrich
DTNB	5,5-dithio-bis(2-nitrobenzoic acid), ≥ 98%	Sigma
EDTA	ethylenediaminetetraacetic acid	Merck
EDTA tripotassium salt dihydrate	ethylenediaminetetraacetic acid tripotassium salt dihydrate, ≥ 99%	Roth
Ethanol	≥ 99.8%	Sigma Aldrich
FeCl ₃ *6H ₂ O	Iron chloride hexahydrate, ≥ 98%	Roth
Glycerol	Reagent plus TM, ≥ 99%	Sigma Aldrich

GR	Glutathione reductase from baker's yeast (<i>S. cerevisiae</i>), 1.5 mg protein/ml, 170 units/mg protein	Sigma
GSH	Reduced glutathione, $\geq 99\%$	Sigma Aldrich
GSSG	Glutathione disulfide, $\geq 98\%$	Sigma Aldrich
Guajacol	2-methoxy-phenol, 98%	Sigma Aldrich
H ₂ O ₂	Hydrogen peroxide, 30%	Chemsolute
H ₂ SO ₄	Sulfuric acid, $\geq 98\%$	Roth
H ₃ BO ₃	Boric acid, 99%	Sigma
HCl	Hydrochloric acid, 1mol/L $\pm 0.2\%$	Roth
KH ₂ PO ₄	Potassium dihydrogen phosphate, $\geq 99\%$	Merck
KNO ₃	Potassium nitrate, $\geq 99\%$	Roth
Methanol	HPLC-gradient grade and $\geq 99\%$	Roth
MgSO ₄ *7H ₂ O	Magnesium sulfate heptahydrate, $\geq 99.5\%$	Merck
MnSO ₄ *H ₂ O	Manganese sulfate monohydrate, 99%	Alfa Aesar
Na ₂ HPO ₄	Disodium dihydrogen phosphate, $\geq 99.5\%$	Merck
NADPH tetrasodium salt	β -Nicotinamide adenine dinucleotide phosphate, $\geq 97\%$	Roth
NaH ₂ PO ₄	Sodium dihydrogen phosphate, $\geq 99\%$	Merck
NEM	N-ethylmaleimide, $\geq 99\%$	Sigma
TCA	Trichloroacetic acid, $\geq 99\%$	Roth
TFA	Trifluoroacetic acid, $\geq 99\%$	Sigma Aldrich
TiCl ₄	Titanium chloride, $\geq 99\%$	Fluka
Tris	PUFFERAN®, $\geq 99.9\%$	Roth
ZnSO ₄ *7H ₂ O	Zinc sulfate heptahydrate, $\geq 99.5\%$	Roth

2.1.3 Modified Hoagland's nutrient solution

A modified Hoagland's nutrient solution (Table 5) was used for the test organism cultures and all exposures. As this study included investigations of co-contaminant sorption onto TiO₂-NPs, the iron chloride as plant available iron source was used instead of originally iron chelate to avoid sorption competition. A stock solution of each macronutrient (1 M) was prepared separately and appropriate volumes of this stock solutions were mixed and adjusted with hydrogen chloride (HCl) (1 M) to a pH 6.3 ± 0.05 . The micronutrient and iron stock solutions were added and the 100% Hoagland's nutrient solution was then finally

diluted with deionized water to the 5% test medium. Before exposure, macrophytes were cultured for 7 d to assure their acclimation to laboratory conditions.

Table 5. Composition and recipe of the modified Hoagland's nutrient solution.

Macronutrients	Concentration of stock solutions (g/L)	Volume of stock solution per litre of 100% medium (ml)	Concentration (ppm) in 100% medium	Final concentration (ppm) in test Medium (5%)
KNO ₃	101.1	5	505.5	25.3
Ca(NO ₃) ₂ *4H ₂ O	236.2	2	472.3	32.6
KH ₂ PO ₄	136.1	1	136.1	6.8
MgSO ₄ *7H ₂ O	246.5	2	493.0	24.6
Micronutrients	Concentration for 1 litre of stock solution (g/L)	Volume of stock solution per litre of 100% medium (ml)	Concentration (ppm) in 100% medium	Final concentration (ppm) in test medium (5%)
MnSO ₄ *H ₂ O	2	1	2.73	0.14
ZnSO ₄ *7H ₂ O	0.22		0.2	0.01
CuSO ₄ *5H ₂ O	0.08		0.08	0.004
(NH ₄) ₆ Mo ₇ O ₂₄ *4H ₂ O	0.2		0.198	0.01
H ₃ BO ₃	2.86		2.86	0.14
Iron stock solution				
FeCl ₃ *6H ₂ O	50	0.1	5	0.25

2.1.4 Cultivation of the test organism

H. verticillata was provided by Extraplant (Extragroup GmbH, Germany) and cultivated in a glass tank (60 cm × 60 cm × 60 cm) at 25 ± 1 °C in a 14:10-hour light-dark photoperiod under cool white fluorescent light (38 µE/m²/s). Macrophytes were cultured in a modified 5% Hoagland's nutrient solution (chapter 2.1.3). Approximately every week 30% of the medium was replaced by new nutrient solution.

2.1.5 TiO₂-nanoparticles and bulk TiO₂

2.1.5.1 Particles

Experiments with *H. verticillata* were performed with different crystalline structures of TiO₂-NPs. Next to a pure anatase and rutile TiO₂, a commercial standard TiO₂ (P25, Evonik Degussa) was tested. Moreover, all investigations included a micron-sized TiO₂ counterpart, to assess nano-size related toxic effects. Table 6 lists the TiO₂-based particles investigated in the study.

Table 6. List of the studied TiO₂-nanoparticles and bulk TiO₂.

Particle	Description by the supplier	Supplier
TiO ₂ nanopowders	Anatase, < 25 nm, 45-50 m ² /g Rutile, 10-30 nm, 50 m ² /g Aeroxide P25, 21 nm, 50 ± 15 m ² /g	Sigma Aldrich Iolitec Evonik Degussa Corporation
Bulk TiO ₂	< 5 µm, rutile and ≈ 5% of anatase	Sigma Aldrich

2.1.5.2 Preparation of TiO₂ nanoparticle suspensions

TiO₂-NP stock solutions (100 mg/L) were prepared by weighing and direct transfer into the test medium. NP suspensions were sonicated in an ultrasonic bath (Allpax Palsson, Germany) at 40 kHz for 2 h, as this time proved to be sufficient to increase the dispersion stability of the NP stock solution. For bulk TiO₂ suspensions the same protocol was applied to ensure comparability. The respective exposure concentrations were prepared by diluting the nano- and microparticle stock solution with the test medium.

2.1.6 Cyanobacterial microcystin-LR as aquatic Co-contaminant

2.1.6.1 Microcystin-LR

For the adsorption study with TiO₂-NPs and cyanotoxins, MC-LR was used as environmental relevant representative of cyanotoxins. MC-LR (HPLC-grade, ≥ 95%) isolated from the cyanobacterial species *Microcystis aeruginosa* was purchased from Enzo Life Sciences (Germany).

2.1.6.2 Preparation of Microcystin-LR suspensions

Cyanobacterial toxin was resuspended and diluted with HPLC-grade methanol to receive a MC-LR stock concentration of 10 mg/L. Before the start of the sorption experiments, the stock concentration was checked *via* liquid chromatography tandem mass spectrometry (LC-MS/MS) analysis (see chapter 2.2.3.3). The final experimental concentration of 5 µg/L MC-LR was achieved by further dilution with the TiO₂ particle suspensions.

2.2 Methods

2.2.1 Nanoparticle characterization

The primary particle sizes and morphologies were verified by ultra-high resolution scanning electron microscopy (SEM) (Hitachi SU8030, Japan) in the ZELMI of TU Berlin. Additionally, a characterization under experimental conditions for zeta potential and size was done after bath sonication using a Zetasizer Nano ZS (Malvern Instruments, Germany). The z-average (intensity weighted) hydrodynamic diameter and the polydispersity index (PDI) were determined by dynamic light scattering (DLS). Size measurements were done in triplicate with each measurement being an average of 5 runs of 10 seconds. Average zeta potential measurements were carried out 30 runs of 11 seconds in triplicate. In addition, the pI_{IEP} was determined by means of zeta potential measurements at varying pH values.

2.2.2 Nanoparticle sedimentation analysis

To evaluate the stability of the three investigated TiO₂-NP suspensions throughout the exposure time a settling experiment was conducted. Results of the sedimentation analysis provided the basis for decisions regarding the exposure medium renewal during the experiments. The respective TiO₂-NP stock solution were prepared as explained previously (chapter 2.1.5.2) and left for sedimentation. During a test period of 7 d aliquots of the dispersion were carefully taken from the supernatant at a certain height to avoid disturbance of the sedimentation process. The states of sedimentation were observed after 1 h, 3 h, 6 h, 24 h, 48 h. and 168 h. Changes of the z-average hydrodynamic diameter were determined by DLS and were performed in triplicate with each measurement being an average of 5 runs of 10 seconds. Moreover, the absorption of light was measured in an UV/Vis-spectrophotometer (UVIKON 922, Kontron Instrument, Italy) at varying wavelengths

(290 nm for P25, 320 nm for anatase TiO₂, 328 nm for rutile TiO₂). Therefore, the specific absorption maxima of the different NPs were analyzed beforehand. Each of the TiO₂-NP experiments has run in triplicate and the results presented are the average of the runs. The change of optical absorbance with time can be related to the normalized NP concentration C/C_0 where C represents the concentration in time, and C_0 is the initial concentration.

2.2.3 Adsorption of microcystin-LR onto TiO₂-NPs

2.2.3.1 Batch adsorption experiments

Batch adsorption experiments were conducted in 250 ml erlenmeyer flasks capped with parafilm to avoid contamination and minimize evaporation of the test solution. Each flask contained 50 ml of the NP suspension at a concentration of 10 mg/L. Nano- and microparticle stock solutions were prepared immediately before initiation of adsorption to minimize particle aggregation and sedimentation. For all experiments, a concentration of 5 µg/L MC-LR was used, as this concentration has been reported to be of environmental relevance for German water bodies (Wiedner et al., 2004). Organic solvent concentration was kept at a level of 0.05% of the total solution volume preventing sorption competition. Measurement of the final pH (526 MultiCal®, WTW, Germany) of each sample was conducted in order to access differences of pH between the batches probably influencing toxin adsorption. The flasks were agitated on a horizontal motion shaker (Edmund Bühler SM25, Germany) with an agitation speed of 125 rpm and a temperature of 20 ± 5 °C to keep the solutions in a completely mixed state. After shaking, the test solutions were centrifuged twice in an ultracentrifuge (Optima MAX-XP, Beckman Coulter, Germany) at $7,800 \times g$ for 10 min to separate the liquid from the solid phase. The supernatant was removed and analysed *via* LC-MS/MS. To assess the loss of MC-LR on the glass walls and from other processes than adsorption (loss in system) a blank without adsorbent was examined in parallel. Additionally, blanks with the adsorbent but without MC-LR served as control of any background contamination during the experiments.

2.2.3.2 Adsorption kinetic study

A kinetic study with a constant TiO₂-NP concentration of 10 mg/L but varying sorption times (0 h, 1 h, 3 h, 6 h, 16 h, 24 h, 48 h, 72 h) was conducted for each NP separately in triplicate. Equilibration was considered to be sufficient when toxin concentration changes

were less than 5% between two successive measurements. The adsorption capacity of each TiO₂-NP after varying time was determined by the following mass balance equation:

$$q_e = \frac{v (C_0 - C_e)}{m}$$

q_e – equilibrium adsorption capacity of MC-LR [$\mu\text{g/g}$] adsorbed on unit mass of TiO₂-NP representative, C_0 – initial liquid-phase concentrations of MC-LR [$\mu\text{g/L}$], C_e – equilibrium liquid-phase concentrations of MC-LR [$\mu\text{g/L}$], v – solution volume [L], m – mass of adsorbent [g].

In order to investigate the adsorption mechanism of MC-LR on the TiO₂-NPs and to determine the rate-limiting step of adsorption, the following kinetic models were adopted to examine the time-dependent experimental adsorption data: pseudo-first-order equation, pseudo-second-order equation and intraparticle diffusion model.

The pseudo-first-order rate equation (Lagergren's equation) (Ho, 2004) can be expressed as:

$$\log(q_e - q_t) = \log q_e - \frac{k_1}{2.303} t$$

q_e – adsorption capacity [$\mu\text{g/g}$] at equilibrium, q_t – adsorption capacity [$\mu\text{g/g}$] at time t , k_1 – first-order rate constant of pseudo-first-order equation [1/h], the values of $\log (q_e - q_t)$ were linearly correlated with t .

The pseudo-second-order model (Ho and Mc Kay, 1999) was equally applied using the linear form equation:

$$\frac{t}{q_t} = \frac{1}{k_2 q_e^2} + \frac{1}{q_e} t$$

q_e – adsorption capacity [$\mu\text{g/g}$] at equilibrium, q_t – adsorption capacity [$\mu\text{g/g}$] at time t , k_2 – rate constant of pseudo-second-order [$\text{g}/\mu\text{g h}$]

The values of k_1 and k_2 were determined from the slope and intercept of the corresponding plot.

Contribution of intra particle diffusion mechanism can be tested by applying the Weber and Morris equation (Weber and Morris, 1963):

$$q_t = k_{id}t^{1/2} + C$$

k_{id} – intraparticle diffusion rate constant [$\mu\text{g/g h}^{1/2}$], C – boundary layer effect [$\mu\text{g/g}$]

The value k_{id} can be evaluated from the slope of the linear plot of q_t versus $t^{1/2}$, if the intraparticle diffusion is the rate-limiting step, the plot passes through the origin.

2.2.3.3 Influence of adsorbent concentration and particle size

Batch adsorption experiments with varying adsorbent concentrations (0.01 mg/L, 0.1 mg/L, 1 mg/L, 10 mg/L TiO_2 -NPs and bulk TiO_2) were performed in quadruplicate. Samples were shaken for 48 h to ensure that the equilibrium was reached for all TiO_2 -NPs.

The residual concentration of MC-LR was calculated as follows:

$$100 \times \frac{C_e}{C_0}$$

C_0 – initial liquid-phase concentrations of MC-LR [$\mu\text{g/L}$], C_e – equilibrium liquid-phase concentrations of MC-LR [$\mu\text{g/L}$]

2.2.3.4 Cyanobacterial toxin determination

To reach detectable concentrations of MC-LR for a quantification in LC-MS/MS analysis, a preconcentration of MC-LR *via* solid-phase-extraction (SPE) was done beforehand using reversed-phase cartridges (Sep-Pak[®] tC18, 400 mg sorbent, Waters, Ireland). The sample was passed through the SPE tube for toxin enrichment followed by an elution step with 5 ml of methanol (99%). Subsequently, all methanol was removed in a vacuum centrifuge (Concentrator plus/Vacufo[®] plus, Eppendorf AG, Germany) at a temperature of 30 °C and finally resuspended with 500 μl HPLC-grade methanol.

MC-LR quantification was performed by LC-MS/MS (Alliance 2695 UHPLC combined with a Micromass Quattro microTM, Waters, USA) using the reverse phase column KinetexTM C18 (2.1 mm * 50 mm, 2.6 μm pore size, Phenomenex, USA). The column oven temperature was set at 40 °C with an injection volume of 20 μl . The mobile phase consisted

of solution A (Mili-Q water containing 0.1% TFA and 5% acetonitrile (ACN)) and solution B (ACN containing 0.1% TFA) at a flow rate of 0.2 ml/min. A gradient was generated between both solutions. The gradient conditions (solution A: solution B) were 65:35 at 3 min, 35:65 from 3.75 to 7 min and 0:100 from 7.8 to 12 min. Elution peaks for MC-LR were observed at 7.44 min. Spectral mass data analysis was performed using electrospray ionization (ESI) in a positive ion mode with a collision energy of 65 V. Desolvation gas N₂ was set as trigger gas and Argon (Ar) as collision gas. For the subsequent MS/MS detection the MRM mode was used with a mass transfer of 995.5 (Q1) and 107.3, 135.1, 213.2, and 357.2 (Q3) for MC-LR. Calibration was linear ($R^2 = 0.999$) between 5 and 500 µg/L. The limit of detection was 1 µg/L.

2.2.4 Oxidative stress response analysis in *Hydrilla verticillata*

2.2.4.1 Exposure design

Oxidative stress related effects in the aquatic macrophyte *H. verticillata* were investigated in a concentration- and time-dependent trial with the model aquatic plant *H. verticillata*. The first exposure system was comprised of different concentrations of TiO₂-NPs and bulk TiO₂ (0.01 mg/L, 0.1 mg/L, 1 mg/L, 10 mg/L) at a fixed exposure time of 24 h. Thus, experiments included a TiO₂-NP level within the range of current predictions (10⁻³ µg/L to 10 µg/L) for surface waters (Gottschalk et al., 2013). The second exposure system studied the time-dependence of the oxidative stress response in *H. verticillata* by evaluating oxidative stress markers after TiO₂-NP and bulk TiO₂ exposure for 0 h, 24 h, 48 h, 96 h. and 168 h. Exposure levels of 0.1 mg/L and 10 mg/L of TiO₂ particles were applied at each time point.

Whole plants, including shoot apical meristem, main stem, and leaves, were cut one week prior the experiment and pre-cultured in modified Hoagland's nutrient solution to avoid plants stress due to pretreatment. The conditions for the cultivation of the plants are listed in the previous chapter 2.1.4. Under the same controlled light- and temperature conditions as for the pre-culture, the plants were exposed to the different TiO₂-particles. Immediately after the particle suspensions have been prepared, plants were introduced into the exposure medium. Controls (containing test medium without TiO₂-particles) were prepared in parallel to consider oxidative stress levels due to the normal experimental setup. Therefore, the study

of time-dependent effects included control plants for each treatment time. Additionally, the time-dependent trial included plants taken directly from the pre-culture as 0 h controls.

To avoid progressive particle sedimentation, and thus decreased exposure of plants during the experiment, the time-dependent study included exposure medium renewal every 24 h. For this purpose, *H. verticillata* was removed from the old exposure medium, gently blotted with a paper towel, and immediately introduced into fresh exposure solution. The same procedure was applied for the control plants for reasons of comparability. Controls, nano-TiO₂, and bulk TiO₂ treatments were conducted in quadruplicate. Due to the influence of the pH on NP suspension stability and its importance for macrophytes biological response, the pH was checked for both exposure systems at the beginning and the end of the experiments using a mobile pH meter (pH 330i, WTW, Germany).

After exposure, macrophytes were washed twice with 100 ml of deionized water, shock-frozen in liquid nitrogen, and stored at -80 °C. The frozen macrophytes were pulverized in liquid nitrogen, using a mortar and pestle, and corresponding amounts of the tissue powder were homogenized with a mechanical TissueLyser LT (Quiagen) for 6 min at 50 oscillation/s using two 7 mm stainless steel beads.

To gain insight into the oxidative stress response after TiO₂-NP exposure, various biochemical markers and the ROS status were analyzed for both exposure settings. The ROS status in *H. verticillata* was investigated by measuring the level of H₂O₂. Moreover, the GSH status and antioxidative enzyme activities were assessed. Regarding the latter, the concentration-dependence study included analysis of POD activity, which was not performed for the time-dependent trial as POD activity was unaffected after such exposures.

2.2.4.2 Measurements of internal H₂O₂

Levels of H₂O₂ were determined colorimetrically according to Jana and Choudhuri (1982). H₂O₂ was extracted by homogenizing 0.2 g of pulverized macrophyte tissue with 3 ml sodium phosphate buffer (50 mM, pH 7.0). The homogenate was centrifuged at 20,800 × g for 15 min at 4 °C and the supernatant was collected. Supernatant amounting to 600 µl was mixed with 200 µl of 0.1% titanium chloride in 20% H₂SO₄ and the red-orange coloration of titanium peroxide was detected at 410 nm in an UV/Vis-spectrophotometer (UVIKON 922, Kontron Instrument, France). Three replicates of each sample were monitored in three individual measurements of the same sample. As the supernatants were not completely

transparent the blank also included sample. H_2O_2 contents were calculated with the following formula using the extinction coefficient (ε) 0.28 L/mmol cm and expressed as $\mu\text{mol/g FW}$.

$$H_2O_2 = \frac{OD_{410} \times v_t}{\varepsilon \times d \times v_s \times \frac{s_p}{v}}$$

OD_{410} – optical density 410 nm, v_t – total volume [ml], ε – molar extinction coefficient [L/ mmol cm], d – cuvette width [cm], v_s – sample volume [ml], s_p – sample weight [g], v – buffer volume [ml]

2.2.4.3 Non-enzymatic antioxidants: GSH status analysis

Non-enzymatic antioxidant status was assessed within this study *via* analysis of the GSH status. Therefore, the levels of GSSG and GSH were determined, the latter by measuring the amount of tGSH, representing GSH and GSSG. Concentrations of tGSH and GSSG were carried out using the GSH spectrophotometrically recycling method (Figure 5) according to Giustarini et al. (2003) and Aravind and Prasad (2005) with modifications. In order to determine the level of GSSG, 0.2 g of pulverized macrophyte tissue was homogenized for 10 min in 0.72 ml of 50 mM Tris base buffer (Tris-(hydroxymethyl)-aminomethane) containing 31 mM of N-Ethylmaleimide (NEM) which covalently reacts with GSH in the sample. After derivatization, sample aliquots were acidified with 80 μl of 60% Trichloroacetic acid (TCA) and again thoroughly mixed for 10 min before centrifugation (Minispin centrifuge 5417 R, Eppendorf, Germany) at $20,800 \times g$ for 5 min at 4°C . Thereafter, the acid de-proteinized supernatant amounting to 250 μl was extracted with three volumes of methylene chloride (Merck, purity $\geq 99.5\%$) and centrifuged at $20,800 \times g$ for 5 min at 4°C to obtain supernatants for GSSG level investigation. To determine the amount of tGSH, pulverized macrophyte tissue (0.2 g) was homogenized in 0.8 ml of 7.5% TCA buffer containing 2.3 mM ethylenediaminetetraacetic acid tripotassium salt dihydrate (Tripotassium EDTA). After mixing for 10 min the solution was centrifuged at $20,800 \times g$ for 5 min at 4°C . The concentration of tGSH was measured in the prepared supernatants. Levels of tGSH and GSSG were determined spectrophotometrically (Infinite M200 plate reader, Tecan, USA) *via* analysis of the increase of absorbance at 412 nm based on the reduction of DTNB (5,5-dithio-bis(2-nitrobenzoic acid)) to TNB (2-nitro-5-thiobenzoic

acid) in the presence of GR (10 U/ml) and 4.8 mM nicotinamide adenine dinucleotide phosphate hydrate (NADPH) in a 200 mM phosphate buffer at 4 °C. Standard curves containing known concentrations of purified solid GSH ($\geq 99\%$) and GSSG ($\geq 98\%$) were used for calculating the amount of tGSH and GSSG (0.05–50 μM GSH and 0.05–10 μM GSSG). Both calibration curves showed excellent correlation ($R^2 = 0.98$ for GSH; $R^2 = 0.99$ for GSSG). The concentrations of GSH and GSSG were reported in nmol/g FW or expressed as GSH/GSSG ratio. Calculations were performed as follows:

$$tGSH \text{ or } GSSG [\mu\text{mol/g FW}] = \frac{(FW + v_s) \times (Abs - n)}{m \times 1000 \times FW}$$

FW – fresh weight of the plant tissue, *v_s* – solvent volume [ml], *Abs* – extinction measured at 420 nm, *n* – intercept of the standard curve, *m* – slope of the standard curve

In order to calculate the content of GSH, the amount of GSSG was multiplied by 2 and subtracted from the level of tGSH.

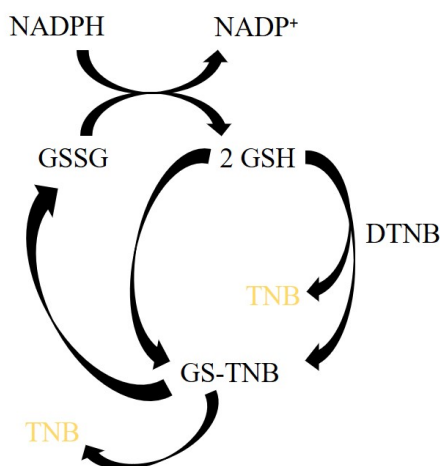


Figure 5. Mechanism of the GSH recycling method. The assay measures reduced glutathione (GSH) and oxidized glutathione (GSSG) after its reduction to two molecules of GSH by glutathione reductase (GR) in the presence of nicotinamide adenine dinucleotide phosphate (NADPH). GSH reacts with 5,5-dithio-bis(2-nitrobenzoic acid) (DTNB) to 2-nitro-5-thiobenzoic acid (TNB) and the glutathione adduct of TNB (GS-TNB). GS-TNB is either reduced by GSH with the formation of GSSG and TNB or by GR and NADPH with the generation of GSH and TNB. The yellow chromophore TNB can be quantified at an absorbance of 412 nm (Giustarini et al., 2013).

2.2.4.4 Enzymatic antioxidants

2.2.4.4.1 Enzyme extraction

Enzyme extraction was prepared according to Pflugmacher (2004) with minor modifications. Pulverized macrophyte tissue ($1.5 \text{ g} \pm 0.1 \text{ g}$) was resuspended in 3 ml of sodium phosphate buffer (0.1 M, pH 6.5) containing 20% (v/v) glycerol, 1.4 mM dithioerythritol (DTE), and 1 mM EDTA. The homogenate was centrifuged at $5,400 \times g$ for 10 min in an ultracentrifuge (Optima MAX-XP, Beckman Coulter, Germany). In order to collect the microsomal protein fraction, the supernatant was again centrifuged at $86,900 \times g$ for 60 min. The supernatant was precipitated twice with solid ammonium sulfate (0–35% and 35–80% saturation) with another centrifugation step at $21,700 \times g$ for 20 min in between. Precipitation was performed on a magnetic stirrer (Variomag, Thermo Fisher Scientific, USA). Solutions were centrifuged for 30 min at $48,900 \times g$ and pellets (cytosolic protein fraction) were resuspended in 1 ml of sodium phosphate buffer (20 mM, pH 7). All centrifugation steps were carried out at 4°C . Solutions were desalted by gel filtration using sephadex columns (NAP-10, GE Healthcare, UK), immediately snap-frozen in liquid nitrogen, and stored at -80°C for enzyme activity assay. Protein concentrations were determined at 595 nm (Infinite M200 plate reader, Tecan, USA) using the protein dye Bradford according to the method of Bradford (1976). Bovine serum albumin (BSA) was used as protein standard at the concentrations of 0 mg/L, 0.025 mg/L, 0.05 mg/L, 0.125 mg/L, 0.25 mg/L, 0.5 mg/L, 0.75 mg/L, and 1 mg/L and revealed a calibration curve with a correlation coefficient of $R^2 = 0.996$.

2.2.4.4.2 Enzyme activity measurements

Peroxidase (POD) (Paper II): POD activity was measured using guajacol as substrate, according to Pütter (1974) by measuring the POD-catalyzed oxidation of guajacol to tetraguajacol at 436 nm. The reaction mixture for activity analysis consisted of sodium phosphate buffer (0.1 M, pH 5), guajacol (100 mM) dissolved in dimethyl sulfoxide (DMSO), H_2O_2 (200 mM) dissolved in sodium phosphate buffer, and enzyme extract. The molar extinction coefficient (ϵ) for enzyme activity calculation is 25.5 L/mmole cm .

Catalase (CAT) (Paper II, III): CAT activity was measured according to Aebi (1974) by monitoring the degradation of H₂O₂ at an absorbance of 240 nm. The reaction mixture for activity analysis consisted of sodium phosphate buffer (0.05 M, pH 7), H₂O₂ (150 mM) dissolved in sodium phosphate buffer, and enzyme extract. The molar extinction coefficient (ϵ) for enzyme activity calculation is 0.036 L/mmol cm.

Glutathione reductase (GR) (Paper II, III): GR was measured according to Carlberg and Mannervik (1985) by monitoring the consumption of NADPH during the regeneration of GSH from GSSG at an absorbance of 340 nm. The reaction mixture for activity analysis consisted of sodium phosphate buffer (0.1 M, pH 7.5), GSSG (20 mM), and NADPH tetrasodium salt (2 mM), both dissolved in deionized water, and enzyme extract. The molar extinction coefficient (ϵ) for enzyme activity calculation is 6.3 L/mmol cm.

Protein concentration analysis and all enzymatic measurements were performed in triplicate for each replicate of the cytosolic protein fraction in a spectrophotometer (Infinite M200 plate reader, Tecan, USA). Enzymatic activities were expressed either in μ kat/mg protein or nkat/mg protein, with [kat] being the conversion rate of 1 mol of substrate per second. For the calculation of the enzyme activity the following formula was used.

$$A_E[\text{kat/mg protein}] = \frac{\Delta E \times v_w}{v_p \times \epsilon \times d \times c_{prot} \times \Delta t}$$

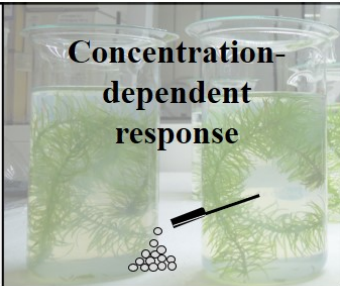
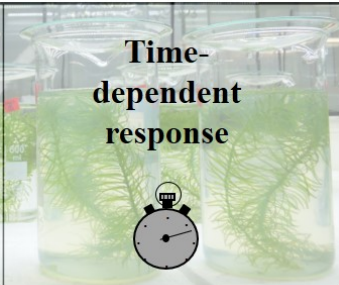
A_E – enzyme activity [kat], ΔE – extinction change, v_w – test volume [μ l], v_p – volume of enzyme extract, ϵ – molar extinction coefficient [L/ mmol cm], d – cuvette width [cm], c_{prot} – protein content of the enzyme extract [mg/L], Δt – measuring interval [s]

Table 7 summarizes the reaction principle of the antioxidative stress enzymes investigated in the study with *H. verticillata*. In addition, table 8 provides an overview of the experiments conducted to assess the oxidative stress response in *H. verticillata*.

Table 7. Catalytic reaction of guajacol peroxidase (POD), catalase (CAT), and glutathione reductase (GR) studied to assess the oxidative stress response in *H. verticillata*.

Antioxidative enzyme	Enzyme code	Reaction principle
POD	EC 1.11.1.7	$4 \text{ Guajacol} + 4 \text{ H}_2\text{O}_2 \rightarrow \text{Tetraguajacol} + 8 \text{ H}_2\text{O}$
CAT	EC 1.11.1.6	$2 \text{ H}_2\text{O}_2 \rightarrow 2 \text{ H}_2\text{O} + \text{O}_2$
GR	EC 1.6.4.2	$\text{GSSG} + \text{NADPH} + \text{H}^+ \rightarrow 2 \text{ GSH} + \text{NADP}^+$

Table 8. Overview of the experiments conducted to assess the oxidative stress response in *H. verticillata* after exposure to TiO₂-based nano- and microparticles.

Exposure conditions and determined effects		 Concentration-dependent response	 Time-dependent response
Macrophyte biomass		4.3 ± 0.2 g fresh weight	3.5 ± 0.1 g fresh weight
TiO ₂ particle concentration		0.01 mg/L, 0.1 mg/L, 1 mg/L 10 mg/L	0.1 mg/L, 10 mg/L
Exposure time		24 h	0 h, 24 h, 48 h, 96 h, 168 h
Oxidative stress related biochemical parameter	ROS formation	H ₂ O ₂ level	H ₂ O ₂ level
	Enzymatic antioxidative stress response	Enzyme activity assessment: POD, CAT, GR	Enzyme activity assessment: CAT, GR
	Non-enzymatic antioxidative stress response	antioxidant status assessment: GSH status	antioxidant status assessment: GSH status

2.2.5 Statistics

Three different kinetic theories were applied to the adsorption data obtained in the experiments studying cyanobacterial toxin adsorption onto the different TiO₂-NPs and bulk TiO₂ (Paper I). The regression correlation coefficients (R^2) of the kinetic plots were used to test the accuracy of the proposed adsorption kinetic models. For investigating the concentration-dependence of adsorption (Paper I) and the concentration-dependence of the oxidative stress response in the test organisms (Paper II) a one way analysis of variance (ANOVA) followed by a post-hoc Dunnett test was performed to determine statistical significant differences between the various concentration levels of the TiO₂-NPs and the respective bulk TiO₂ concentration (Paper I and II) or the control treatment (Paper II). Additionally, a post hoc comparison of all concentration levels was done for each TiO₂-NP separately with Tukey's HSD test to assess the concentration dependence of MC-LR adsorption. For the experiments dealing with time-dependent oxidative stress related effects in *H. verticillata* (Paper III) the same statistical methods were applied to evaluate significant differences between the TiO₂-NP treatment and the bulk TiO₂ exposure at a certain time. Prior to ANOVA, all data were tested for normality and homogeneity of variances using Shapiro-Wilks test and Levene's test, respectively. For data sets not normally distributed, a logarithmic (log10) or square root transformation was applied. Kruskal-Wallis one-way analysis of variance and Mann-Whitney U test were performed for data sets not fitting normal distribution and homogeneity of variances. Statistical analysis was performed using commercial software SPSS 21.0 (SPSS Inc, Chicago, IL, USA). A significance level of $p < 0.05$ was considered significant for all comparisons.

3 Results

3.1 Nanoparticle characterization

Ultra-high resolution SEM images indicated differences in the TiO₂-NPs morphology (Paper I, Figure 1). Whereas P25 showed up as a nearly homogenous sample of spherical NPs, the rutile and anatase product consisted of heterogeneous shaped particles. Moreover, the primarily NP samples showed polydispersity. Thus, the NP images displayed small particles, representing the sizes provided by the manufacturer, and individual larger NPs, however, still below 1 μm . All TiO₂-NPs showed aggregates of the primary particles which might have been a characteristic of the NP product itself or a result of the sample preparation method required for the microscopic imaging.

Ultrasonication was applied to all TiO₂-NP samples and decreased secondary particle size in the exposure medium with time. However, an ultrasonication time study revealed that the average particle size decreased quickly within a sonication time of 2 h and then became more constant with increasing sonication time (Figure 6). For this purpose, all TiO₂-NP suspension preparations throughout this thesis were sonicated for 2 h.

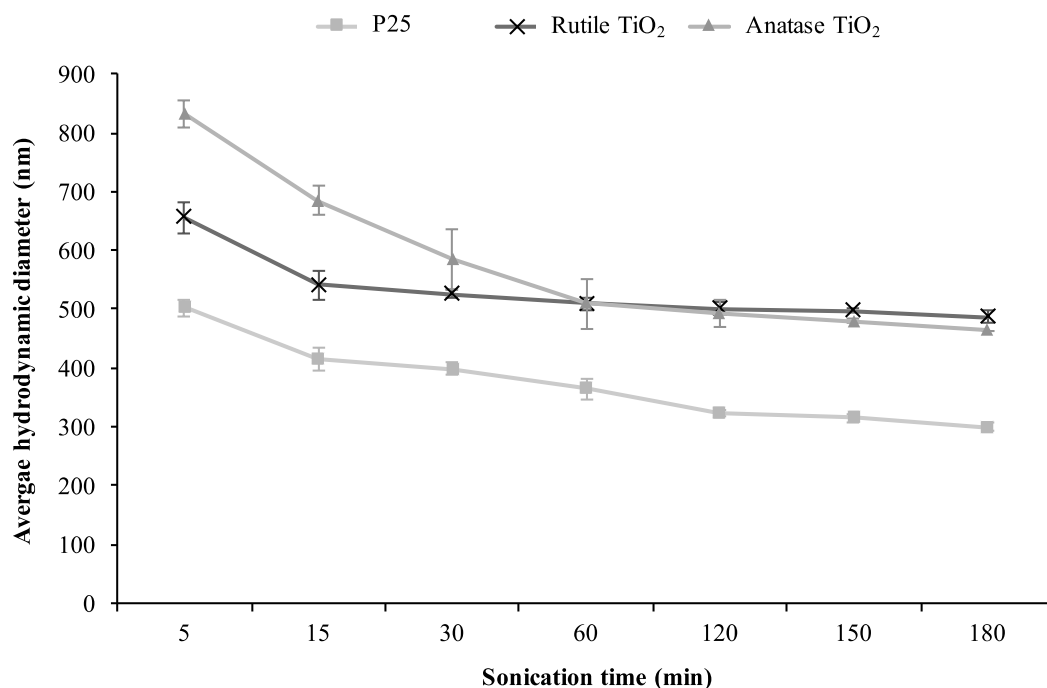


Figure 6. Average hydrodynamic diameter of the investigated TiO₂-NPs as a function of sonication time.

DLS and zeta potential measurements of the TiO₂-NPs suspensions were performed to assess the NPs characteristics under experimental conditions. DLS results indicated an almost bimodal size distribution of the TiO₂ particles. All TiO₂-NPs tended to aggregate in the test medium. Immediately after sonication, about 90% of the particles exhibited average sizes in the 400 to 500 nm range (Paper I, Table 2) and thus much larger than the vendor reported sizes. However, compared to the investigated bulk TiO₂, with average particle sizes of about 1.5 μ m, the TiO₂-NP aggregates still showed smaller sizes. Clearly, the surface charge was a function of solution pH and the pH_{IEP} was pH 2.78, pH 2.83, pH 3.52 and pH 3.63 for rutile TiO₂, bulk TiO₂, anatase TiO₂ and P25, respectively. At a pH below the respective pH_{IEP} the NP surface was characterized by a net positive charge. In contrast, at pH above the respective pH_{IEP} the surface charge was negative. Thus, zeta potential analysis of all investigated TiO₂-NPs showed a negative zeta potential under experimental conditions (Paper I, Figure 2). With respect to the pH_{IEP}, similar patterns of the zeta potential development occurred for particles with comparable crystallinity status (bulk TiO₂ and rutile TiO₂, P25 and anatase TiO₂). However, only marginal differences between the crystal phases became apparent.

3.2 Nanoparticle sedimentation analysis

Nanoparticle sedimentation analysis indicated instability of the respective TiO₂-NP suspensions. Immediately after the start of the sedimentation analysis, a progressing drop of the optical absorbance indicated NPs settling in the suspensions (Paper III, Figure 1B). Within 24 h, the absorbance decreased by 78%, 65% and 51% for P25, rutile TiO₂ and anatase TiO₂, respectively. P25 in particular showed an outstanding particle settling behavior compared to suspensions of anatase and rutile TiO₂. After 168 h of absorbance analysis, only 6%, 20% and 23% of P25, rutile TiO₂, and anatase TiO₂, respectively, remained in solution. The results of the spectrophotometer analysis were in accordance with the results of the particle size analysis *via* DLS (Paper III, Figure 1A). After suspending the TiO₂-NPs in the test medium, NP aggregate formation became apparent. Whereas anatase TiO₂ and rutile TiO₂ only showed minor changes in their aggregate sizes in the first hours of DLS analysis, suspensions containing P25 were characterized by large particle aggregates with increasing sizes from \sim 440 nm to $>$ 800 nm within the first 6 h. After 24 h, all tested TiO₂-NPs displayed a rapid decrease of their z-average hydrodynamic diameters which continued with settling time, however, to a lesser extent.

3.3 Cyanobacterial toxin adsorption onto TiO₂ nanoparticles

3.3.1 Adsorption kinetic study

All TiO₂-NPs showed a continuous increase in the adsorption of MC-LR with time (Paper I, Figure 3). The adsorption capacity of anatase TiO₂ progressively flattened after 24 h. Rutile TiO₂ and P25 reached toxin adsorption equilibrium at 48 h. P25 exhibited the highest capacity for MC-LR removal followed by anatase TiO₂ and rutile TiO₂ (282 µg/g, 188 µg/g, 128 µg/g for $t = 72$ h). As the loss of the MC-LR was negligible and no background contamination was detected during the batch adsorption experiments, the variation of toxin concentration could be directly linked to its adsorption onto the TiO₂-NPs.

For all TiO₂-NPs the correlation coefficients of the first-order kinetic were lower compared to the second-order kinetic model (Paper I, Table 2). Thus, the pseudo-second-order kinetic model might explain the adsorption kinetic of MC-LR onto TiO₂-NPs most effectively. Moreover, as the data for the intraparticle diffusion model exhibited multi-linear plots (Paper I, Figure 4) it can be assumed that an intraparticle diffusion of MC-LR is not the sole mechanism to explain toxin adsorption.

3.3.2 Influence of the particle size and concentration on the toxin adsorption process

All TiO₂-NPs showed a higher toxin adsorption at all applied concentrations compared to the bulk TiO₂. Statistical significant differences in toxin adsorption between TiO₂-NPs and bulk TiO₂ were assessed for all TiO₂-NPs at a concentration level of 0.01 mg/L ($p < 0.01$), 0.1 mg/L ($p < 0.001$ for P25 and anatase TiO₂, $p < 0.01$ for rutile TiO₂) and anatase TiO₂ at a concentration of 1 mg/L ($p < 0.01$). For the lowest applied dose of TiO₂-based adsorbents almost identical residual MC-LR values were detected (60% for P25, 58% for anatase TiO₂, 62% for rutile TiO₂). Both, P25 and anatase TiO₂ exhibited residual toxin levels of 55% at a concentration of 0.1 mg/L. Rutile TiO₂ showed a slightly lower adsorption of MC-LR at the same concentration level, as 60% of residual toxin was detected. With the exception of anatase TiO₂, further elevation of the adsorbent dose resulted in constant or slightly higher residual toxin levels, however, still lower compared to respective bulk TiO₂ treatments.

3.4 Oxidative stress response in *Hydrilla verticillata*

H₂O₂ formation

Results of the concentration-dependent study of the ROS generation in *H. verticillata* revealed no altered H₂O₂ levels for macrophytes treated with anatase TiO₂, rutile TiO₂, and bulk TiO₂ for 24 h (Figure 1B-D, Paper II). Instead, an exposure to P25 at the highest investigated concentration of 10 mg/L caused an increase in H₂O₂ by 30%, which turned out to be significant ($p = 0.017$) (Figure 1A, Paper II).

No clear time-dependence in the H₂O₂ formation after exposure to both tested concentrations, 0.1 mg/L and 10 mg/L TiO₂-NPs, could be observed. However, after 96 h of nano-TiO₂ treatment, exposure to 10 mg/L rutile TiO₂, P25, and anatase TiO₂ caused significant ($p < 0.05$) elevated H₂O₂ levels by 16%, 20% and 30%, respectively, compared with non-treated macrophytes. Instead, no altered H₂O₂ levels were detected in *H. verticillata* exposed to bulk TiO₂ compared to the respective control. A comparison of the ROS formation after TiO₂ nano- and microparticle treatment (Figure 2, Paper III) revealed significantly ($p = 0.02$) elevated H₂O₂ levels for both tested P25 concentrations already after 24 h of exposure. An elongation of the exposure time solely caused a shift in the ROS status for the high exposure scenario. Again, after 96 h of exposure to 10 mg/L of nano-TiO₂, all NPs induced significantly ($p < 0.001$) increased H₂O₂ levels in nano-exposed *H. verticillata* compared to bulk-TiO₂ treated plants. This increase amounted to 33%, 37%, and 47% for rutile TiO₂, P25, and anatase TiO₂, respectively. After 168 h of exposure, P25 still caused a significantly elevated H₂O₂ level by 31% compared to the bulk-sized control ($p = 0.02$).

Non-enzymatic antioxidants: GSH status analysis

Analysis of the levels of GSH and GSSG revealed that nano-TiO₂ exposure induced a shift in the GSH status in *H. verticillata* in the concentration-dependent and in the time-dependent trial.

Nano-exposed macrophytes showed a tendency of a concentration-dependent shift in the GSH status (Figure 2, Paper II). Already a low-level exposure of 0.01 mg/L TiO₂-NPs caused significantly decreased levels of GSH ($p < 0.05$) by 30%, 37%, and 57% for rutile TiO₂, anatase TiO₂, and P25, respectively. In parallel the GSSG levels increased

significantly ($p < 0.01$) and surpassed by more than 2-fold (P25 and anatase TiO₂) and 3-fold (rutile TiO₂) the GSSG levels of the respective negative controls. Moreover, all further exposure settings revealed decreased GSH levels in such exposed plants, which turned out to be significantly different to non-treated plants ($p < 0.05$), with the exception of 1 mg/L rutile TiO₂. An exposure to 10 mg/L anatase TiO₂, 0.1 mg/L P25 and rutile TiO₂ induced the highest drop of GSH, amounting to 62%, 69%, and 48%, respectively. In accordance, GSSG levels surpassed more than 2-fold and 5-fold the respective control GSSG levels after exposure to 0.1 mg/L of P25 and rutile TiO₂. Bulk TiO₂ treatments did not reveal such clear tendencies of decreased GSH or increased GSSG levels. Whereas GSSG levels remained uninfluenced, solely an exposure to 0.1 mg/L TiO₂-based microparticles revealed a significantly decreased amount of GSH ($p < 0.05$) by 25%. However, this decrease was to a significantly lesser extent ($p < 0.001$) compared to the TiO₂-NP treatments at the same concentration level.

Results of the time-dependent trial revealed that all investigated TiO₂-NPs decreased the GSH/GSSG ratios for the investigated exposure times (Figure 3, Paper III). After 96 h of exposure, the highest drop of the ratio compared to non-exposed plants accounted for 69%, 76%, and 83% in plant exposed to 10 mg/L of P25, rutile TiO₂, and anatase TiO₂, respectively. This drop turned out to be significant ($p < 0.001$). After 168 h, a tendency of increased GSH/GSSG ratios can be suggested, however, still with lower ratios than in non-treated macrophytes. In accordance, results of the low-level exposure setting revealed decreased GSH/GSSG ratios after an exposure time of 96 h, but not significantly different to control plants. By comparing the GSH status in plants exposed to bulk TiO₂ and TiO₂-NPs, the GSH status seemed to be less affected in microparticle exposures as broadly higher ratio values were measured for durations up to 96 h in such exposed plants. However, bulk TiO₂ treated plants showed a drop in their GSH status. Compared to the control, the maximum decrease amounted to 55% and 42% after an exposure time of 96 h for the low- and high-level exposure scenario, respectively, but only significant ($p < 0.001$) for plants exposed to 10 mg/L bulk TiO₂. Regarding crystal phase related differences, especially the mixture-phased P25 and anatase TiO₂ appear outstanding, as a significant decrease ($p < 0.05$) in the GSH status was observed already after 24 h for both tested concentrations. In such exposed macrophytes the drop in the GSH status amounted to 72% and 43% or 67% and 65% compared to bulk TiO₂ exposed plants for the high- and low-level exposure to P25 and anatase TiO₂, respectively.

Antioxidative enzyme activity

Based on the results of the antioxidative enzyme activity analysis in the concentration-dependent and in the time-dependent trial, macrophytes exposed to TiO₂-NPs showed an altered activity status of the investigated enzymes GR and CAT.

Nano-exposed plants did not show a change in the activity pattern of POD for none of the investigated concentrations of the first trial. However, a concentration-dependent increase in the activities of GR and CAT became obvious for all TiO₂-NPs (Figure 3, Paper II). With respect to untreated macrophytes, an exposure to 10 mg/L of anatase TiO₂ and concentrations of rutile TiO₂ exceeding 0.01 mg/L exhibited a significant raise of the GR activity ($p < 0.05$). This raise amounted to a maximum of 1.5- and 1.9-times increased activity levels for 1 mg/L of rutile TiO₂ and 10 mg/L of anatase TiO₂, respectively. For plants exposed to 10 mg/L of P25 a progressing GR activity increase was measured. However, the by 29% increased activity for the highest tested concentration of 10 mg/L of P25 did not turn out to be statistically significant. In accordance, a by 25% increased activity was observed in plants treated with the highest concentration of 10 mg/L bulk TiO₂, but again not statistically proven. The comparison of bulk and nano-TiO₂ treated plants showed a clear tendency of higher enzyme activity levels for all TiO₂-NPs over the entire particle concentration range. In this regard, significant elevated GR activities were detected after an exposure to 1 mg/L P25, 0.1 mg/L and 1 mg/L rutile TiO₂, and 10 mg/L anatase TiO₂ (Figure 3 A, Paper II).

CAT activity analysis in TiO₂-NP exposed plants revealed higher enzyme activities compared to unexposed plants, whereas a treatment with bulk TiO₂ did not cause changes in the CAT activity pattern. A significantly increased enzyme activity compared to control plants ($p < 0.05$) was detected in *H. verticillata* exposed to 10 mg/L of P25 and anatase TiO₂. In accordance with the results for the GR activity pattern, significantly increased CAT activities ($p < 0.05$) were measured for rutile TiO₂ concentration exceeding a concentration of 0.01 mg/L. Altogether, CAT activity showed a maximum increase compared to control plants by a factor of 2.1, 2.3, and 2.5 after exposure to 10 mg/L of P25, anatase TiO₂, and rutile TiO₂. Comparable with the results of a shifted GR activity, a comparison of the enzyme activity pattern in nano- and microparticle treated plants revealed elevated CAT activities for all concentration levels of TiO₂-NPs. This increase turned out to be significant

($p < 0.05$) for the exposure setting with 10 mg/L P25, 0.1 mg/L and 10 mg/L rutile TiO₂ and all concentrations of anatase TiO₂ (Figure 3 B, Paper II).

Results of the time-dependent trial (Figure 4, Paper III) revealed a different impact on the antioxidative enzyme activity between the tested crystal structures of TiO₂-NPs for both studied enzymes. An almost similar response to an exposure of macrophytes treated with anatase TiO₂ and P25 became obvious, as such exposed plants exhibited an increased CAT activity ($p < 0.05$) for the high exposure scenario after 24 h. Compared to the respective control as well as the bulk sized counterpart, the change in CAT activity was significant ($p < 0.05$) and amounted to a 1.95- and 2.24-fold enzyme activity raise compared to unexposed plants and a 1.6- and 1.8-fold enzyme activity raise compared to bulk exposed plants for 10 mg/L of anatase TiO₂ and P25, respectively. After 48 h of exposure, CAT activity subsequently decreased, however, was still significantly higher for the P25 exposure setting ($p < 0.05$) compared to the control and bulk TiO₂. Further elongation of the exposure time revealed a drop in the CAT activity in plants treated with 10 mg/L of anatase TiO₂ and P25. After 168 h, such exposed plants showed a significantly decreased CAT activity ($p < 0.01$) compared to bulk TiO₂ exposed plants amounting to about 60% for both TiO₂-NPs. Moreover, anatase TiO₂ exposure provoked a significantly decreased CAT activity ($p < 0.05$) for the low-level exposure setting. No significant alteration in the CAT activity was observed until 96 h of exposure with rutile TiO₂. However, compared to control treated plants the raise of CAT activity by 77% was significant ($p < 0.01$). Again, a decreased enzyme activity became obvious after 168 h. With respect to the bulk sized control, both tested concentrations caused a significant drop in the CAT activity by 95% and 34% for a rutile TiO₂ treatment of 10 mg/L ($p < 0.01$) and 0.1 mg/L ($p < 0.05$). GR activity was affected by all investigated TiO₂-NPs. Immediately after 24 h, enzyme activities were significantly ($p < 0.05$) 1.3-, 1.4-, and 1.6-fold higher than in control treated plants after high-level exposure to rutile TiO₂, anatase TiO₂, and P25, respectively. Compared to bulk TiO₂, a significantly elevated enzyme activity ($p < 0.05$) was detected for plants exposed to 10 mg/L P25 (1.56 times) and anatase-TiO₂ (1.38 times) after 24 h. Moreover, also a low-level exposure with P25 caused an elevated GR activity after 24 h, however, only significant when compared to the bulk sized control ($p < 0.05$). Elongation of the exposure time revealed a subsequent drop of the GR activity for both tested P25 concentrations. In contrast, both tested concentrations of anatase and rutile TiO₂ induced an enhanced GR activity after 48 h, which turned out to be significant compared to bulk TiO₂ treated plants ($p < 0.05$). A

concentration dependence in the GR activity increase became obvious, as the enzyme activity surpassed by about 30% and 60% the levels of the GR activity for the bulk TiO₂ exposure setting for low- and high-level NP treatments, respectively. Thereafter, no clear influence on the GR activity became apparent for the pure phase NP treatments. For none of the tested bulk TiO₂ concentrations a significant influence on GR activity was observed when compared to the negative control.

The following tables summarize the investigated changes in the oxidative stress related parameters of *H. verticillata* after exposure to TiO₂-NPs and bulk TiO₂.

Table 9. Changes in the biochemical response in *H. verticillata* after exposure to TiO₂-NPs for 24 h (Paper II).

Particle	Concentration (mg/L)	Biochemical parameter				
		ROS formation H ₂ O ₂	Enzymatic defense		Non-enzymatic defense	
			CAT	GR	GSH	GSSG
P25	0.01	-	-	-	57% ↓ (*) ^c	114% ↑ (**) ^c
	0.1	-	-	-	69% ↓ (*) ^c	166% ↑ (***) ^c
	1	-	-	48% ↑ (**) ^b	36% ↓ (*) ^c	-
	10	30% ↑ (*) ^c	105% ↑ (*) ^c 73% ↑ (*) ^b	-	68% ↓ (*) ^c	104% ↑ (**) ^c
Rutile TiO ₂	0.01	-	-	-	30% ↓ (*) ^c	211% ↑ (*) ^c
	0.1	-	90% ↑ (*) ^c 120% ↑ (*) ^b	37% ↑ (*) ^c 74% ↑ (**) ^b	48% ↓ (**) ^c	420% ↑ (*) ^c
	1	-	114% ↑ (**) ^c	48% ↑ (**) ^c 93% ↑ (***) ^b	-	210% ↑ (*) ^c
	10	-	153% ↑ (*) ^c 125% ↑ (*) ^b	30% ↑ (*) ^c	39% ↓ (**) ^c	323% ↑ (*) ^c
Anatase TiO ₂	0.01	-	69% ↑ (**) ^b	-	37% ↓ (**) ^c	123% ↑ (*) ^c
	0.1	-	133% ↑ (**) ^b	-	38% ↓ (**) ^c	144% ↑ (*) ^c
	1	-	73% ↑ (*) ^b	-	38% ↓ (**) ^c	-
	10	-	126% ↑ (***) ^c 179% ↑ (*) ^b	91% ↑ (***) ^c 47% ↑ (*) ^b	62% ↓ (***) ^c	-
Bulk TiO ₂	0.01	-	-	-	-	-
	0.1	-	-	-	26% ↓ (*) ^c	-
	1	-	-	-	-	-
	10	-	-	-	-	-

Significant differences to the control (c) and bulk TiO₂ (b) treatment are indicated with * ($p < 0.05$), ** ($p < 0.01$), *** ($p < 0.001$)

Table 10. Changes in the biochemical response in *H. verticillata* during 168 h exposure to TiO₂-NPs (Paper III).

Biochemical parameter	Particle	24 h		48 h		96 h		168 h	
		0.1 mg/L	10 mg/L	0.1 mg/L	10 mg/L	0.1 mg/L	10 mg/L	0.1 mg/L	10 mg/L
ROS formation H ₂ O ₂	P25	34% ↑ (*) ^b	23% ↑ (*) ^b	-	-	-	20% ↑ (**) ^c 37% ↑ (****) ^b	-	31% ↑ (*) ^b
	Rutile TiO ₂	-	-	-	-	-	16% ↑ (*) ^c 33% ↑ (****) ^b	-	-
	Anatase TiO ₂	-	-	-	-	-	30% ↑ (****) ^c 48% ↑ (****) ^b	-	-
	Bulk TiO ₂	-	-	-	-	-	-	-	-
Enzymatic defense CAT	P25	-	124% ↑ (**) ^c 81% ↑ (*) ^b	-	54% ↑ (*) ^c 39% ↑ (*) ^b	-	-	-	32% ↓ (*) ^c 60% ↓ (**) ^b
	Rutile TiO ₂	-	-	-	-	-	77% ↑ (**) ^c	34% ↓ (*) ^b	95% ↓ (**) ^b
	Anatase TiO ₂	-	95% ↑ (**) ^c 58% ↑ (*) ^b	-	-	-	-	38% ↓ (**) ^b	61% ↓ (**) ^b
	Bulk TiO ₂	-	-	-	-	-	-	-	70% ↑ (*) ^c
GR	P25	47% ↑ (*) ^b	60% ↑ (*) ^c 56% ↑ (**) ^b	-	-	-	-	-	-
	Rutile TiO ₂	-	34% ↑ (*) ^c	51% ↑ (*) ^c 33% ↑ (*) ^b	58% ↑ (*) ^b	-	-	-	-
	Anatase TiO ₂	-	43% ↑ (*) ^c 39% ↑ (*) ^b	44% ↑ (**) ^c 27% ↑ (*) ^b	47% ↑ (**) ^c 63% ↑ (*) ^b	-	-	-	-
	Bulk TiO ₂	-	-	-	-	-	-	-	-
Non-enzymatic defense GSH/GSSG ratio	P25	52% ↓ (****) ^c 43% ↓ (*) ^b	64% ↓ (*) ^c 72% ↓ (****) ^b	63% ↓ (****) ^c 49% ↓ (**) ^b	57% ↓ (**) ^c 48% ↓ (*) ^b	-	69% ↓ (****) ^c 31% ↓ (**) ^b	-	-
	Rutile TiO ₂	-	-	66% ↓ (****) ^c 52% ↓ (****) ^b	45% ↓ (*) ^c	-	76% ↓ (****) ^c 47% ↓ (****) ^b	-	-
	Anatase TiO ₂	71% ↓ (****) ^c 65% ↓ (****) ^b	58% ↓ (*) ^c 67% ↓ (****) ^b	73% ↓ (****) ^c 63% ↓ (****) ^b	83% ↓ (****) ^c 82% ↓ (****) ^b	-	83% ↓ (****) ^c 62% ↓ (****) ^b	-	41% ↑ (*) ^b
	Bulk TiO ₂	-	-	-	-	-	55% ↓ (****) ^c	-	-

Significant differences to the control (c) and bulk TiO₂ (b) treatment are indicated with * ($p < 0.05$), ** ($p < 0.01$), *** ($p < 0.001$)

4 Discussion

4.1 Characteristics of the investigated TiO₂-nanoparticles and stability of TiO₂-nanoparticle suspensions

Nanoparticle characterization throughout the study was critical in order to correlate their specific properties to their toxicity potential. In this regard, multiple properties were of importance including size, surface charge (zeta potential), and degree of interaction (agglomeration/aggregation) of the NPs (Jiang et al., 2009). First, particle characterization should address the “as received-powder” form of the respective NPs (Powers et al., 2006). For this purpose, electron microscopy represents a powerful technique to capture images of NPs with the necessary resolution. Moreover, it provides reliable information regarding the particle shape, morphology, and size (Powers et al., 2006). In the present thesis, SEM analysis of the primary TiO₂-NPs in its dry form indicated aggregate formation of the investigated TiO₂-NPs. As SEM imaging required transfer of the sample from a dispersed hydrated state to a dried high vacuum state, a preparation method which is known to induce aggregate formation (Hassellöv et al., 2008; Michen et al., 2015), this could be a possible explanation for the formation of primary particle aggregates in the purchased NP samples. Also, the NP powder may have been composed of aggregates after its manufacture as already proposed by Jiang et al. (2009) for the TiO₂-NP P25. In order to evaluate the size, size distribution, state of dispersion, and the zeta potential of the TiO₂-NPs in the exposure medium, a DLS analysis was performed. Compared to electron microscopy imaging, DLS is a versatile technique that offers the possibility to accurately reflect the nature of NPs in the respective exposure suspension with only a minimum of sample perturbation. Therefore, DLS is the method of choice for studying nanoparticles in liquids (Pecora, 2000). In toxicological studies, it is the rule rather than the exception that NPs size distribution changes in the suspension; thus, particle size and shape may differ dramatically from its original form (Powers et al., 2006). In accordance, the formation of large scale TiO₂-NP secondary particles in the range of 400 to 500 nm was observed in the aqueous dispersion. As ultrasonication was applied before DLS analysis was performed, it can be concluded that these secondary particles comprised of aggregates. Ultrasonication is a commonly used technique to disperse agglomerates of NPs (Jiang et al., 2009). In accordance, ultrasonic bath treatment was able to disperse agglomerates present in the NP suspensions, as the

sonication time study revealed decreased average particle sizes for all TiO₂-NPs within a sonication time of 2 h. Nonetheless, the hard-bonded aggregates were not broken up by bath sonication even after an elongation of the sonication time. NP suspensions are often polydisperse (Percora, 2000) and referring to the investigated PDI, all investigated TiO₂-NP suspensions represented polydisperse systems as well. However, with a PDI of less than 0.7, DLS technique still was suitable for NP size characterization (Kim et al., 2014). In a polydisperse NP solution, with a distribution of particle sizes and the presence of large scale NP aggregates, the light scattering signal of small sized NPs can be masked when performing DLS analysis (Hassellöv et al., 2008). Therefore, the presence of TiO₂-NPs cannot be completely excluded in the respective NP dispersions of the study. Moreover, NP size characterization was performed at a fixed concentration of 100 mg/L, representing the NP stock concentration for all experiments. This approach might have been influential for the results of the NP characterization, as there is evidence that the particle concentration affects the rate and degree of secondary particle formation by enhancing the rate of direct particle-to-particle interaction with increasing NP concentration (Allouni et al., 2009). As all experiments were performed with lower NP concentrations after diluting the respective NP stock suspension, a decreased particle interaction, hence decreased secondary particle sizes can be suggested during the studies. Nonetheless, based on the present DLS results, aggregates of TiO₂-NPs were smaller in size compared to the investigated bulk TiO₂, thus, an assessment of size related effects was enabled.

The particle surface charge is a major factor in determining the particle dispersion stability (Powers et al., 2006). Thus, it was an important characteristic to assess NPs stability in the test medium. As a rough criterion, it is proposed that the zeta potential of NPs provides sufficient repulsive force against particle-to-particle interaction if its absolute value is greater than 30 mV (Bihari et al., 2008; Jiang et al., 2009). According to that, the attraction between the TiO₂-NPs exceeded their repulsion supporting the results of the particle size characterization. Analysis of the p*H*_{IEP} of the respective TiO₂-NPs revealed that a manipulation of the pH in the test medium would not have had a major positive impact on the dispersion stability. Consistent with previous studies (Kosmulski, 2002; Suttiponpannit, 2011), the results of the p*H*_{IEP} assessment suggested that this particle characteristic was rather insensitive to the crystalline structure of TiO₂-NPs as only marginal differences between the crystal phases became obvious. Altogether, results of the particle size and surface charge analysis indicated that TiO₂-NP suspensions suffered from instability.

As the present thesis included an investigation of the time-dependent oxidative stress response in *H. verticillata*, a sedimentation study was performed to provide information about methodical adaptations during the experiment aiming at a steadily exposure of the test organism. Measurements of the optical absorbance of the respective TiO₂-NP over the entire exposure time coupled with a particle size analysis *via* DLS revealed progressing sedimentation. Hence, the results were in agreement with the results of the particle characterization as they indicated suspensions instability. In accordance with a previous study by Ji et al. (2010), especially the TiO₂-NP P25 was characterized by large scale aggregates with progressing time leading to increased sedimentation compared to the other investigated TiO₂-NPs.

Overall, it can be suggested that the prevalent composition of the Hoagland's nutrient solution was unfavorable for obtaining a stable NP suspension. The colloidal stability of TiO₂-NPs is strongly influenced by the chemistry of the surrounding water. Thus, a combined effect of several medium characteristics, like pH, ionic strength, and the content of NOM (Keller et al., 2010; Ottoufelling et al., 2011), were decisive for TiO₂-NPs characteristics in the suspension. As already introduced, it is considered unlikely to find "bare" NPs in the environment and an adsorption of NOM onto NPs is likely, leading to electrosteric stabilization of NPs (Yang et al., 2009; Hotze et al., 2010). Therefore, it can be suggested that NOM addition to the test medium would have been linked to a decreased aggregate formation after NOM adsorption onto the TiO₂-NPs. However, the usage of NOM was not considered for this study. On the one hand, NOM concentration in surface waters varies; moreover, NOM is heterogeneous in its chemical composition, molecular weight, size, and structure (Gu et al., 1996; Sillanpää, 2014). Hence, the decision for a distinct NOM and concentration level would not have reflected a more realistic scenario leaving behind the complex nature of NOM. In general, it is a restriction of laboratory studies to reflect the complexity of natural waters. Previous study results confirm that TiO₂-NP aggregation and sedimentation depend on the aqueous media they are suspended in (Keller et al., 2010; Brunelli et al., 2013). Nevertheless, NPs will form aggregates after being released in the aquatic ecosystem (Handy et al., 2008) and sediment feeding organisms may accumulate high NP concentrations (Baun et al., 2008). However, organisms in the water column like aquatic macrophytes might suffer long-term exposure due to mixing processes in moving bodies of natural waters (rivers, streams) or a continuously or frequent NP loading. Thus, the regular medium renewal performed in the time-dependent study with

H. verticillata, aiming at the maintenance of TiO₂-NP exposure, can be considered as environmental relevant.

4.2 Cyanobacterial toxin adsorption onto TiO₂ nanoparticles

Mixture interactions of TiO₂-NPs with other aquatic contaminants are of special interest as they may influence the bioavailability, the bioconcentration of co-contaminants, and hence the toxicity of the individual compounds (Canesi et al., 2015). As MCs account to the most frequently found cyanotoxins in algal blooms globally, which were recognized as a potent stress factor and health hazard for aquatic organisms, the adsorption process of the environmental relevant representative MC-LR onto TiO₂-NPs was assessed. Results indicate the potential of TiO₂-NPs to adsorb MC-LR likely *via* a chemisorption process involving valence forces through sharing or the exchange of electrons between sorbent and sorbate (Ho and McKay, 1999). At the initial state of toxin adsorption, a high adsorption rate was assessed due to high availability of free adsorption sites. With progressing time, the adsorption rate decreased as an increasing number of adsorption sites was occupied by the toxin. Differences in the adsorption site availability between TiO₂-NPs and bulk TiO₂ may also be an explanation for the observed size-dependence of MC-LR adsorption when comparing toxin adsorption onto nano- and microparticles. As evident from the particle characterization, even at an aggregated status of the TiO₂-NPs, they exhibited smaller sizes of their secondary particles compared to the bulk sized counterpart. Hence, a larger surface of TiO₂-NPs for an interaction with MC-LR can be suggested. Both, the size-dependence of adsorption and the chemisorption of MC-LR onto NPs are in accordance with results by Gao et al. (2012) who investigated MC-LR adsorption onto iron oxide NPs. Moreover, analysis of the plot of the intraparticle diffusion model revealed multi-linearity which suggests two phases of toxin adsorption. Here, the slopes of the respective linear portions indicated the rate of adsorption (Cheung et al., 2007). The first sharp portion can be attributed to a rapid boundary layer diffusion of MC-LR, followed by a slower toxin diffusion from the surface site into the inner pores (Zhang et al., 2013; Gupta et al., 2014). Differences in the slopes of the TiO₂-NPs indicated differences in the rate of the respective adsorption phase. Moreover, the plots not passed through the origin. This confirmed a complex adsorption process, in which surface adsorption as well as intraparticle diffusion contribute to the adsorption process (Cheung et al., 2007; Fan et al., 2012). In respect to the results of the adsorption kinetic study, the crystallinity status of TiO₂-NPs

might have influenced MC-LR adsorption. The highest adsorption capacity was observed for P25, which mostly consists of an anatase crystal structure, followed by the pure phase anatase TiO₂ and rutile TiO₂. A differential adsorption behavior of the TiO₂ isomorphs was already observed in former studies, but the underlying reason has not yet been fully understood (Barbour et al., 2007; Suriyaraja et al., 2014). However, even if only marginal, differences in the pI_{EP} of the TiO₂ isomorphs might have influenced electrostatic attraction between the respective TiO₂-NP and MC-LR. Moreover, results of the particle size characterization revealed the formation of aggregates in the test medium. Thus, the aggregate morphology might have caused differences in the adsorptive capacity as they can occur as compact clusters or structures with high porosity, probably leading to a different adsorptive potential of the TiO₂-NP suspensions.

The surface charge of NPs is an important parameter for controlling the adsorption of biomolecules (Powers et al., 2006). As the initial and final pH of the solution did not significantly change throughout the study it can be concluded that changes in the toxin adsorption were not a result of pH driven changes in the particle surface charge or particle size. Further, the results of the zeta potential analysis revealed a negative surface charge for all TiO₂-NPs in the test medium, which might be in accordance with TiO₂-NP characteristics in natural waters (Keller et al., 2010; Ottofuelling et al., 2011). Moreover, cyanobacterial-driven pH increases (Ibelings and Maberly, 1998; Xu et al., 2010) will probably cause elevated absolute values of the zeta potential with a positive effect on TiO₂-NPs stability in water and thus toxin adsorption. In general, electrostatic attraction might have been outweighed by electrostatic repulsion between TiO₂-NPs and MC-LR due to their negative surface potential in the test medium. This would be in accordance to a previous study result by Gao et al. (2012), who postulated an electrostatic repulsion between negatively charged iron oxide NPs and MC-LR. Whereas an electrostatic interaction between the aquatic contaminants was apparently not the driving force behind the investigated adsorption processes, a chemical reaction mechanism is conceivable to be the major mechanism of cyanobacterial toxin adsorption. Such a chemical reaction mechanism between adsorbent and adsorbate is likely to be controlled by the surface hydroxyl groups of the TiO₂-NPs and the carboxylic functional groups of MC-LR (Lee and Walker, 2011; Gao et al., 2012; Thomas and Syres, 2012).

Despite the assumption that the addition of NOM to the test medium would have caused increased NP suspension stability and thereby increased MC-LR adsorption, current studies indicate that NOM competes for adsorption sites onto mineral surfaces depending on the concentration and the tested NOM subcomponent (Gu et al., 1996, Lee and Walker, 2011). Therefore, the potential of NOM to individually influence the results of NP adsorption studies is emphasized and underlines the difficulty of NOM investigation not taking into account its heterogeneity.

In accordance to Gao et al. (2012), the present results of the concentration-dependent adsorption study indicated that high NP concentrations inevitably could not cause increased contaminant adsorption. Hence, the exceptional behavior of NPs in aqueous solutions is emphasized. It is known that the rate of aggregation and the aggregate size increases with increasing particle concentration (Allouni et al., 2009; Brunelli et al., 2013). Thus, decreased aggregate sizes in low-level TiO₂-NP suspensions can be suggested which led to increased MC-LR adsorption compared to a higher concentration scenario. Next to the result that all TiO₂-NPs caused elevated toxin adsorption compared to the bulk-sized counterpart, this would further contribute to the conclusion that MC-LR adsorption onto TiO₂-NPs is a size-dependent process.

4.3 Oxidative stress response in *Hydrilla verticillata*

H₂O₂ formation

ROS represent unavoidable byproducts of normal cell metabolism either generated by electron transport processes or various metabolic pathways in different cellular components (Gill and Tuteja, 2010). Under non-stressed conditions an equilibrium between the ROS production and scavenging ensures low levels of ROS (Mittler, 2002; Gill and Tuteja, 2010). However, marked increases in the ROS production after exposure to xenobiotics or a decreased antioxidant capacity can overwhelm the antioxidant defense system and might cause oxidative stress (Livingstone, 2003; Ray et al., 2012). As a consequence of excess ROS or LPO products, several deleterious effects on proteins, lipids, and DNA can ultimately result in cell death (Sharma et al., 2012). H₂O₂, the most representative and potent ROS, is probably the most common assayed primary ROS to assess biochemical changes related to oxidative stress effects in organisms (Gill and Tuteja, 2010, Noctor et al., 2015).

In the present study, concentration- and time-dependent changes in the H₂O₂ levels of *H. verticillata* were analyzed after its exposure to TiO₂ nano- and microparticles (Paper II, III). Results imply a concentration-dependent effect on the H₂O₂ status as in particular high-level exposures of 10 mg/L TiO₂-NPs provoked increased ROS concentrations compared to unexposed macrophytes for both tested exposure systems. Thus, TiO₂-NPs' potential to overwhelm the antioxidative capacity of *H. verticillata* in a concentration-dependent manner became obvious. No clear time-dependent changes in the H₂O₂ level were assessed. However, an elongation of the nano-TiO₂ exposure up to 96 h revealed ROS levels which significantly exceeded those measured in the unexposed and bulk TiO₂ exposed plants. Moreover, the observed drop in the ROS level after 168 h of TiO₂-NP treatment might be attributed to the investigated adaptations in the antioxidative stress response of the macrophyte. Despite the current uncertainties of environmental relevant TiO₂-NP concentrations in surface waters, nano-TiO₂ exposures of 10 mg/L might be unlikely to occur at present. However, considering a further expanding production of TiO₂-NPs in the coming years (Robichaud et al., 2009), concentrations in the low mg/L range will probably represent a realistic future scenario. Nevertheless, H₂O₂ levels were uninfluenced after low-level exposures in the µg/L range. Therefore, severe oxidative damage of macrophytes due to an excess in ROS production may currently not be likely after TiO₂-NP exposure. Next to the concentration-dependence of H₂O₂ formation, a size-dependent effect can be suggested. Solely nano-TiO₂ treatments provoked a raise of the H₂O₂ concentration in the studies, whereas bulk-TiO₂ exposure did not reveal obvious changes in the ROS status compared to unexposed macrophytes for none of the performed trials. In respect to the absence of distinct adaptations in the antioxidative stress response, ROS homeostasis seemed to be unaffected in such exposed plants.

H₂O₂ is generated under normal as well as stressful conditions in plants *via* the electron transport chain of chloroplasts, mitochondria, endoplasmic reticulum, plasma membrane, an oxidation of fatty acids, and photorespiration (Sharma et al., 2012). Moreover, various enzymatic sources like NADPH-oxidases and cell wall peroxidases are known to play an important role in the H₂O₂ formation in plants (Neill et al., 2002).

Regarding the localization of the investigated H₂O₂ generation after TiO₂-NP exposure it can be assumed that a direct intracellular stimulation of the ROS formation was unlikely as the investigated TiO₂-NPs suspensions suffered instability and were characterized by the

formation of large sized aggregates. A plant's cell wall constitutes the primary site of interaction and a barrier for the TiO₂-NP entrance into the cell (Navarro et al., 2008). Concerning the limiting pore diameter of a plant cell wall, which is considered to be in the range of only a few nm (Raid and Bacic, 1996), such aggregates would have been unable to pass through the cell wall. However, the ROS increase in plant cells might have been a result of an external localized cell wall damage. Hence, TiO₂-NPs interaction with the cell wall might have led to the formation of large sized pores with the result of an internalization of TiO₂-NPs through the cell wall (Navarro et al., 2008). As H₂O₂ is relatively stable compared to other ROS and can readily cross biological membranes (Sharma et al., 2012), and thus a plant's plasma membrane, it might have contributed to oxidative stress related effects far away from its site of generation. This could be an explanation for the investigated internal H₂O₂ level adaptations after TiO₂-NP exposure. As soon as H₂O₂ enters the plant cell, it can bind to different cell organelles, influencing their metabolic processes (Navarro et al., 2008). Moreover, the conversion of the moderately active H₂O₂ to the highly reactive •OH, which depends on the activity of H₂O₂-degradating enzymes in plants under stress, has the potential to cause severe oxidative damage in macrophytes. In this respect, Song et al. (2012) have found increased contents of malondialdehyde, a decomposition product of polyunsaturated fatty acids of biomembranes, after anatase TiO₂ exposure of *Lemna minor*. Hence, a such related disruption of the cell membrane by TiO₂-NPs probably caused increased TiO₂-NPs influx in the plant cell probably affecting sensitive organelles like mitochondria and chloroplasts.

H₂O₂ has the potential to regulate the expression of various genes, including those encoding antioxidative stress related enzymes (Neill et al., 2002). Therefore, an up- and down-regulation of antioxidative stress enzymes linked to intracellular H₂O₂ levels is possible and might explain the investigated adaptations of the enzymatic antioxidative defense and the GSH status in *H. verticillata* after TiO₂-NP exposure.

Non-enzymatic antioxidants: GSH status analysis

The importance of GSH pool measurements as an oxidative stress marker is based on its role in the antioxidative defense system (Sharma et al., 2012). GSH accounts to the most important components in the antioxidative stress response as it participates in the AsA-GSH cycle and is reducing equivalent for GPx. Therefore, GSH significantly influences the capacity of H₂O₂ removal (Mittler, 2002). Moreover, it acts as a co-substrate for the

conjugation reaction with electrophilic xenobiotics during biotransformation catalyzed by GST (Gill and Tuteja, 2010). Interestingly, the GSH status seems to be a better marker for changes in the redox state driven by increased H_2O_2 contents in the plant cell compared to the AsA pool (Noctor et al., 2015).

The results of the present thesis imply that H_2O_2 degrading pathways, which depend on GSH, were enhanced during exposure to TiO_2 -NPs as a shift in the GSH/GSSG ratio became apparent. Results of the concentration- as well as the time-dependent study suggest an immediate high GSH-dependent metabolism to counteract excess ROS (Paper II, III). In accordance, a previous study observed elevated levels of total GSH in the gills and decreased total GSH levels in the liver of rainbow trout after a long-term exposure (14 d) with 1 mg/L and 0.5 mg/L P25, respectively (Federici et al., 2007). Even if not analyzed, the H_2O_2 breakdown *via* APx is likely as it is characterized by a higher affinity for H_2O_2 compared to CAT (Sharma et al., 2012). Hence, the ubiquitous AsA-GSH cycle might have contributed to ROS status stabilization. Inevitably, this would have caused enhanced oxidation of AsA and GSH, the latter proven by increased levels of GSSG in nano- TiO_2 exposed macrophytes. However, with progressing exposure time the appropriate function of the AsA-GSH cycle can be questioned due to the lack of GSSG reduction resulting in the observed drop in the GSH/GSSG ratio for exposure times up to 96 h. Without appropriate levels of GSH, the enzymatic regeneration of AsA from DHA as well as the H_2O_2 degradation *via* GPx might have been successively decreased. This could explain the rise in H_2O_2 levels after 96 h of nano- TiO_2 exposure. Nevertheless, after 168 h nano-exposed plants had GSH/GSSG ratios comparable to unexposed plants irrespective of the tested concentration; thus, a metabolic stabilization is likely and corresponds to decreased H_2O_2 levels.

Next to the previously mentioned potential of H_2O_2 to influence the gene expression of antioxidative stress related enzymes (Neill et al., 2002), the GSH status in plant cells is another sensitive modulator of the gene expression (Foyer et al., 1997). Therefore, an upregulation of the GSH synthesis due to an elevated expression of its catalyzing enzymes glutamylcysteine synthetase and glutathione synthetase can be suggested and would be conform with unaffected GR activities in TiO_2 -NP treated plants after 96 h. Moreover, the current state of research indicates that increased activity of the GSH synthesizing enzymes

and an enhanced cysteine synthesis leads to an accelerated GSH generation (Noctor and Foyer, 1998).

In accordance with the results of the H_2O_2 analysis, the shift in the GSH/GSSG ratio appeared to be size-dependent. Whereas an exposure with TiO_2 -NPs provoked a drop of the GSH/GSSG ratio immediately at the beginning of the experiments, antioxidant levels rather remained stable until 96 h of a bulk- TiO_2 treatment. Nevertheless, also a microparticle exposure led to adaptations in the GSH-dependent metabolism after long-term exposure accompanied by decreased GSH levels, however, in all experiments to a lesser extent than in NP exposed plants.

Overall, the present results clearly indicate the importance of GSH-dependent metabolic pathways in the plant to combat ROS increase due to TiO_2 -NP exposure. Further, the results suggest that the GSH status in plant cells is a sensitive indicator of oxidative stress related effects caused by TiO_2 -NPs, as already low-level TiO_2 -NP concentrations revealed a shift in the antioxidant concentration after a short exposure time.

Antioxidative enzyme activity

Enzymatic components of the antioxidative defense system in plants comprise of several enzymes, which are crucial for suppressing toxic ROS levels in cells. An imbalance of a scavenging enzyme, due to excess in ROS, will induce compensatory effects on other enzymes to maintain ROS homeostasis (Apel and Hirt, 2004). In the present thesis, the activity of the antioxidative enzymes POD, CAT, and GR were studied after macrophyte exposure to TiO_2 -NPs.

Results of the concentration-dependent trial imply that POD was not considerable activated after nano- TiO_2 exposure (Paper II). Therefore, POD might be less sensitive to increased levels of H_2O_2 after short-term TiO_2 -NP treatment compared to other H_2O_2 -degrading enzymes like CAT. This assumption is supported by study results of Song et al. (2012), who have observed significantly increased POD levels in *L. minor* after an extended exposure time to anatase TiO_2 -NPs for 168 h. Moreover, the authors investigated a concentration-dependent effect on the enzyme activity as the activity of POD and CAT increased in *L. minor* exposed to TiO_2 -NP concentrations higher than 100 mg/L. Hence, changes in the POD activity might be a result of ROS status changes solely occurring after high-level TiO_2 -NPs exposures, by far surpassing environmental relevant concentrations. In contrast to the

results by Song et al. (2012), the present study results revealed significantly increased CAT activities compared to the unexposed plants at a lower exposure level of 10 mg/L anatase TiO₂. As it is known that the characteristics of NPs affect their toxicity potential, this could be attributed to the smaller particle size investigated for the investigated NPs in the culture medium at a comparable concentration level (< 500 nm *versus* > 1500 nm). Based on the particle size differences in the studies, it can be proposed that the exposure of *L. minor* to large particles with a small surface-to-volume ratio may have contributed to less interaction of anatase TiO₂ with *L. minor* than in the present study with *H. verticillata*. Furthermore, Song et al. (2012) investigated a different plant species, which might have displayed individual strategies against oxidative stress related effects, differing from those of another species like *H. verticillata* (Romero-Oliva et al., 2015b).

The antioxidative enzyme CAT is characterized by a very fast turnover rate and does not depend on reducing equivalents for H₂O₂ breakdown. Thus, in the group of H₂O₂-degrading enzymes CATs are unique (Sharma et al., 2012). The present study results revealed an increased activity of CAT after TiO₂-NP exposure, which implies that CAT is a relevant enzymatic component of the antioxidative defense system of *H. verticillata* to prevent from a nano-driven ROS accumulation. In this regard, NPs' potential to induce a shift in the CAT activity seems to depend on the NP concentration, exposure time, and crystal phase (Paper II, III). Elevated CAT activities were noticed together with increased exposure concentrations of all TiO₂-NPs in both study trials. Moreover, results of the time-dependent trial suggest that the crystalline structure of the TiO₂-NPs influenced the enzymatic response (Paper III). Already after 24 h of exposure to 10 mg/L P25 (~ 80% anatase) and pure anatase TiO₂, increased CAT activities were measured. With prolonged exposure time, such exposed plants showed successively decreased CAT activities. In contrast, rutile TiO₂ exposure led to a delayed CAT activity increase after 96 h. However, irrespective of the different patterns of CAT activity changes, all high-level exposures showed significant decreased CAT activities after 168 h compared to bulk TiO₂ treated plants. Even if a decrease in the enzyme activity can be considered as a hint for high stress conditions in plants (Song et al., 2012), investigations of the pigment status, which were performed throughout the time-dependent exposure study, revealed no significant effects of ROS increase after TiO₂-NP exposure. Therefore, it can be suggested that the inhibition of CAT in *H. verticillata* did not cause severe effects on the physiological level, probably due to compensatory ROS scavenging by other antioxidative enzymes. This would also be in

accordance with the trend of ROS status normalization after 168 h of exposure to 10 mg/L TiO₂-NPs. Nevertheless, in respect to the results of the H₂O₂ level changes after TiO₂-NP treatment, the investigated CAT activity increase after 24 h of exposure to 10 mg/L anatase TiO₂ and P25 indicates the importance of CAT to maintain low H₂O₂ levels in plant cells. Next to the previously discussed putative absence of GPx and APx catalyzed H₂O₂ degradation, due to the lack of appropriate GSH levels with progressing exposure time, the decreased CAT activity might explain the H₂O₂ level increase after 96 h in such exposed macrophytes. In accordance, the increased H₂O₂ concentrations in rutile TiO₂ treated plants indicate that the promoted CAT activity was not sufficient to combat ROS increase.

As it is known that the limitation of one component of the oxidative stress response system results in the up-regulation of various antioxidant processes to compensate (Foyer et al., 1997), other H₂O₂-scavenging enzymes probably took over the role of CAT with the result of decreased H₂O₂ concentrations after 168 h. Although not considerably affected after 24 h of exposure to TiO₂-NPs (Paper II), POD can be considered as a compensatory enzyme after an elongation of the exposure time, which would be in accordance with the previously discussed study result by Song et al. (2012). In addition, H₂O₂ degrading pathways, dependent on GSH, might have been of importance at the beginning and the end of the exposure, when GSH status normalization was detected. Moreover, the putative activity increase of APx and GPx after low-level nano-TiO₂ exposure might explain the absence of significant H₂O₂ elevations after 96 h, as no significant effects on the GSH status and CAT activity were detected compared to the control plants.

The increased GR activity after a concentration- as well as time-dependent exposure of *H. verticillata* to TiO₂-NPs (Paper II, III) reflects the metabolic adaptation of such exposed plants suffering from elevated GSH oxidation which became obvious for low and high exposure settings. However, in both study trials the elevated GR activity was insufficient to maintain high ratios of GSH/GSSG over the entire exposure duration. As GR catalysis represents the rate limiting step of the AsA-GSH-pathway (Ahmad et al., 2008), it contributes to the conclusion that the appropriate function of this important scavenging system for ROS was unlikely to occur in the macrophyte with significantly dropped GSH/GSSG ratios. Moreover, due to the lack of GR activity adaptations for exposure times exceeding 96 h, the investigated normalization of the GSH status in plants exposed to 10 mg/L TiO₂-NPs for 168 h cannot be directly linked to adaptations in the GR activity.

Instead, the previously discussed putative up-regulation of GSH synthesis after induction of the expression of such related genes appears to be a more conceivable explanation.

In accordance to the other investigated oxidative stress related parameters, a particle size-dependent influence on the enzymatic antioxidative stress response in the plant cell became obvious. None of the exposure trials revealed a distinct trend of an affected enzyme activity pattern after bulk-TiO₂ exposure, whereas in particular high-level nano-TiO₂ exposed macrophytes showed significant differences in their CAT and GR activities compared to microparticle exposed plants.

5 Conclusions and Outlook

This thesis was carried out to estimate the impact of a TiO₂-NPs exposure in the aquatic environment. For this purpose, the potential role of TiO₂-NPs as contaminant carriers was assessed by studying the adsorption of the environmental contaminant MC-LR onto nano-TiO₂. Moreover, the thesis focused on the biochemical response of the model aquatic freshwater macrophyte *H. verticillata* after nano-exposure to evaluate TiO₂-NPs potential to induce oxidative stress related effects as a possible mode of nano-toxicity.

The following points represent the main findings of the present thesis in summarized form:

- The cyanobacterial toxin MC-LR can be adsorbed by TiO₂-NPs of varying crystalline status based on chemisorption processes. Therefore, TiO₂-NPs can act as ‘Trojan horse’ like carriers for MC-LR in freshwater systems probably influencing its fate and toxicity in aquatic ecosystems.
- MC-LR adsorption onto TiO₂-NPs depends on the particle size, probably due to the increased presence of active adsorption sites of nanostructured particles compared to larger sized microparticles.
- MC-LR adsorption is influenced by the crystalline status of TiO₂-NPs with anatase TiO₂ based NPs exhibiting a higher adsorption capacity compared to rutile TiO₂ based NPs. This might be a result of crystal phase specific surface properties (pH_{IEP}) or general differences in the respective NP characteristic in the suspension (aggregate size and aggregate morphology).
- Low concentrations of TiO₂-NPs exhibit a higher potential for MC-LR adsorption. As the level of NPs in a suspension affects the rate of aggregation, this underlines the influence of colloidal stability on the adsorption efficiency.
- The induction of oxidative stress is a likely mechanism of TiO₂-NP toxicity towards aquatic macrophytes.

- TiO₂-NPs stimulate activity changes of antioxidative enzymes GR and CAT. Further, an imbalance in the GSH homeostasis in *H. verticillata* is provoked, indicating increased activity of GSH-dependent enzymes to counteract elevated ROS generation after nano-TiO₂ exposure.
- ROS status normalization after TiO₂-NP exposure is ensured by a compensatory ROS scavenging of the various antioxidative enzymes in macrophytes.
- The sensitive response of the GSH and GSSG levels in *H. verticillata* suggests that the GSH status is a suitable indicator for oxidative stress related metabolic adaptations in nano-TiO₂ exposed macrophytes, due to the importance of the GSH-dependent metabolism for cellular protection against increased ROS after TiO₂-NP exposure.
- The major polymorphs of TiO₂, anatase and rutile, induce different patterns of the antioxidative stress response, however, oxidative stress related effects in macrophytes after exposure to TiO₂-NPs seem not to be related to a distinct crystalline phase.
- Taking into account the predicted freshwater concentrations of TiO₂-NPs, nano-TiO₂ exposure may currently not cause severe oxidative damage to macrophytes.
- As adaptations in the antioxidative stress response in *H. verticillata* could be related to the nano-scaled character of the TiO₂-NPs, the toxicity potential of NPs should not be equated with their respective bulk-sized counterpart, even after aggregate formation and thus particle size increase.

The present thesis underlined that TiO₂-NPs interact with cyanotoxins *via* adsorption processes. Next to the proven dependence of MC-LR adsorption on the TiO₂ particle size, other aqueous suspension characteristics like varying pH values, especially in an alkaline range, varying ionic strengths, as well as NOM compositions and concentrations should be considered in future studies in order to take the complexity of aquatic ecosystems into account. This would contribute to a more realistic assessment of TiO₂-NPs potential for MC-LR adsorption in natural waters. Moreover, future study approaches should focus on NPs mixture toxicity, evaluating MC-LR toxicity after an interaction with TiO₂-NPs.

In this regard, TiO₂-NPs might lead to decreased toxin bioavailability due to sedimentation of toxin-loaded TiO₂-NPs after aggregate formation, or just as well may cause increased toxicity to plants due to their carrier function for MC-LR. Regarding the oxidative stress related effects in macrophytes after TiO₂-NP exposure, further insights into the localization of ROS generation in such exposed aquatic plants are required. Hereby, an assessment of the formation of LPO products in the plant cell after nano-TiO₂ treatment would probably clarify if TiO₂-NP influx in the plant cell after membrane damage is likely to occur, subsequently contributing to internal ROS generation due to effects on plant cell organelles.

6 References

- Aebi M., 1974. Catalase. *In* Bergmeyer H.U. (eds). *Methods of Enzymatic Analysis*, 2nd edition, Vol. 2. Academic Press, New York, 673-684.
- Ahmad, P., John, R., Sarwat, M., Umar, S., 2008. Responses of proline, lipid peroxidation and antioxidative enzymes in two varieties of *Pisum sativum* L. under salt stress. *Int. J. Plant Prod.* 2, 353-365.
- Aitken, R.J., Chaudhry, M.Q., Boxall, A.B.A., Hull, M., 2006. Manufacture and use of nanomaterials: current status in the UK and global trends. *Occup. Med. Oxford* 56, 300-306.
- Alscher, R.G., 1989. Biosynthesis and antioxidant function of glutathione in plants. *Physiol. Plant.* 77, 457-64.
- Allouni, Z.E., Cipman, M.R., Hol, P.J., Skodvin, T., Gjerdet, N.R., 2009. Agglomeration and sedimentation of TiO₂ nanoparticles in cell culture medium. *Colloids Surf. B* 68, 83-87.
- Apel, K., Hirt, H., 2004. Reactive oxygen species: metabolism, oxidative stress, and signal transduction. *Annu. Rev. Plant. Biol.* 55, 373-399.
- Aravind, P., Prasad, M.N., 2005. Cadmium-induced toxicity reversal by zinc in *Ceratophyllum demersum* L. (a free floating aquatic macrophyte) together with exogenous supplements of amino- and organic acids. *Chemosphere* 61, 1720-1733.
- Bailey, H.C., Lui, D.H.W., 1980. *Lumbriculus variegatus*, a benthic oligochaete, as a bioassay organism. *In* Eaton, J.C., Parrisch, P.R., Hendricks, A.C. (eds). *Aquatic Toxicology*. ASTM, 205-215.
- Balasubramanian, G., Dionysiou, D. D., Suidan, M. T., Baudin, I., Laine, J.-M., 2004. Evaluating the activities of immobilized TiO₂ powder films for the photocatalytic degradation of organic contaminants in water. *Appl. Catal. B* 47, 73-84.
- Barbour, M.E., O'Sullivan, D.J., Jagger, D.C., 2007. Chlorhexidine adsorption to anatase and rutile titanium dioxide. *Colloid. Surface. A* 307, 116-120.
- Bartram, J., Carmichael, W.W., Chorus, I., Jones, G., Skulberg, O.M., 1999. Introduction. *In* Chorus, I., Bartram, J. (eds). *Toxic cyanobacteria in water: a guide to their public health consequences, monitoring and management*. WHO & E&FN Spon, London, 1-14.

- Baun, A., Hartmann, N. B., Grieger, K., Kusk, K. O., 2008. Ecotoxicity of engineered nanoparticles to aquatic invertebrates: a brief review and recommendations for future toxicity testing. *Ecotoxicology* 17, 387-395.
- Baun, A., Sørensen, S.N., Rasmussen, R.F., Hartmann, N.B., Koch, C.B., 2008. Toxicity and bioaccumulation of xenobiotic organic compounds in the presence of aqueous suspensions of aggregates of nano-C60. *Aquat. Toxicol.* 86, 379-397.
- Bayne, B.L., Brown, D.A., Burns, K., Dixon, D.R., Ivanovici, A., Livingstone, D.A., Lowe, D.M., 1985. The effects of stress and pollution on marine animals. Praeger, New York, USA.
- Bihari, P., Vippola, M., Schultes, S., Praetner, M., Khandoga, A.G., Reichel, C.A., Coester, C., Tuomi, T., Rehberg, M., Krombach, F., 2008. Optimized dispersion of nanoparticles for biological in vitro and in vivo studies. Part. *Fibre Toxicol.* 5, 1-14.
- Blankenship, R.E., Sadekar, S., Raymond, J., 2007. The evolutionary transition from anoxygenic to oxygenic photosynthesis. In Falkowski, P., Knoll A.H. (eds). *Evolution of Aquatic Photoautotrophs*. Academic Press, New York, 21-35.
- Botta, C., Labille, J., Auffan, M., Borschneck, D., Miche, H., Cabie, M., Masion, A., Rose, J., Bottero, J. Y., 2011. TiO₂-based nanoparticles released in water from commercialized sunscreens in a life-cycle perspective: Structures and quantities. *Environ. Pollut.* 159(6), 1543-1548.
- Bradford, M.M. 1976. A rapid and sensitive method for the quantitation of microgram quantities of protein utilizing the principle of protein-dye binding. *Anal. Biochem.* 72, 248-254.
- Brunelli, A., Pojana, G., Callegaro, S., Marcomini, A., 2013. Agglomeration and sedimentation of titanium dioxide nanoparticles (n-TiO₂) in synthetic and real waters. *J. Nanopart. Res.* 15, 1684.
- Buzea, C., Pacheco Blandino, I.I., Robbie, K., 2007. Nanomaterials and nanoparticles: Sources and toxicity. *Biointerphases* 2(4), 1-103.
- Canesi, L., Ciacci, C., Balbi, T., 2015. Interactive effects of nanoparticles with other contaminants in aquatic organisms: friend or foe? *Mar. Environ. Res.* 111, 128-134.
- Carlberg I, Mannervik B. 1985. Glutathione reductase. *Methods Enzymol.* 113, 484-490.
- Carmichael, W.W., 1992. A status report on planktonic cyanobacteria (blue-green algae) and their toxins. Report EPA/600/SR-92/079, Washington D.C, 1-4.
- Carp, O., Huisman, C.L., Reller, A., 2004. Photoinduced reactivity of titanium dioxide. *Prog. Solid State Ch.* 32, 33-177.

- Carpenter, S.R., Lodge, D.M., 1986. Effects of submersed macrophytes on ecosystem processes. *Aquat. Bot.* 26(3-4), 341-370.
- Chen, L., Chen, J., Zhang, X., Xie, P., 2016. A review of reproductive toxicity of microcystins. *J. Hazard. Mater.* 30, 381-399.
- Cheung, W.H., Szeto, Y.S., McKay, G., 2007. Intraparticle diffusion processes during acid dye adsorption onto chitosan. *Bioresour. Technol.* 98, 2897–2904.
- Chorus I., 2001. Introduction: Cyanotoxins – research for environmental safety and human health. *In* Chorus, I. (eds). *Cyanotoxins – Occurrence, Causes, Consequences*. Berlin: Springer-Verlag, 1-4.
- Codd, G., Bell, S., Kaya, K., Ward, C., Beattie, K., Metcalf, J., 1999. Cyanobacterial toxins, exposure routes and human health, *Eur. J. Philos.* 34(4), 405-415.
- Cole, J., 1982. Interactions between bacteria and algae in aquatic ecosystems, *Ann. Rev. Ecol. Syst.* 13(1), 291-314.
- Cook, C.D.K., Luond, R., 1982. A revision of the genus *Hydrilla* (Hydrocharitaceae). *Aquat. Bot.* 13, 485-504.
- Cromer, D.T., Herrington, K., 1954. The structures of anatase and rutile. *J. Am. Chem. Soc.* 77, 4708-4709.
- Dawson, R.M., 1998. Toxicology of microcystins. *Toxicon* 7, 953-962.
- de Figueiredo, D.R., Azeiteiro, U.M., Esteves, S.M. Gonçalves, F.J.M., Pereira, M.J., 2004. Microcystin-producing blooms – A serious global public health issue. *Ecotoxicol. Environ. Saf.* 59, 151-163.
- D'Autreaux, B., Toledano, M.B., 2007. ROS as signalling molecules: mechanisms that generate specificity in ROS homeostasis. *Nat. Rev. Mol. Cell Biol.* 8, 813-824.
- DeMott, W.R., Zhang, Q.X., Charnichael, W.W., 1991. Effects of toxic cyanobacteria and purified toxins on the survival and feeding of a copepod and three species of *Daphnia*. *Limnol. Oceanogr.* 36, 1346-1357.
- Drewes, C.D., Fournier, C.R., 1990. Morphallaxis in an aquatic oligochaete *Lumbriculus variegatus*: Reorganization of escape reflexes in regenerating body fragments. *Dev. Biol.* 13, 894-103.
- Drotar, A., Phelps, P., Fall, R., 1985. Evidence for glutathione peroxidase activities in cultured plant cells. *Plant Sci.* 42, 35-40.
- Duster, T.A., Fein, J.B., 2014. Comparison of the Aggregation behavior of TiO₂ nanoparticles exposed to fulvic acid and *Bacillus subtilis* exudates. *Water Air Soil Pollut.* 225, 2189.

- Engates, K.E., Shipley, H.J., 2011. Adsorption of Pb, Cd, Cu, Zn, and Ni to titanium dioxide nanoparticles: effect of particle size, solid concentration, and exhaustion. *Environ. Sci. Pollut. Res.* 18, 386-395.
- EPA, 2007. Nanotechnology White Paper. U.S. Environmental Protection Agency Report EPA 100/B-07/001, Washington DC, USA.
- Fan, L.L., Luo, C.N., Li, X.J., Lu, F.G., Qiu, H. M., Sun, M., 2012. Fabrication of novel magnetic chitosan grafted with graphene oxide to enhance adsorption properties for methyl blue, *J. Hazard. Mater.* 215, 272-279.
- Fastner, J., Neumann, U., Wirsing, B., Weckesser, J., Wiedner, C., Nixdorf, B., Chorus, I., 1999. Microcystins (hepatotoxic heptapeptides) in German fresh water bodies. *Environ. Toxicol.* 14, 13-22.
- Federici, G., Shaw, B.J., Handy, R.D., 2007. Toxicity of titanium dioxide nanoparticles to rainbow trout (*Oncorhynchus mykiss*): Gill injury, oxidative stress, and other physiological effects. *Aquat. Toxicol.* 84, 415-430.
- Foyer, C.H., Lopez-Delgado, H., Dat, J.F., Scott, I.M., 1997. Hydrogen peroxide- and glutathione-associated mechanisms of acclimatory stress tolerance and signalling. *Physiol. Plantarum* 100, 241-254.
- French, R.A., Jacobson, A.R., Kim, B., Isley, S.L., Penn, R.L., Baveye, P.C., 2009. Influence of ionic strength, pH, and cation valence on aggregation kinetics of titanium dioxide nanoparticles. *Environ. Sci. Technol.* 43(5), 1354-1359.
- Gao, Y. Q., Gao, N. Y., Deng, Y., Gu, J. S., Shen, Y. C. Wang, S.X., 2012. Adsorption of microcystin-LR from water with iron oxide nanoparticles. *Water Environ. Res.* 84, 562-568.
- Gerardi, M.H., Lytle, B., 2015. Blue-Green Algae (Cyanobacteria). In Gerardi, M.H. (eds). *The biology and troubleshooting of facultative lagoons*, John Wiley & Sons, Inc, Hoboken, New Jersey, 97-104.
- Gill, S.S., Tuteja, N., 2010. Reactive oxygen species and antioxidant machinery in abiotic stress tolerance in crop plants. *Plant Physiol. Biochem.* 48, 909-930.
- Giustarini, D., Dalle-Donne, I., Colombo, R., Milzani, A., Rossi, R., 2003. An improved HPLC measurement for GSH and GSSG in human blood. *Free Radical Bio. Med.* 35, 1365-1372.
- Gondikas, A.P., von der Kammer, F., Reed, R.B., Wagner, S., Ranville, J.F., Hofmann, T., 2014. Release of TiO₂ nanoparticles from sunscreens into surface waters: A one-year survey at the Old Danube Recreational Lake. *Environ. Sci. Technol.* 48, 5415-5422.

- Gottschalk, F., Sun, T. Y., Nowack, B., 2013. Environmental concentrations of engineered nanomaterials: Review of modeling and analytical studies. *Environ. Pollut.* 181, 287-300.
- Gu, B., Mehlhorn, T.L., Liang, L., McCarthy, J.F., 1996. Competitive adsorption, displacement, and transport of organic matter on iron oxide, II. Displacement and transport. *Geochim. Cosmochim. Acta* 60, 2977-2992.
- Gupta, S.M., Tripathi, M., 2010. A review of TiO₂ nanoparticles. *Phys. Chem.* 56(16), 1639-1657.
- Gupta, V.K., Pathania, D., Kothiyal, N.C., Sharma, G., 2014. Polyaniline zirconium (IV) silicophosphate nanocomposite for remediation of methylene blue dye from waste water, *J. Mol. Liq.* 190, 139-145.
- Guzman, K.A.D., Finnegan, M.P., Banfield, J.F., 2006. Influence of surface potential on aggregation and transport of titania nanoparticles. *Environ. Sci. Technol.* 40, 7688-7693.
- Habig, W. H., Pabst, M. J., Jakoby, W. B., 1974. Glutathione S-transferases: The first enzymatic step in mercapturic acid formation. *J. Biol. Chem.* 249, 7130-7139.
- Hadjiivanov, K.L., Klissurski, D.G., 1996. Surface chemistry of titania (anatase) and titania-supported catalysts. *Chem. Soc. Rev.* 25, 61-69.
- Handy, R.D., Owen, R., Valsami-Jones, E., 2008. The ecotoxicology of nanoparticles and nanomaterials: current status, knowledge gaps, challenges, and future needs. *Ecotoxicology* 17, 315-325.
- Hansson, L., Gustafsson, S., Rengefors, K., Bomark, L., 2007. Cyanobacterial chemical warfare affects zooplankton community composition. *Freshw. Biol.* 52, 1290-1301.
- Hartmann, N.B., Baun, A., 2010. The nano cocktail: Ecotoxicological effects of engineered nanoparticles in chemical mixtures, *Integr. Environ. Assess. Manage.* 6, 311-313.
- Hartmann, N.B., Legros, S., von der Kammer, F., Hofmann, T., Baun, A., 2012. The potential of TiO₂ nanoparticles as carriers for cadmium uptake in *Lumbriculus variegatus* and *Daphnia magna*. *Aquat. Toxicol.* 118-119, 1-8.
- Hartmann, N.B., von der Kammer, F., Hofmann, T., Baalousha, M., Ottofuelling, S., Baun, A., 2010. Algal testing of titanium dioxide nanoparticles—testing considerations, inhibitory effects and modification of cadmium bioavailability. *Toxicology* 269, 190-197.

- Hassellöv, M., Readman, J.W., Ranville, R.F., Tiede, K., 2008. Nanoparticle analysis and characterization methodologies in environmental risk assessment of engineered nanoparticles. *Ecotoxicology* 17(5), 344-361.
- Ho, Y. S., 2004. Citation review of Lagergren kinetic rate equation on adsorption reactions, *Scientometrics* 59, 171-177.
- Ho, Y. S. and McKay, G., 1999. Pseudo-second order model for sorption processes, *Process Biochem.* 34, 451-465.
- Holland, A., Kinnear, S., 2013. Interpreting the possible ecological role(s) of cyanotoxins: compounds for competitive advantage and/or physiological aide? *Mar. Drugs* 11(7), 2239-2258.
- Hotze, E. M., Phenrat, T., Lowry, G. V., 2010. Nanoparticle aggregation: challenges to understanding transport and reactivity in the environment. *J. Environ. Qual.* 39(6), 1909-1924.
- Ibelings, B.W., Maberly, S.C., 1998. Photoinhibition and the availability of inorganic carbon restrict photosynthesis by surface blooms of cyanobacteria, *Limnol. Oceanogr.* 43, 408-419.
- Ibelings, B.W., Bruning, K., de Jonge, J., Wolfstein, K., Pires, L.M.D., Postma, J., Burger, T., 2005. Distribution of microcystins in a lake foodweb: No evidence for biomagnifications. *Microb. Ecol.* 49, 487-500.
- Jana, S., Choudhuri, M.A., 1982. Glycolate metabolism of 3 submersed aquatic angiosperms during aging. *Aquat. Bot.* 12, 345-354.
- Ji, Z., Jin, X., George, S., Xia, T., Meng, H., Wang, X., Suarez, E., Zhang, H., Hoek, E.M., Godwin, H., Nel, A.E., Zink, J.I., 2010. Dispersion and stability optimization of TiO₂ nanoparticles in cell culture media. *Environ. Sci. Technol.* 44, 7309-7314.
- Jiang, J., Oberdörster G., Biswas, P., 2009. Characterization of size, surface charge, and agglomeration state of nanoparticle dispersions for toxicological studies, *J. Nanopart. Res.* 11, 77-89.
- Kaegi, R., Ulrich, A., Sinnet, B., Vonbank, R., Wichser, A., Zuleeg, S., Simmler, H., Brunner, S., Vonmont, H., Burkhardt, M., Boller, M., 2008. Synthetic TiO₂ nanoparticle emission from exterior facades into the aquatic environment. *Environ. Pollut.* 156(2), 233-239.
- Keller, A. A., Wang, H., Zhou, D., Lenihan, H. S., Cherr, G., Cardinale, B. J., Miller, R., & Ji, Z., 2010. Stability and aggregation of metal oxide nanoparticles in natural aqueous matrices. *Environ. Sci. Technol.* 44(6), 1962-1967.

- Kim, N.A., An, I.B., Lim, D.G. Lim, J.Y., Lee, S.Y., Shim, W.S., Kang, N.-G., Jeong, S.H., 2014. Effects of pH and buffer concentration on the thermal stability of etanercept using DSC and DLS. *Biol. Pharm. Bull.* 37, 808-816.
- Knauer, K., Sobek, A., Bucheli, T.D., 2007. Reduced toxicity of diuron to the freshwater green alga *Pseudokirchneriella subcapitata* in the presence of black carbon. *Aquat. Toxicol.* 83,143-148.
- Kosmulski, M., 2002. The significance of the difference in the point of zero charge between rutile and anatase. *Adv. Colloid Interface Sci.* 99, 255-264.
- Landmann, M., Rauls, E., Schmidt, W.G., 2012. The electronic structure and optical response of rutile, anatase and brookite TiO₂. *J. Phys.: Condens. Matter* 24, 1-6.
- Langeland, K. A., 1996. *Hydrilla verticillata* (L.F.) Royle (Hydrocharitaceae), "The perfect aquatic weed". *Castanea* 61, 293-304.
- Lee, J., Walker, H. W., 2011. Adsorption of microcystin-LR onto iron oxide nanoparticles. *Colloid. Surface. A* 373, 94-100.
- Livingstone, D.R., 2003. Oxidative stress in aquatic organisms in relation to pollution and aquaculture. *Rev. Med. Vet.* 154, 427-430.
- Loosli, F., Le Coustumer, P., Stoll, S., 2013. TiO₂ nanoparticles aggregation and disaggregation in presence of alginate and suwannee river humic acids. pH and concentration effects on nanoparticle stability. *Water Res.* 47, 6052-6063.
- MacKintosh, C., Beattie, K.A., Klumpp, S., Cohen, P., Codd, G.A., 1990. Cyanobacterial microcystin-LR is a potent and specific inhibitor of protein phosphatases 1 and 2A from both mammals and higher plants. *FEBS Lett.* 264, 187-192.
- Madsen, J.D., Chambers, P.A., James, W.F., Koch, E.W., Westlake, D.F., 2001. The interaction between water movement, sediment dynamics and submersed macrophytes. *Hydrobiologia* 444, 71-84.
- Michen, B., Geers, G., Vanhecke, D., Endes, C., Rothen-Rutishauser, B., Balog, S., Petri-Fink, A., 2015. Avoiding drying-artifacts in transmission electron microscopy: Characterizing the size and colloidal state of nanoparticles. *Sci. Rep.* 5, 9793.
- Mittler R., 2002. Oxidative stress, antioxidants and stress tolerance. *Trends Plant Sci.* 7, 405-410.
- Mo, S., Ching, W.Y., 1995. Electronic Structure and Optical Properties of the Three Phases of TiO₂: Rutile, anatase, and brookite. *Phys. Rev. B* 51(19), 13023-13032.

- Navarro, E., Baun, A., Behra, R., Hartmann, N.B., Filser, J., Miao, A.J., Quigg, A., Santschi, P.H., Sigg, L., 2008. Environmental behavior and ecotoxicity of engineered nanoparticles to algae, plants, and fungi. *Ecotoxicology* 17, 372-386.
- Neal, C., Jarvie, H., Rowland, P., Lawler, A., Sleep, D., Scholefield, P., 2011. Titanium in UK rural, agricultural and urban/industrial rivers: Geogenic and anthropogenic colloidal/sub-colloidal sources and the significance of within-river retention. *Sci. Total Environ.* 409(10), 1843-53.
- Neill, S., Desikan, R., Hancock, J., 2002. Hydrogen peroxide signalling. *Curr. Opin. Plant Biol.* 5, 388-395.
- Nishiwaki-Matsushima R., Ohta T., Nishiwaki S., Suganuma M., Kohyama K., Ishikawa T., Carmichael W.W., Fujiki H., 1992. Liver tumor promotion by the cyanobacterial cyclic peptid toxin microcystin-LR. *J. Canc. Res. Clin. Oncol.* 118, 420-424.
- Nizan, S., Dimentman, C., Shilo, M., 1986. Acute toxic effects of the cyanobacterium on *Daphnia magna*. *Limnol. Oceanogr.*, 31(3), 497-502.
- O'Neil, J.M., Davis, T.M., Burford, M.A., Gobler C.J., 2012. The rise of harmful cyanobacteria blooms: The potential roles of eutrophication and climate change. *Harmful Algae* 14, 313-334.
- Noctor, G., Foyer, C.H., 1998. Ascorbate and glutathione: Keeping active oxygen under control. *Annu. Rev. Plant Phys.* 49, 249-279.
- Noctor, G., Lelarge-Trouverie, C., Mhamdi, A., 2015. The metabolomics of oxidative stress. *Phytochemistry* 112, 33-53.
- Nowack, B., Bucheli, T., 2007. Occurrence, behavior and effects of nanoparticles in the environment. *Environ. Pollut.* 150, 5-22.
- Ottofuelling, S., von der Kammer, F., Hofmann, T., 2011. Commercial titanium dioxide nanoparticles in both natural and synthetic water: Comprehensive multidimensional testing and prediction of aggregation behavior. *Environ. Sci. Technol.* 45, 10045-10052.
- Pecora, R., 2000. Dynamic light scattering measurement of nanometer particles in liquids. *J. Nanopart. Res.* 2, 123-131.
- Peijnenburg, W.J.G.M., Baalousha, M., Chen, j., Chaudry, Q., von der Kammer, F., Kuhlbusch, T.A.J., Lead, J., Nickel, C., Quik, J.T.K., Renker, M., Wang, Z., Koelmans, A.A., 2015. A review of the properties and processes determining the fate of engineered nanomaterials in the aquatic environment. *Crit. Rev. Environ. Sci. Technol.* 45(19), 2084-2134.

- Phipps, G.L., Ankley, G.T., Benoit, D.A., Mattson, V.R., 1993. Use of the aquatic oligochaete *Lumbriculus variegatus* for assessing the toxicity and bioaccumulation of sediment-associated contaminants. *Environ. Toxicol. Chem.* 12, 269-279.
- Pflugmacher, S., Wiegand, C., Beattie, K.A., Codd, G.A., Steinberg, C.E.W., 1999a. Uptake of the cyanobacterial hepatotoxin microcystin-LR by aquatic macrophytes. *J. Appl. Bot.* 72, 228-232.
- Pflugmacher, S., Codd, G.A., Steinberg, C.E.W., 1999b. Effects of cyanobacterial toxin microcystin-LR on detoxification enzymes in aquatic plants. *Environ. Toxicol.* 14, 111-115.
- Pflugmacher, S., Wiegand, C., Beattie, K.A., Krause, E., Steinberg, C.E.W., Codd, G.A., 2001. Uptake, effects and metabolism of cyanobacterial toxins in the emergent reed plant *Phragmites australis* (Cav.) Trin. Ex. Steud. *Environ. Toxicol. Chem.* 20, 846-852.
- Pflugmacher, S., 2002. Possible allelopathic effects of cyanotoxins, with reference to microcystin-LR, in aquatic Ecosystems. *Environ. Toxicol.* 17, 407-413.
- Pflugmacher, S., 2004. Promotion of oxidative stress in the aquatic macrophyte *Ceratophyllum demersum* during biotransformation of the cyanobacterial toxin microcystin-LR. *Aquat. Toxicol.* 70(3), 169-178.
- Pflugmacher, S., Jung, K., Lundvall, L., Neumann, S., Peuthert, A., 2006. Effects of cyanobacterial toxins and cyanobacterial cell-free crude extract on germination of alfalfa (*Medicago sativa*) and induction of oxidative stress. *Environ. Toxicol. Chem.* 25(9), 2381-2387.
- Powers, K., Brown, S., Krishna, V., Wasdo, S., Moudgil, B., Roberts, S., 2006. Research strategies for safety evaluation of nanomaterials. Part VI. Characterization of nanoscale particles for toxicological evaluation. *Toxicol. Sci.* 90, 296-303.
- Praetorius, A., Scheringer, M., Hungerbühler, K., 2012. Development of environmental fate models for engineered nanoparticles - A case study of TiO₂ nanoparticles in the Rhine River. *Environ. Sci. Technol.* 46, 6705-6713.
- Prezelin, B.B., 2007. Algal blooms. In Denny, M. W., Gaines, S.D. (eds). *Encyclopedia of Tidepools and Rocky Shores*, University of California Press, Los Angeles, 30-33.
- Puddu, V., Choi, H., Dionysiou, D. D., Puma, G. L., 2010. TiO₂ photocatalyst for indoor air remediation: Influence of crystallinity, crystal phase, and UV radiation intensity on trichloroethylene degradation. *Appl. Catal. B* 94(3-4), 211-218.

- Pütter, J., 1974. Peroxidases. In Bergmeyer, H.U., (eds). Methods of Enzymatic Analysis, Vol 2. Academic Press, New York, 685-690.
- Qu, X.L., Alvarez, P.J.J., Li, Q.L., 2013. Applications of nanotechnology in water and wastewater treatment. Water Res. 47(12), 3931-3946.
- Raid, S.M., Bacic, A., 1996. Cell wall porosity and its determination. In Linskens, H.F., Jackson, J.F. (eds). Modern Methods of Plant Analysis, Vol 17: Plant Cell Wall Analysis, Springer-Verlag, Berlin, 63-80.
- Ray, P.D., Huang, B.W., Tsuji, Y., 2012. Reactive oxygen species (ROS) homeostasis and redox regulation in cellular signaling. Cell. Signal. 24, 981-990.
- Ray, P.Z., Shipley, H.J., 2015. Inorganic nano-adsorbents for the removal of heavy metals and arsenic: a review. RSC Adv. 5, 29885-29907.
- Reilly, K., Gómez-Vásquez, R., Buschmann, H., Tohme, J., Beeching, J.R., 2003. Oxidative stress responses during cassava post-harvest physiological deterioration. Plant. Mol. Biol. 53, 669-685.
- Rinehart, K., Namikoshi, M., Choi, B., 1994. Structure and biosynthesis of toxins from blue-green algae (cyanobacteria). J. Appl. Phycol. 6, 159-176.
- Robichaud, C.O., Uyar, A.E., Darby, M.R., Zucker, L.G., Wiesner, M.R., 2009. Estimates of upper bounds and trends in nano-TiO₂ production as a basis for exposure assessment. Environ. Sci. Technol. 43, 4227-4233.
- Rohrlack, T., Christoffersen, K., Dittman, E., Noguiera, I., Vasconcelos, V., Börner, T., 2005. Ingestion of microcystin by *Daphnia*: intestinal uptake and toxic effects. Limnol. Oceanogr. 50, 440-448.
- Romero-Oliva, C.S., Contardo-Jara, V., Block, T., Pflugmacher, S., 2014. Accumulation of microcystin congeners in different aquatic plants and crops - A case study from Lake Amatitlán, Guatemala. Ecotoxicol. Environ. Saf. 102, 121-128.
- Romero-Oliva, C.S., Contardo-Jara, V., Pflugmacher, S., 2015a. Time dependent uptake, bioaccumulation and biotransformation of cell free crude extract microcystins from Lake Amatitlán, Guatemala by *Ceratophyllum demersum*, *Egeria densa* and *Hydrilla verticillata*. Toxicon 105, 62-73.
- Romero-Oliva, C.S., Contardo-Jara, V., Pflugmacher, S., 2015b. Antioxidative response of the three cell-free crude extracts containing three microcystins from cyanobacterial blooms of Lake Amatitlán, Guatemala. Aquat. Toxicol. 163, 130-139.

- Sharma, P., Jha, A. B., Dubey, R. S., Pessarakli, M., 2012. Reactive oxygen species, oxidative damage, and antioxidative defense mechanism in plants under stressful conditions. *J. Bot.* 2012, 1-26.
- Sharma, R., Yang, Y., Sharma, P., Awasthi, S., Awasthi, Y.C., 2004. Antioxidant role of glutathione S transferases: protection against oxidant toxicity and regulation of stress-mediated apoptosis *Antioxid. Redox Signal.* 6, 289-300.
- Sillanpää, M., 2014. General introduction. *In* Sillanpää, M. (eds). *Natural organic matter in water: characterization and treatment methods*. Elsevier Science, Burlington, 1-15.
- Sivonen, K., Jones, G., 1999. Cyanobacterial toxins. *In* Chorus, I. and Bartram, J. (eds). *Toxic cyanobacteria in water: A guide to their public health consequences, monitoring and management* WHO & E&FN Spon, London, 41-111.
- Song, G.L., Gao, Y., Wu, H., Hou, W.H., Zhang, C.Y., Ma, H.Q., 2012. Physiological effect of anatase TiO₂ nanoparticles on *Lemna minor*. *Environ. Toxicol. Chem.* 31, 2147-2152.
- Suriyaraja, S.P., Vijayaraghavanb, T., Bijic, P., Selvakumara, R., 2014. Adsorption of fluoride from aqueous solution using different phases of microbially synthesized TiO₂ nanoparticles. *J. Environ. Chem. Eng.* 2, 444-454.
- Suttiponparnit, K., Jiang, J. K., Sahu, M., Suvachittanont, S., Charinpanitkul, T., Biswas, P., 2011. Role of surface area, primary particle size, and crystal phase on titanium dioxide nanoparticle dispersion properties, *Nanoscale Res. Lett.* 6(27), 1-8.
- Thomas, A.G., Syres, K.L., 2012. Adsorption of organic molecules on rutile TiO₂ and anatase TiO₂ single crystal surfaces. *Chem. Soc. Rev.* 41, 4207-4217.
- Thomaz, S.M., Cunha, E.R., 2010. The role of macrophytes in habitat structuring in aquatic ecosystems: Methods of measurement, causes and consequences on animal assemblages' composition and biodiversity. *Acta Limnol. Bras.* 22, 218-236.
- Valko, M., Rhodes, C.J., Moncol, J., Izakovic, M., Mazur, M., 2006. Free radicals, metals and antioxidants in oxidative stress-induced cancer. *Chem. Biol. Interact.* 160, 1-40.
- Van, T. K., Haller, W. T., Bowes, G., 1976. Comparison of the photosynthetic characteristics of three submersed aquatic plants. *Plant Phys.* 58, 761-768.
- Varner, K.E., Rindfusz, K., Gaglione, A., Viveiros, E., 2010. Nano titanium dioxide environmental matters. EPA/600/R-10/089. State-Of-The-Science Review. US Environmental Protection Agency, Washington, DC.

- von der Kammer, F., Ferguson, P.L., Holden, P.A., Masion, A., Rogers, K.P., Klaine, S.J., Koelmans, A.A., Horne, N., Unrine, J.M., 2012. Analysis of engineered nanomaterials in complex matrices (environment and biota): general considerations and conceptual case studies. *Environ. Toxicol. Chem.* 31, 32-49.
- Weber, W. J. and Morris, J. C., 1963. Kinetics of adsorption on carbon from solution, *J. San. Eng. Div.* 89, 31-60.
- Weir, A., Westerhoff, P., Fabricius, L., Hristovski, K., von Goetz, N., 2012. Titanium dioxide nanoparticles in food and personal care products, *Environ. Sci. Technol.* 46, 2242-2250.
- Westerhoff, P., Song, G., Hristovski, K., Kiser, M.A., 2011. Occurrence and removal of titanium at full scale wastewater treatment plants: Implications for TiO₂ nanomaterials, *J. Environ. Monit.* 13, 1195-1203.
- WHO, 1998. Cyanobacterial toxins: Microcystin-LR in drinking-water. Guidelines for drinking-water quality, World Health Organization, Geneva.
- Wiedner, C., Chorus, I., Fastner, J., 2004. The Waterbodies surveyed for cyanotoxins in Germany. Cyanotoxins- occurrence, causes, consequences, Springer, Berlin, 6-21.
- Wiegand, C., Pflugmacher, S., 2005. Ecotoxicological effects of selected cyanobacterial secondary metabolites: a short review. *Toxicol. Appl. Pharmacol.* 203, 201-218.
- Wiesner, M.R., Lowry, G.V., Alvarez, P., Dionysiou, D., Biswas, P., 2006. Assessing the risks of manufactured nanomaterials. *Environ. Sci. Technol.* 40, 4336-4345.
- Wunderlich, W., Oekermann, T., Miao, L., Hue, N.T., Tanemura, S., Tanemura, M., 2004. Electronic properties of nano-porous TiO₂-and ZnO-thin films-comparison of simulations and experiments. *J. Ceram. Process. Res.* 5, 343-335.
- Xu, H., Paerl, H.W., Qin, B.Q., Zhu, G.W., Gao, G., 2010. Nitrogen and phosphorus inputs control phytoplankton growth in eutrophic Lake Taihu, China, *Limnol. Oceanogr.* 55, 420-432.
- Yang, K., Lin, D.H., Xing, B.S., 2009. Interactions of humic acid with nanosized inorganic oxides. *Langmuir* 25(6), 3571-3576.
- Yang, W.W., Miao, A.J., Yang, L.Y., 2012. Cd²⁺ Toxicity to green alga *Chlamydomonas reinhardtii* as influenced by its adsorption on TiO₂ engineered nanoparticles. *PLoS One* 7, 1-8.
- Zastepa, A., Pick, F.R., Blais, J.M., 2014. Fate and persistence of particulate and dissolved microcystin-LA from *Microcystis* blooms. *Hum. Ecol. Risk Assess.* 20, 1670-1686.

-
- Zeng, J., Tu, W.W., Lazar, L., Chen, D.N., Zhao, J.S., Xu, J., 2014. Hyperphosphorylation of microfilament-associated proteins is involved in microcystin-LR-induced toxicity in HL7702 cells. *Environ. Toxicol.* 30, 981-988.
- Zhang, X.Z., Sun, H.W., Zhang, Z.Y., Niu, Q., Chen, Y.S., Crittenden, J.C., 2007. Enhanced bioaccumulation of cadmium in carp in the presence of titanium dioxide nanoparticles. *Chemosphere* 67, 160-166.
- Zhang, F., Lan, J., Yang, Y., Wei, T. F., Tan, R. Q., Song, W. J., 2013. Adsorption behavior and mechanism of methyl blue on zinc oxide nanoparticles. *J. Nanopart. Res.* 15, 1-10.

7 Figure Index

Figure 1. Molecular structure of the cyanobacterial heptapeptide microcystin-LR. ...	9
Figure 2. Generation of reactive oxygen species (ROS) from molecular oxygen and likely inter-conversion pathways.	11
Figure 3. Antioxidative pathway.	13
Figure 4. <i>Hydrilla verticillata</i>	15
Figure 5 Mechanism of the GSH recycling method.	28
Figure 6. Average hydrodynamic diameter of the investigated TiO ₂ -NPs as a function of sonication time.	35

8 Table Index

Table 1. Properties of anatase, rutile, and brookite TiO ₂	1
Table 2. List of technical devices used for analytical chemistry and biological experiments.	17
Table 3. List of software.	18
Table 4. List of chemicals.	18
Table 5. Composition and recipe of the modified Hoagland's nutrient solution.	20
Table 6. List of the studied TiO ₂ -nanoparticles and bulk TiO ₂	21
Table 7. Catalytic reaction of guajacol peroxidase (POD), catalase (CAT), and glutathione reductase (GR) studied to assess the oxidative stress response in <i>H. verticillata</i>	32
Table 8. Overview of the experiments conducted to assess the oxidative stress response in <i>H. verticillata</i> after exposure to TiO ₂ -based nano- and microparticles.	33
Table 9. Changes in the biochemical response in <i>H. verticillata</i> after exposure to TiO ₂ -NPs for 24 h (Paper II).	43
Table 10. Changes in the biochemical response in <i>H. verticillata</i> during 168 h exposure to TiO ₂ -NPs (Paper III).	44

Appendix I

Publication I

Potential role of engineered nanoparticles as contaminant carriers in aquatic ecosystems: Estimating sorption processes of the cyanobacterial toxin microcystin-LR by TiO₂ nanoparticles

Annette Okupnik, Valeska Contardo-Jara, Stephan Pflugmacher

This work was published in Colloids and Surfaces A (2015) 481, 460-467.

DOI: <http://dx.doi.org/10.1016/j.colsurfa.2015.06.013>

Own contribution:

Literature review

Design of the experiments

Nanoparticle characterization

Performance of all required laboratory studies including method optimization

Interpretation of the experimental results

Statistical analysis

Manuscript preparation

Revision of the manuscript according to the reviewers' comments

Abstract

In the present study, the adsorption of a cyanobacterial toxin, microcystin-LR (MC-LR), onto titanium dioxide nanoparticles (TiO₂-NPs) was investigated in aqueous solution. TiO₂-NPs with different crystalline phases (anatase, rutile, anatase-rutile mixture) and MC-LR in an environmental relevant concentration for German water bodies were used to make results more applicable to environmental conditions. To investigate the adsorption mechanism as well as to determine the rate-limiting step of adsorption, analysis of the adsorption kinetic was performed and common kinetic models were applied to the experimental data. Additionally, the influence of nano-TiO₂ dosage (0.01-10 mg/L) and particle size on adsorption capacity was examined, the latter by comparing the adsorption data of TiO₂-NPs to a bulk sized counterpart. The analysis of the adsorption kinetic indicates a complex adsorption mechanism and the involvement of pseudo-second-order chemisorption in the adsorption process. While only anatase TiO₂ showed a variation of MC-LR adsorption at different adsorbent concentrations, the particle size of the adsorbents appears to be the most influencing factor on toxin adsorption. All TiO₂-NPs exhibited higher adsorption capacities compared to the bulk TiO₂ counterpart, which was statistically significant for the environmental relevant concentration levels of TiO₂-NPs. The obtained results emphasise the potential of TiO₂-NPs to act as carriers for environmental contaminants such as the cyanobacterial toxin MC-LR, and thus to influence its fate in aquatic ecosystems.

Introduction

Manufactured titanium dioxide nanoparticles (TiO₂-NPs) are one of the most commonly employed metal oxide NPs [1]. Produced in thousands of tons per year and an estimated increasing production until 2025, the production of TiO₂-NPs will probably catch up the non-nano TiO₂ production [2]. The naturally occurring mineral exists in three crystalline phases brookite, anatase and rutile in which only the last two play a significant role for industrial applications [3, 4]. Because of its optical properties TiO₂-NPs are used as white pigments in numerous commercial utilizations as e.g. cosmetics, personal care products (e.g. sunscreens, toothpastes), paints, pharmaceuticals and even food [5, 6]. Inevitably, TiO₂-NPs are increasingly released into the aquatic environment. Here, they will be part of a complex mixture of chemical compounds with supposed interactions between the NPs and other environmental contaminants [7]. The nanoscale size of the particles leads to novel properties

which differ from their bulk scale counterparts [8]. Particularly, the increased surface-to-volume ratio of NPs as one characteristic feature may increase the possibility of interactions with other contaminants in surface waters [7]. Thereby, TiO₂-NPs might become transport facilitators for aquatic contaminants, such as cyanobacterial toxins.

In general, cyanobacterial toxins represent a wide range of secondary metabolites, which have been identified as potent stress factors and serious toxicological hazard in the aquatic environment [9-11]. High temperature and pH values, low turbulence and high nutrient input are environmental conditions which enhance the development of cyanobacteria [12]. In such eutrophic surface waters cyanobacteria can reach massive cell densities, so-called cyanobacterial blooms, with high concentrations of cyanotoxins released into the surrounding water principally owing to cell lysis of the cyanobacteria. Since eutrophication has become a global environmental problem, more and more lakes and reservoirs offer favourable conditions of temperature, light and nutrient status for such a cyanobacterial mass development [13]. Within the diverse group of cyanotoxins, microcystins are the most frequently identified cyanobacterial toxins [14]. These cyclic heptapeptides (d-Ala1-X2-d-MeAsp3-Y4-Adda-Arg5-d-Glu6-Mdha7) are potent inhibitors of protein phosphatases 1 and 2A, and have hepatotoxicity and tumor promotion activity [9, 15, 16]. Besides the threat for the human health, multiple studies have recorded an ecotoxicological risk of microcystins for aquatic organisms [10, 11, 17-19]. Microcystin-LR (MC-LR), which contains leucine and arginine in the variable positions X and Y, is the most commonly found microcystin congener [9] and is regulated by the WHO in the guidelines for drinking-water quality at a value of 1 µg/L [20].

TiO₂-NPs with a large surface area and thus a high adsorption capacity have the potential to affect the transport, fate and bioavailability of MC-LR in the environment, whereby an interaction of TiO₂-NPs with the cyanotoxin could amplify as well as alleviate their toxicity. Previous studies focused on the photocatalytic activity of TiO₂-NPs to assess their potential for environmental remediation by degradation of different contaminants including cyanobacterial toxins [21-24]. The adsorption of microcystins onto TiO₂-NPs have not yet been investigated sufficiently to draw conclusions about their potential to modify the toxicity of microcystins. To date, the few existing studies that evaluated the adsorption behavior of microcystins onto NPs used contaminant levels much higher than expected for the aquatic environment [25-27].

The aim of the study was to elucidate the adsorption behavior at environmentally relevant concentrations of MC-LR and TiO₂-NPs as representative cyanobacterial toxin and putative adsorbent material, respectively. For the evaluation of the carrier function of TiO₂-NPs for cyanotoxins probably leading to changes in MC-LR toxicity and bioconcentration, three TiO₂-NPs with different crystalline phases and MC-LR at an environmental realistic concentration for German water bodies were investigated in batch adsorption studies. TiO₂-NPs were characterised to assess differences in their morphology, particle size and surface electrical properties. Measurements of remaining MC-LR in solution after contact to TiO₂-NPs revealed the amount of toxin adsorption. To better understand the adsorption process a kinetic analysis based on common sorption kinetic models was performed. Additionally, the effect of adsorbent dosage (0.01-10 mg/L) was studied and compared to a bulk sized counterpart to estimate nano-specific adsorption characteristics.

Materials and Methods

Test medium

Batch adsorption experiments were conducted in a modified Hoagland's nutrient solution (Table 1) representing a hydroponic culture medium with optimal conditions for macrophyte growth in laboratory settings. To avoid sorption competition iron chloride as plant available iron source was used instead of iron chelate. A stock solution of each macronutrient (1 M) was prepared separately and appropriate volumes of this stock solutions were mixed and adjusted with HCl (1 M) to a pH 6.3 ± 0.05 . The micronutrient and iron stock solutions were added and the 100 % Hoagland's nutrient solution was then finally diluted with deionized water to the 5 % test medium.

Table 1. Composition and recipe of the modified Hoagland's nutrient solution used for the batch adsorption experiments.

Macronutrients	Concentration of stock solutions (g/L)	Volume of stock solution per litre of 100% medium (ml)	Concentration (ppm) in 100% medium	Final concentration (ppm) in test Medium (5%)
KNO ₃	101.1	5	505.5	25.3
Ca(NO ₃) ₂ *4H ₂ O	236.2	2	472.3	32.6
KH ₂ PO ₄	136.1	1	136.1	6.8
MgSO ₄ *7H ₂ O	246.5	2	493.0	24.6
Micronutrients	Concentration for 1 litre of stock solution (g/L)	Volume of stock solution per litre of 100% medium (ml)	Concentration (ppm) in 100% medium	Final concentration (ppm) in test medium (5%)
MnSO ₄ *H ₂ O	2	1	2.73	0.14
ZnSO ₄ *7H ₂ O	0.22		0.2	0.01
CuSO ₄ *5H ₂ O	0.08		0.08	0.004
(NH ₄) ₆ Mo ₇ O ₂₄ *4H ₂ O	0.2		0.198	0.01
H ₃ BO ₃	2.86		2.86	0.14
Iron stock solution				
FeCl ₃ *6H ₂ O	50	0.1	5	0.25

Adsorbent

TiO₂-NPs

In order to propose a potential release into the aquatic environment, three commercially available titanium based NPs with different crystallinity status were used. All NPs were provided as nanopowders. Anatase TiO₂ (100 % anatase, < 25 nm, specific surface area 45-50 m²/g) was purchased from Sigma Aldrich Co. Ltd. (Germany). Rutile TiO₂ (100 % rutile, 10- 30 nm, specific surface area 50 m²/g) was obtained from Iolitec (Germany). The AEROXIDE[®] P25 TiO₂ nanoparticles (~ 20/80 % rutile/anatase, 21 nm, specific surface area of 50 ± 15 m²/g) were provided by the manufacturer Evonik Degussa Corporation (Germany).

Characterisation of the TiO₂-NPs and bulk TiO₂

The primary particle sizes and morphologies were verified by a ultra-high resolution scanning electron microscope (Hitachi SU8030, Japan). Additionally, a characterisation under experimental conditions for zeta potential and size was done using a Zetasizer Nano ZS (Malvern Instruments, Germany). The z-average hydrodynamic diameter and the polydispersity index (PDI) were determined by dynamic light scattering (DLS). Size measurements were done in triplicate with each measurement being an average of 5 runs of 10 seconds. Average zeta potential measurements were carried out 30 runs of 11 seconds in triplicate. In addition, the isoelectric point (pH_{IIEP}, pH at which the zeta potential is zero) was determined by means of zeta potential measurements at varying pH values adjusted with NaOH (1 M) or HCl (1 M) respectively (pH 2 to pH 10).

Preparation of the nanoparticle suspensions

NP stock solutions (100 mg/L) were prepared by weighing and direct transfer into the test medium. As the appropriate preparation method for NP suspensions should be adjusted and validated for each nanomaterial separately, varying sonication times were investigated. NP suspensions were ultrasonicated for different time intervalls (5 min to 180 min) in an ultrasonic bath (Allpax Palsson, Germany) at 40 kHz. Aliquots of the suspensions were analyzed for absorbance values in an UV/Vis-spectrophotometer (UVIKON 922, Kontron Instrument, Italy) at varying wavelengths (290 nm for P25, 320 nm for anatase TiO₂, 328 nm for rutile TiO₂). The specific absorption maxima of the different NPs was analysed beforehand. A sonication time of two hours proved to be sufficient to increase the dispersion stability.

Adsorbate

MC-LR

MC-LR (HPLC-grade; purity ≥ 95 %) isolated from *Microcystis aeruginosa* was obtained from Enzo Life Sciences (Germany). The toxin was resuspended and diluted with HPLC-grade methanol (VWR International GmbH, France) to a MC-LR stock solution of 10 mg/L before storage at -20 °C.

MC-LR determination

To reach detectable MC-LR concentrations for toxin analysis *via* HPLC a preconcentration of MC-LR *via* solid-phase-extraction (SPE) was done beforehand using reversed-phase cartridges (Sep-Pak® tC18, 400 mg sorbent, Waters, Ireland). The sample was passed through the SPE tube for toxin enrichment followed by eluting with 5 mL of 99 % methanol (Carl Roth, Germany). Subsequently all methanol was removed in a vacuum centrifuge (Concentrator plus/Vacufouge® plus, Eppendorf AG, Germany) at a temperature of 30 °C and finally resuspended with 500 µL HPLC-grade methanol.

MC-LR quantification was performed by LC-MS/MS (Alliance 2695 UHPLC combined with a Micromass Quattro microTM, Waters) using the reverse phase column Kinetex™ C18 (2.1 mm * 50 mm, 2.6 µm pore size, Phenomenex, USA). The column oven temperature was set at 40 °C with an injection volume of 20 µL. The mobile phase consisted of solution A (Mili-Q water containing 0.1 % TFA and 5 % acetonitrile (ACN)) and solution B (ACN containing 0.1 % TFA) at a flow rate of 0.2 mL/min. A gradient was generated between both solutions. The gradient conditions (solution A: solution B) were 65:35 at 3 min, 35:65 from 3.75 to 7 min and 0:100 from 7.8 to 12 min. Elution peaks for MC-LR were observed at 7.44 min. Spectral mass data analyses was performed using electrospray ionization (ESI) in a positive ion mode with a collision energy of 65 V. Desolvation gas N₂ was set as trigger gas and Argon (Ar) as collision gas. For the subsequent MS/MS detection the MRM mode was used with a mass transfer of 995.5 (Q1) and 107.3, 135.1, 213.2 and 357.2 (Q3) for MC-LR. Calibration was linear ($R^2 = 0.999$) between 5 and 500 µg/L. The limit of detection was 1 µg/L.

Batch adsorption experiments

Batch adsorption experiments were conducted in 250 mL erlenmeyer flasks capped with parafilm to avoid contamination and minimize evaporation of the test solution. Each flask contained 50 mL of the NP suspension obtained by diluting the respective NP stock solution. Particle stock solutions were prepared immediately before initiation of adsorption to minimize particle aggregation and sedimentation. The same preparation method was used for the bulk TiO₂ counterpart (< 5 µm, rutile and small amount of anatase, Sigma Aldrich Co. Ltd., Steinheim, Germany). For all experiments a concentration of 5 µg/L MC-LR was used as this concentration has been reported to be of environmental relevance for German

water bodies [28]. Methanol concentration was kept at a level of 0.05 % of the total solution volume preventing sorption competition. Measurement of the final pH (526 MultiCal®, WTW, Germany) of each sample was conducted to access differences of pH between the batches probably influencing toxin adsorption. The flasks were agitated on a horizontal motion shaker (Edmund Bühler SM25, Hechingen, Germany) with an agitation speed of 125 rpm at a temperature of 20 ± 5 °C to keep the solutions in a completely mixed state. After shaking, the samples the test solutions were centrifuged twice in an ultracentrifuge (Optima MAX-XP, Beckman Coulter, Germany) at 12.000 rpm for 10 min to separate the liquid from the solid phase. The supernatant was removed and analyzed *via* LC-MS/MS. To assess the loss of MC-LR on the glass walls and from other processes than adsorption (loss in system) a blank without adsorbent was examined in parallel. Additionally, blanks with the adsorbent but without MC-LR served as control of any background contamination during the experiments.

Adsorption kinetic study

To obtain an appropriate sorption equilibrium time a kinetic study with a constant TiO₂-NP concentration of 10 mg/L but varying sorption times (0, 1, 3, 6, 16, 24, 48, 72 h) was conducted for each NP separately in triplicate. Equilibration was considered to be sufficient when toxin concentration changes were less than 5 % between two successive measurements.

The adsorption capacity of each TiO₂-NP after varying time was determined by the following mass balance equation (i):

$$q_e = \frac{V(C_0 - C_e)}{m}$$

where q_e is the equilibrium adsorption capacity of MC-LR (µg/g) adsorbed on unit mass of TiO₂-NP representative, C_0 and C_e the initial and equilibrium liquid-phase concentrations of MC-LR (µg/L), respectively, V the solution volume (L), and m the mass of adsorbent (g).

In order to investigate the adsorption mechanism of MC-LR on the TiO₂-NPs and to determine the rate-limiting step of adsorption, the following kinetic models were adopted to examine the time-dependent experimental adsorption data: (ii) pseudo-first-order equation, (iii) pseudo-second-order equation and (iiii) intraparticle diffusion model.

(ii) The pseudo-first-order rate equation (Lagergren's equation) can be expressed as [29]:

$$\log(q_e - q_t) = \log q_e - \frac{k_1}{2.303} t$$

where, q_e and q_t are the adsorption capacity ($\mu\text{g/g}$) at equilibrium and at time t , respectively and k_1 the first-order rate constant of pseudo-first-order equation (h^{-1}). The values of $\log(q_e - q_t)$ were linearly correlated with t .

(iii) The pseudo-second-order model was equally applied using the linear form equation [30]:

$$\frac{t}{q_t} = \frac{1}{k_2 q_e^2} + \frac{1}{q_e} t$$

where q_e , q_t and t have the same meaning as in the previous section on pseudo-first-order model. The symbol k_2 is the rate constant of pseudo-second-order sorption ($\text{g}/\mu\text{g h}$).

The values of k_1 and k_2 were determined from the slope and intercept of the corresponding plot.

(iiii) Contribution of intra particle diffusion mechanism can be tested by applying the Weber and Morris equation [31]:

$$q_t = k_{id} t^{1/2} + C$$

where k_{id} is the intraparticle diffusion rate constant ($\mu\text{g/g h}^{1/2}$) which can be evaluated from the slope of the linear plot of q_t versus $t^{1/2}$. The intercept C ($\mu\text{g/g}$) reflects the boundary layer effect. If the intraparticle diffusion is the rate-limiting step, the plot passes through the origin.

Influence of adsorbent concentration and particle size

Batch adsorption experiments with varying adsorbent concentrations (10 mg/L, 1 mg/L, 0.1 mg/L, 0.01 mg/L TiO_2 -NPs and TiO_2) were performed with four replicates. All samples were shaken for 48 h to ensure that the equilibrium was reached for all TiO_2 -NPs.

The residual concentration of MC-LR in % was calculated as follows:

$$100 \times \frac{C_e}{C_0}$$

where C_0 and C_e are the initial and equilibrium liquid-phase concentrations of MC-LR ($\mu\text{g/L}$), respectively.

Statistical analysis

The three different kinetic theories were applied to the adsorption data. The regression correlation coefficients (R^2) of the kinetic plots were used to test the accuracy of the proposed adsorption kinetic models. Data of the concentration-dependent experiment were tested for normality and homogeneity of variances using Shapiro-Wilks test and Levene's test, respectively. A one way analysis of variance (ANOVA) followed by a post-hoc Dunnett test was performed to determine statistical significant differences between the different concentration levels of the TiO_2 -NPs and the bulk TiO_2 . Additionally, a post hoc comparison of all concentration levels of each TiO_2 -NP was done with Tukey's HSD test to assess if MC-LR adsorption showed concentration dependence. Statistical analysis was performed using commercial software SPSS 21.0 (SPSS Inc, Chicago, IL, USA). A significance level of $p < 0.05$ was considered significant for all comparisons.

Results and Discussion

Characterisation of the TiO_2 -NPs

Ultra-high resolution SEM images of the examined TiO_2 -NPs were taken to indicate differences in the NPs morphology (Figure 1). Whereas P25 showed up as a nearly homogenous sample of spherical NPs, the rutile and anatase product consisted of heterogenous shaped particles. The primarily NP samples could be characterised as polydisperse as there was a large variation in the particle size with a number of small particles representing the sizes provided by the manufacturer and individual larger NPs, however, below $1\ \mu\text{m}$. All TiO_2 -NPs showed aggregates of the primary particles which might have been a characteristic of the product itself as already investigated for the well characterized P25 [32] but could also be attributed to the sample preparation method required for the microscopic imaging.

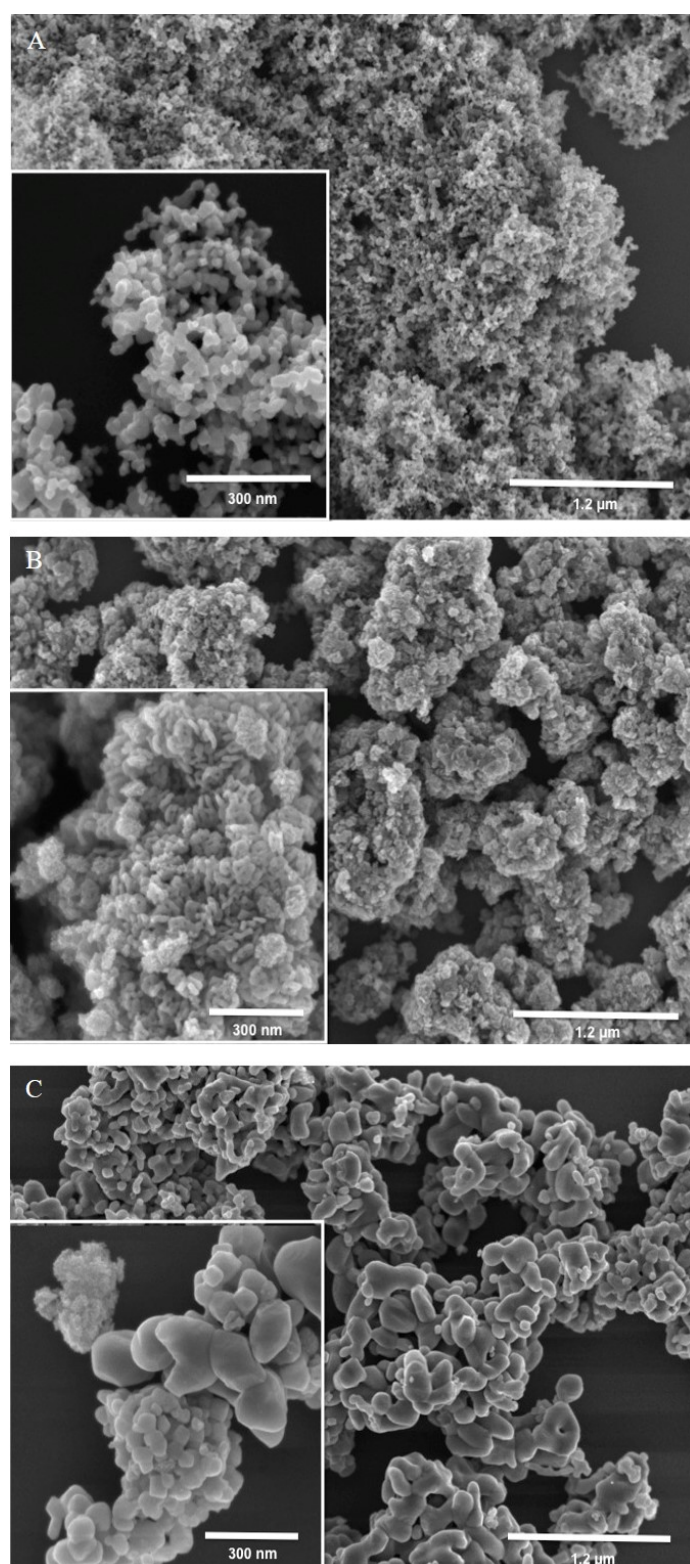


Figure 1. Low and high-magnification SEM micrographes of TiO₂ nanoparticles anatase TiO₂ (A), rutile TiO₂ (B) and P25 (C).

DLS measurements of the NPs in the Hoagland's nutrient solution indicated an almost bimodal size distribution. All NPs tended to aggregate in the test medium. In accordance with previous studies [32-35], sonication failed to break up the NP aggregates. About 90 % of the particles exhibited average sizes in the 400 to 500 nm range (Table 2), much larger than the vendor reported sizes. DLS analysis of the bulk TiO₂ counterpart revealed large average particle sizes of about 1.5 μ m. Even if the reported sizes suggest the formation of larger aggregates in the samples, the presence of smaller aggregates or individual NPs cannot be excluded due to the intensity weighted character of the DLS method.

Table 2. Properties of the three types of TiO₂ nanoparticles and bulk TiO₂. The particles have been characterized suspended in the test medium for the analysis of Z-average particle size, zeta potential and pH_{IEP}. Values for the surface area, average primary particle diameter and crystalline structure are from particle suppliers or other studies.

	Particle type			
	anatase TiO ₂	rutile TiO ₂	P25	bulk TiO ₂
Surface area (m²/g)	45-55 ^a	50 ^a	50±15 ^a	2.5 ^b
Average primary particle diameter	< 25 nm ^a	10-30 nm ^a	21 nm ^a	0.3-1 μ m ^b
Z-average particle size (nm)^c	489 ± 5.7	525 ± 28.3	438 ± 128.0	1458 ± 71.1
PDI^c	0.3 ± 0.02	0.3 ± 0.04	0.4 ± 0.07	0.7 ± 0.07
Zeta potential (mV)^c	-22 ± 0.34	-26 ± 0.45	-22 ± 0.25	-30 ± 1.8
pH_{IEP}	~ 3.5	~ 2.7	~ 3.6	~ 2.7
Crystalline phase	anatase	rutile	73% anatase/ 18% rutile ^d	rutile (contains a small amount of anatase ≈ 5%)

a characteristics provided by the manufacturer

b [52]

c characteristics estimated in the test medium (pH = 6.3 ± 0.05); data shown are the mean ± standard deviation (n = 3)

d [53]

All of the investigated TiO₂-NPs showed a negative zeta potential under experimental conditions with pH values above pH_{IEP} (Figure 2). Similar patterns of the zeta potential development occurred for particles with comparable crystallinity status (bulk TiO₂ and rutile TiO₂, P25 and anatase TiO₂). However only marginal differences between the titania

crystal phases occurred, which is consistent with previous studies [36, 37]. As a zeta potential of at least ± 30 mV is believed to be the approximate threshold for a stable nanodispersion [38]; attraction between the TiO_2 -NPs exceeded their repulsion which is in accordance with DLS size analysis and the observation of NP aggregates.

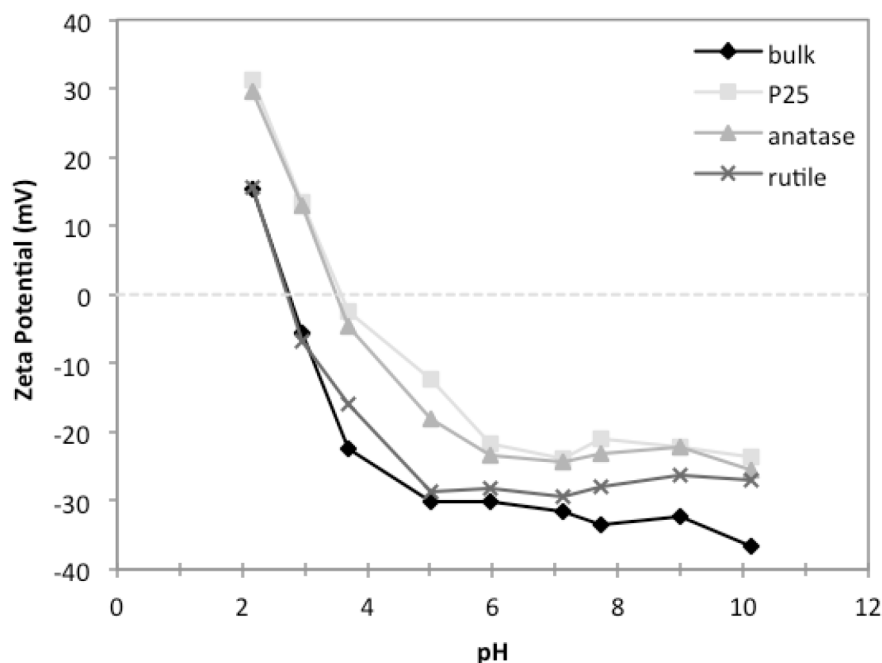


Figure 2. Zeta potential (mV) of TiO_2 nanoparticles and bulk TiO_2 with varying pH in the test medium.

Batch adsorption experiments

Adsorption kinetic study

The adsorption capacity ($\mu\text{g/g}$) for MC-LR by the different TiO_2 -NPs at an initial MC-LR concentration of $5 \mu\text{g/L}$ is displayed as a function of time (Figure 3). Because the loss of the toxin was negligible and no background contamination was detected, the variation of MC-LR concentration could be linked to its adsorption onto the TiO_2 -NPs. All NPs showed a continuous increase in the adsorption of MC-LR with time. The adsorption capacity of anatase TiO_2 progressively flattened after 24 h. Rutile TiO_2 and P25 reached toxin adsorption equilibrium at 48 h which is consistent with a study conducted with MC-LR and iron oxide NPs [25]. Because the adsorption rate is positively associated with the number of active adsorption sites, the highest adsorption capacity of the TiO_2 -NPs occurred initially

when active sites were most available. Hereafter, the adsorption capacity showed a slighter increase over time. P25 exhibited the highest capacity for MC-LR removal followed by anatase TiO_2 and rutile TiO_2 (282 $\mu\text{g/g}$, 188 $\mu\text{g/g}$, 128 $\mu\text{g/g}$ for $t = 72$ h). Interestingly, the order of MC-LR removal followed the order of increasing NP-sizes as revealed by DLS analysis of the NPs in the test medium (438 nm, 489 nm, 525 nm). This result suggests a size dependence of MC-LR adsorption onto TiO_2 -NPs. Besides the size of the NP-aggregates in the samples, their morphology could also explain differential adsorption capacities as aggregates can occur as compact clusters of NPs or structures with high porosity and pore dimensions. Also, the crystallinity status seems to have influenced the toxin adsorption to a certain extent. P25 which mostly consists of the anatase phase, and the pure anatase TiO_2 -NP exhibited the highest adsorption capacity for MC-LR compared to the pure rutile TiO_2 -NP. Differential adsorption behaviors of the two isomorphs have been observed also in former studies but the reasons have not yet been fully understood [39, 40].

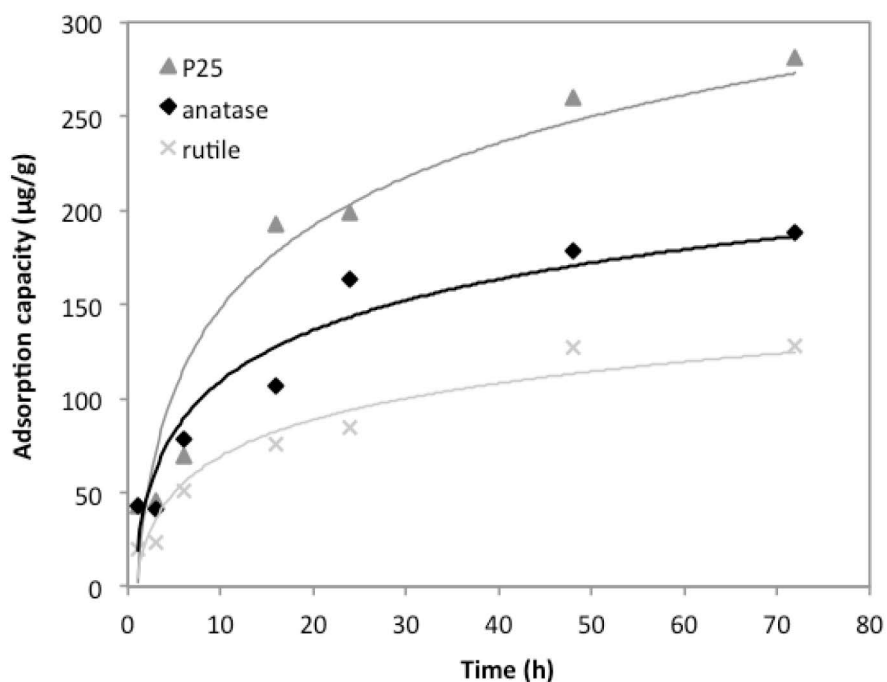


Figure 3. Adsorption capacity ($\mu\text{g/g}$) of MC-LR by TiO_2 -nanoparticles versus time (initial MC-LR = 5 $\mu\text{g/L}$; adsorbent dose = 10 mg/L; final pH \approx 6; $T = 20^\circ\text{C} \pm 5$).

The kinetic models as fitted with the experimental data are presented in the plots (Figure 4). For all TiO_2 -NPs the correlation coefficients of the first-order kinetic were lower than in the case of second-order kinetic model (Table 3), suggesting that kinetics of MC-LR adsorption

by the investigated TiO₂-NPs can be more favorably described by the pseudo-second-order kinetic model. This is in accordance with a former study performed with iron oxide NPs [26], thus MC-LR adsorption onto NPs may be a chemical sorption process involving valence forces through sharing or exchanging of electrons [30]. Since the pseudo-second-order model cannot identify the diffusion mechanism the probability of intraparticle diffusion of MC-LR was tested. As the data exhibit multi-linear plots (Figure 4 c) it can be assumed that intraparticle diffusion is not the only mechanism involved in MC-LR adsorption onto TiO₂-NPs. The first linear portion (phase I) may be attributed to the boundary layer diffusion after diffusion of the adsorbate through the solution to the surface of the adsorbent. Phase II may be due to the diffusion of MC-LR from the surface site into the inner pores (intraparticle diffusion) [41]. It is evident from the plot that the boundary layer diffusion governed the largest part of the adsorption process for all TiO₂-NPs. The rate constants k_{id1} and k_{id2} , respectively, were calculated from the slope of the first and second linear portion of the plots. The higher values of k_{id1} indicate that the initial step (phase I) was rapid and was subsequently followed by a slower step (phase II). The decrease of the diffusion rate constant during the adsorption process has been explained by a decrease in the number of unoccupied adsorption sites and the increase of diffusion resistance [42]. As the intercepts obtained by the extrapolation of the second portion of the plots back towards the y-axis does not pass through the origin, a complex adsorption mechanism including chemisorption and physisorption processes can be assumed [43]. With regard to the latter, it should be kept in mind that electrostatic interactions might have been unfavourable for adsorption, as MC-LR is characterised by a negative surface charge over a broad pH range ($3 < \text{pH} < 12$) [25], and also the TiO₂-NPs exhibited a negative surface charge during the experiments (Table 2). Hence, the adsorption of MC-LR was apparently caused by non-electrostatic forces. A chemical reaction mechanisms between the adsorbent and the adsorbate might underlie the adsorption process and is likely controlled by the surface hydroxyl groups of the TiO₂-NPs and the side groups of MC-LR [25, 44].

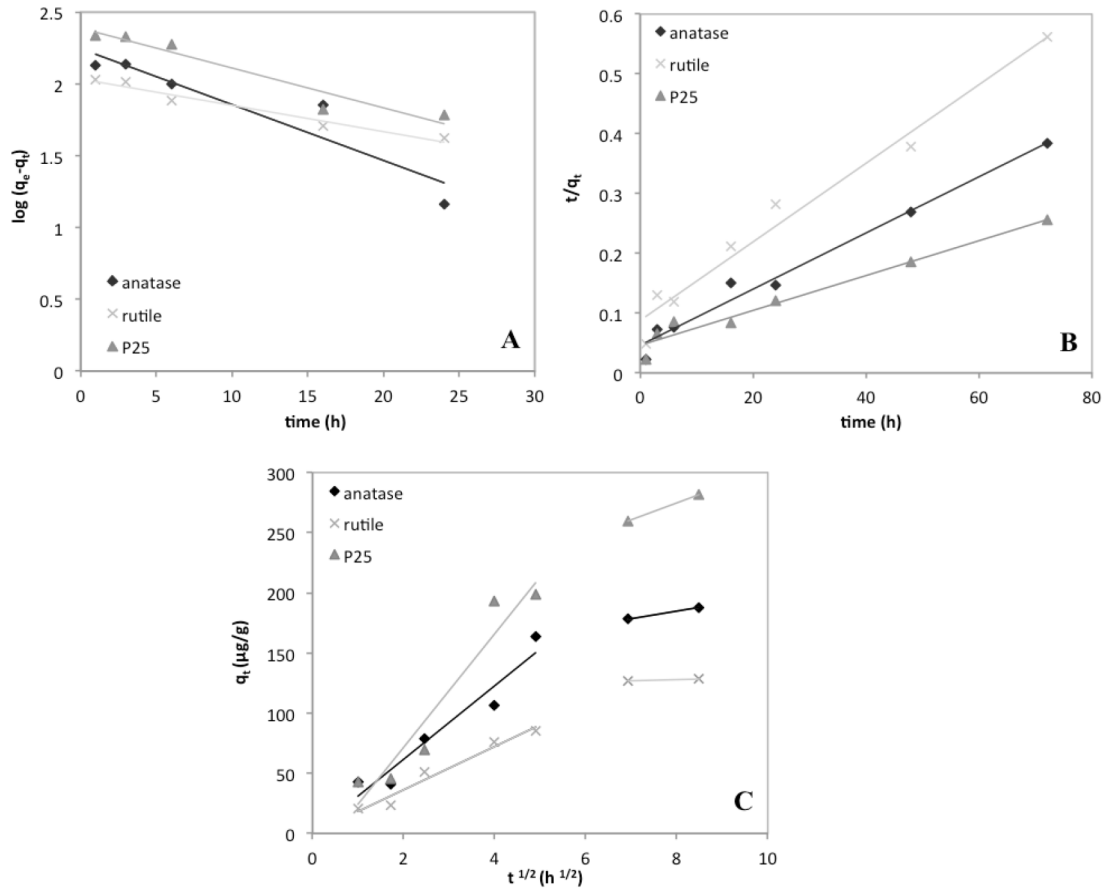


Figure 4. Plots of pseudo-first-order kinetics (A), pseudo-second-order kinetics (B) and intraparticle diffusion model (C) for MC-LR removal by TiO₂-nanoparticles.

Table 3. The constant parameters of pseudo-first-order kinetics, pseudo-second-order kinetics and intraparticle diffusion model for the adsorption of MC-LR onto TiO₂-nanoparticles.

Pseudo-first-order model			
TiO ₂ -nanoparticle	k ₁ (h ⁻¹)	R ²	
anatase	0.0896	0.877	
rutile	0.0421	0.960	
P25	0.0638	0.927	
Pseudo-second-order model			
TiO ₂ -nanoparticle	k ₂ (μgg ⁻¹ h ⁻¹) * 10 ⁻²	R ²	
anatase	0.048	0.980	
rutile	0.050	0.974	
P25	0.018	0.962	
intraparticle diffusion model			
TiO ₂ -nanoparticle	k _{id1} (μg g ⁻¹ h ^{-1/2})	k _{id2} (μg g ⁻¹ h ^{-1/2})	R ² *
anatase	30.55	6.30	0.931
rutile	17.99	0.92	0.960
P25	47.18	14.02	0.924

Influence of particle size and adsorbent concentration

The adsorption of MC-LR onto varying concentrations of TiO₂-NPs and bulk TiO₂ was measured to assess the influence of the particle size and adsorbent dose on the adsorption process. All NPs had the tendency of a higher toxin adsorption compared to the bulk TiO₂ counterpart, which was statistically significant for the concentration levels of 0.1 mg/L and 0.01 mg/L (Figure 5). Under the experimental conditions of this study the particle size seems to be an important factor influencing the MC-LR adsorption. The increased presence of active adsorption sites on the surface of TiO₂-NPs compared to the bulk TiO₂ could be the reason for this observation. It is known that aggregation of NPs is an important factor resulting in loss of surface area and thus limiting the capacity for adsorption. However, it is evident from the characterisation of the particles of the present study that even at an aggregated status the TiO₂-NPs exhibited a larger surface for the interaction with MC-LR caused by the smaller particle size in the test solutions (Table 2).

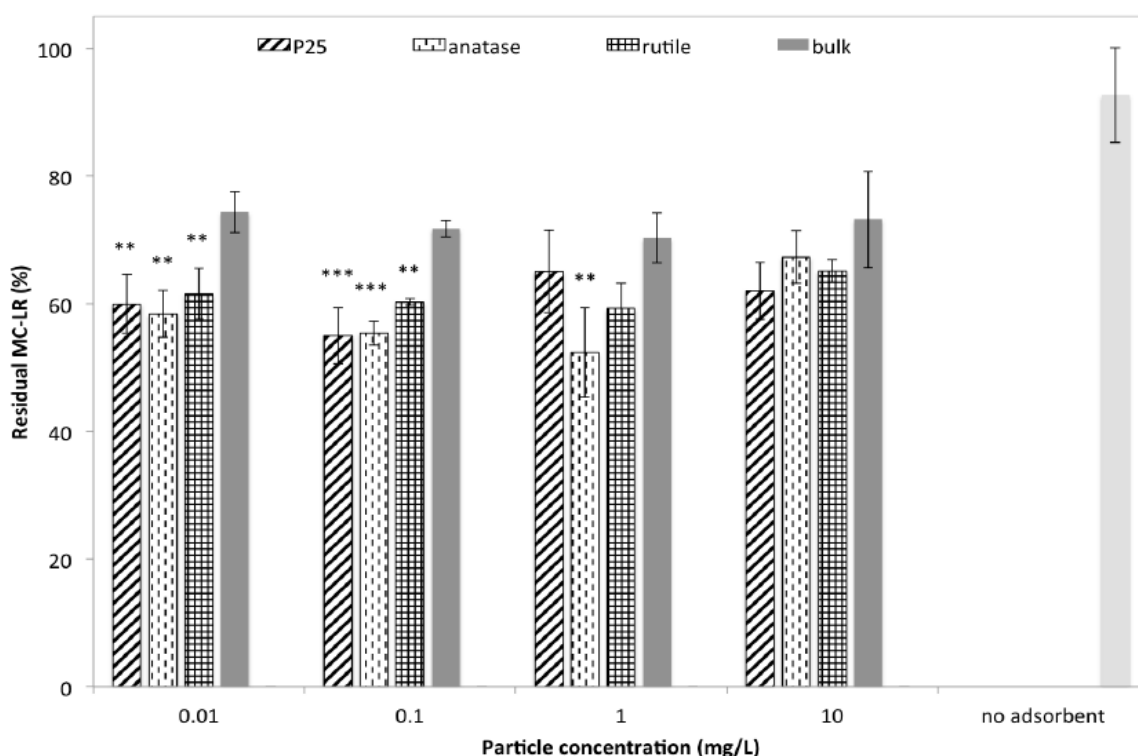


Figure 5. Residual MC-LR (%) after adsorption onto TiO₂-nanoparticles and bulk TiO₂. (initial MC-LR = 5 µg/L; final pH ≈ 6; T = 20 °C ± 5); significant difference to bulk TiO₂, $p < 0.05$ (*), $p < 0.01$ (**); $p < 0.001$ (***)).

Regarding the concentration dependency of MC-LR adsorption, only anatase TiO₂ showed a variation in the toxin adsorption with varying NP concentrations. Interestingly, at lower concentration levels of anatase TiO₂ (1 mg/L and 0.1 mg/L) more MC-LR was adsorbed than at the highest concentration of 10 mg/L ($p < 0.05$). A similar result was found by Gao et al. [26], underlining the exceptional behavior of NPs in solutions and the importance of colloidal stability of NPs for adsorption processes. From literature it is known that the rate of aggregation and the size of individual aggregates increases with increasing particle concentration [45, 46]. Thus, it can be assumed that the sedimentation rate increased in the solutions with high NP concentrations as the formation of large aggregates occurred. The domination of particle-particle interactions over the particle-toxin interactions could also explain the lack of concentration-dependent adsorption behavior onto rutile TiO₂ and P25 during the experiments.

Environmental considerations

Even if there are still major knowledge gaps that affect the aquatic exposure modelling for TiO₂-NPs, the scientific literature agrees that low quantities of nano-TiO₂ in the range of approximately 10- 10⁻³ µg/L exist in surface waters [47]. This underlines the importance of the present observation that TiO₂-NPs can act as carriers for cyanobacterial toxins as the removal of an environmental relevant concentration of MC-LR was about 40% at the lowest concentration level for all TiO₂-NPs (0.01 mg/L). Hence, TiO₂-NPs exhibit the potential to influence the fate of MC-LR in aquatic ecosystems due to an interaction of both, the NPs and the toxin. As the adsorption could facilitate the exposure of aquatic organisms towards MC-LR and thus increase its bioavailability, an amplified toxicity could be the result. Furthermore, the stability of cyanobacterial toxins might be influenced as their adsorption onto TiO₂-NPs could result in a decreased sensitivity against microbial degradation.

The zeta potential of the NPs plays a significant role for the MC-LR adsorption process [25, 26], and thus the properties of the NPs in an experimental adsorption study should be comparable to that existing in the aquatic environment. As previous studies revealed that TiO₂-NPs exhibit a negative zeta potential in natural waters [48, 49] which will probably be enhanced by cyanobacterial-driven pH increases during blooming events [50, 51], the adsorption process of MC-LR onto TiO₂-NPs could follow the mechanisms investigated in the present study. Nevertheless, it should also be considered that aquatic ecosystems are

characterized by a complex water chemistry and under natural conditions adsorption capacities of TiO₂-NPs will most likely be influenced by the presence of other water components like natural organic matter (NOM), being ubiquitous in aquatic systems. As a previous study already investigated a negative impact of NOM on the MC-LR adsorption capacity by maghemite nanoparticles [25], further investigations of the MC-LR adsorption onto TiO₂-NPs in the presence of NOM should be conducted. This should base on environmental relevant concentration levels of all mixture components to gain a further insight into the interaction of TiO₂-NPs and cyanobacterial toxins under realistic environmental conditions.

Conclusions

In this study, the adsorption of MC-LR from aqueous solution by TiO₂-NPs of different crystallinity status was investigated. Batch adsorption studies revealed their potential to act as carriers for cyanobacterial toxins in aquatic environments as a significant toxin removal was observed at environmental relevant concentrations of both, adsorbent and adsorbate. The kinetic data indicate a complex adsorption mechanism and the involvement of pseudo-second-order chemisorption in the adsorption process. Whereas the adsorbent dosage did not have an overall influence on the adsorption process, the adsorbent size was an important influencing factor on MC-LR adsorption. All TiO₂-NPs showed a higher adsorption capacity than the microscale TiO₂. This clarifies the unique chemical and physical properties of NPs compared to the bulk sized counterparts even when tending to aggregate in aqueous suspension. Thus, our results indicate the potential of TiO₂-NPs to influence the fate of MC-LR in the environment due to adsorption and emphasise the importance for further investigations concerning the interaction of TiO₂-NPs and cyanobacterial toxins.

Acknowledgements

The authors acknowledge Dr. T. Bucheli (Agroscope Reckenholz-Tänikon Research Station) for providing laboratory equipment for particle characterisation and U. Gernert (ZELMI-TU Berlin) for the SEM imaging. The authors would also like to thank S. Kühn for her support and assistance during LC-MS/MS analysis.

Reference list

- [1] R. K. Shukla, V. Sharma, A. K. Pandey, S. Singh, S. Sultana and A. Dhawan, ROS-mediated genotoxicity induced by titanium dioxide nanoparticles in human epidermal cells, *Toxicol. In Vitro* 25 (2011) 231-241.
- [2] C. O. Robichaud, A. E. Uyar, M. R. Darby, L. G. Zucker and M. R. Wiesner, Estimates of upper bounds and trends in nano-TiO₂ production as a basis for exposure assessment., *Environ. Sci. Technol.* 43 (2009) 4227-4233.
- [3] K. L. Hadjiivanov and D. G. Klissurski, Surface chemistry of titania (anatase) and titania-supported catalysts, *Chem. Soc. Rev.* 25 (1996) 61-69.
- [4] C. Pagnout, S. Jomini, M. Dadhwal, C. Caillet, F. Thomas and P. Bauda, Role of electrostatic interactions in the toxicity of titanium dioxide nanoparticles toward *Escherichia coli*, *Colloid Surface B* 92 (2012) 315-321.
- [5] ICIS, Titanium Dioxide Uses and Market, <http://www.icis.com/Articles/2007/11/07/9076546/titanium-dioxide-tio2-uses-and-market-data.html> (July 22nd, 2014)
- [6] A. Weir, P. Westerhoff, L. Fabricius, K. Hristovski and N. von Goetz, Titanium Dioxide Nanoparticles in Food and Personal Care Products, *Environ. Sci. Technol.* 46 (2012) 2242-2250.
- [7] N. B. Hartmann and A. Baun, The nano cocktail: Ecotoxicological effects of engineered nanoparticles in chemical mixtures, *Integr. Environ. Assess. Manage.* 6 (2010) 311-313.
- [8] L. K. Adams, D. Y. Lyon and P. J. J. Alvarez, Comparative eco-toxicity of nanoscale TiO₂, SiO₂, and ZnO water suspensions, *Water Res.* 40 (2006) 3527-3532.
- [9] K. Rinehart, M. Namikoshi and B. Choi, Structure and biosynthesis of toxins from blue-green algae (cyanobacteria), *J. Appl. Phycol.* 6 (1994) 159-176.
- [10] S. Pflugmacher, K. Jung, L. Lundvall, S. Neumann and A. Peuthert, Effects of cyanobacterial toxins and cyanobacterial cell-free crude extract on germination of alfalfa (*Medicago sativa*) and induction of oxidative stress, *Environ. Toxicol. Chem.* 25 (2006) 2381-2387.
- [11] S. Pflugmacher, Promotion of oxidative stress in the aquatic macrophyte *Ceratophyllum demersum* during biotransformation of the cyanobacterial toxin microcystin-LR, *Aquat. Toxicol.* 70 (2004) 169-178.

- [12] D. R. de Figueiredo, U. M. Azeiteiro, S. M. Esteves, F. J. M. Gonçalves and M. J. Pereira, Microcystin-producing blooms—A serious global public health issue, *Ecotoxicol. Environ. Saf.* 59 (2004) 151-163.
- [13] J. Bartram, W. W. Carmichael, I. Chorus, G. Jones and O. M. Skulberg, Introduction. Toxic cyanobacteria in water: A guide to their public health consequences, monitoring and management, WHO & E&FN Spon, London 1999, pp. 1-14.
- [14] K. Sivonen and G. Jones, Cyanobacterial toxins. In: Toxic cyanobacteria in water: A guide to public health significance, monitoring and management, WHO & E&FN Spon, London, 1999, pp. 41-111.
- [15] W. W. Carmichael, Cyanobacteria secondary metabolites—the cyanotoxins, *J. Appl. Bacteriol.* 72 (1992) 445-459.
- [16] D. M. Toivola, J. E. Eriksson and D. L. Brautigan, Identification of Protein Phosphatase 2a as the Primary Target for Microcystin-1r in Rat-Liver Homogenates, *FEBS Lett.* 344 (1994) 175-180.
- [17] J. Jiang, X. Gu, R. Song and X. Y. Wang, L., Microcystin-LR induced oxidative stress and ultrastructural alterations in mesophyll cells of submerged macrophyte *Vallisneria natans* (Lour.) Hara, *J. Hazard. Mater.* 190 (2011) 188-196.
- [18] W. Chen, L. Song, D. Ou and N. Gan, Chronic toxicity and responses of several important enzymes in *Daphnia magna* on exposure to sublethal microcystin-LR, *Environ. Toxicol.* 20 (2005) 323-330.
- [19] S. M. Mitrovic, O. Allis, A. Furey and K. J. James, Bioaccumulation and harmful effects of microcystin-LR in the aquatic plants *Lemna minor* and *Wolffia arrhiza* and the filamentous alga *Chladophora fracta*, *Ecotoxicol. Environ. Saf.* 61 (2005) 345-352.
- [20] WHO, Cyanobacterial toxins: Microcystin-LR in Drinking-water. Guidelines for Drinking-Water Quality, WHO, Geneva, 1998.
- [21] L. A. Lawton, P. K. J. Robertson, B. J. P. A. Cornish and M. Jaspars, Detoxification of microcystins (cyanobacterial hepatotoxins) using TiO₂ photocatalytic oxidation, *Environ. Sci. Technol.* 33 (1999) 771-775.
- [22] P. K. J. Robertson, L. A. Lawton, B. Munch and J. Rouzade, Destruction of cyanobacterial toxins by semiconductor photocatalysis, *Chem. Commun.* (1997) 393-394.
- [23] J. Yang, D. X. Chen, A. P. Deng, Y. F. Fang, G. F. Luo, D. J. Li, R. P. Li and Y. P. Huang, Visible light-induced N-doped TiO₂ nanoparticles for the degradation of microcystin-LR, *Sci. China Chem.* 53 (2010) 1793-1800.

- [24] M. Pelaez, A. A. de la Cruz, E. Stathatos, P. Falaras and D. D. Dionysiou, Visible light-activated N-F-codoped TiO₂ nanoparticles for the photocatalytic degradation of microcystin-LR in water, *Catal. Today* 144 (2009) 19-25.
- [25] J. Lee and H. W. Walker, Adsorption of microcystin-Lr onto iron oxide nanoparticles, *Colloid Surface A* 373 (2011) 94-100.
- [26] Y. Q. Gao, N. Y. Gao, Y. Deng, J. S. Gu, Y. C. Shen and S. X. Wang, Adsorption of microcystin-LR from water with iron oxide nanoparticles, *Water Environ. Res.* 84 (2012) 562-568.
- [27] L. A. Lawton, P. K. J. Robertson, B. J. P. A. Cornish, I. L. Marr and M. Jaspars, Processes influencing surface interaction and photocatalytic destruction of microcystins on titanium dioxide photocatalysts, *J. Catal.* 213 (2003) 109-113.
- [28] C. Wiedner, I. Chorus and J. Fastner, The Waterbodies surveyed for cyanotoxins in Germany. Cyanotoxins- Occurrence, Causes, Consequences, Springer, Berlin, 2004, pp. 6-21.
- [29] Y. S. Ho, Citation review of Lagergren kinetic rate equation on adsorption reactions, *Scientometrics* 59 (2004) 171-177.
- [30] Y. S. Ho and G. McKay, Pseudo-second order model for sorption processes, *Process Biochem.* 34 (1999) 451-465.
- [31] W. J. Weber and J. C. Morris, Kinetics of adsorption on carbon from solution, *J. San. Eng. Div* 89 (1963) 31-60.
- [32] J. Jiang, G. Oberdörster and P. Biswas, Characterization of size, surface charge, and agglomeration state of nanoparticle dispersions for toxicological studies, *J. Nanopart. Res.* 11 (2009) 77-89.
- [33] N. Mandzy, E. Grulke and T. Druffel, Breakage of TiO₂ agglomerates in electrostatically stabilized aqueous dispersions, *Powder Technol.* 160 (2005) 121-126.
- [34] Y. Zhang, Y. Chen, P. Westerhoff, K. Hristovski and J. C. Crittenden, Stability of commercial metal oxide nanoparticles in water, *Water Res.* 42 (2008) 2204-2212.
- [35] Z. Ji, X. Jin, S. George, T. Xia, H. Meng, X. Wang, E. Suarez, H. Zhang, E. M. V. Hoek, H. Godwin, A. E. Nel and J. I. Zink, Dispersion and Stability Optimization of TiO₂ Nanoparticles in Cell Culture Media, *Environ. Sci. Technol.* 44 (2010) 7309-7314.
- [36] K. Suttiponpanit, J. K. Jiang, M. Sahu, S. Suvachittanont, T. Charinpanitkul and P. Biswas, Role of Surface Area, Primary Particle Size, and Crystal Phase on Titanium Dioxide Nanoparticle Dispersion Properties, *Nanoscale Res. Lett.* 6 (2011).

- [37] M. Kosmulski, The significance of the difference in the point of zero charge between rutile and anatase, *Adv. Colloid Interface Sci.* 99 (2002) 255-264.
- [38] T. M. Riddick, *Zeta-Meter Operating Manual ZM-75*, Zeta-Meter Inc., New York, 1968.
- [39] M. E. Barbour, D. J. O'Sullivan and D. C. Jagger, Chlorhexidine adsorption to anatase and rutile titanium dioxide, *Colloid Surface A* 307 (2007) 116-120.
- [40] S. P. Suriyaraja, T. Vijayaraghavanb, P. Bijic and R. Selvakumara, Adsorption of fluoride from aqueous solution using different phases of microbially synthesized TiO₂ nanoparticles, *J. Environ. Chem. Eng.* 2 (2014) 444-454.
- [41] V. K. Gupta, D. Pathania, N. C. Kothiyal and G. Sharma, Polyaniline zirconium (IV) silicophosphate nanocomposite for remediation of methylene blue dye from waste water, *J. Mol. Liq.* 190 (2014) 139- 145.
- [42] F. Zhang, J. Lan, Y. Yang, T. F. Wei, R. Q. Tan and W. J. Song, Adsorption behavior and mechanism of methyl blue on zinc oxide nanoparticles, *J. Nanopart. Res.* 15 (2013).
- [43] L. L. Fan, C. N. Luo, X. J. Li, F. G. Lu, H. M. Qiu and M. Sun, Fabrication of novel magnetic chitosan grafted with graphene oxide to enhance adsorption properties for methyl blue, *J. Hazard. Mater.* 215 (2012) 272-279.
- [44] A. G. Thomas and K. L. Syres, Adsorption of organic molecules on rutile TiO₂ and anatase TiO₂ single crystal surfaces, *Chem. Soc. Rev.* 41 (2012) 4207-4217.
- [45] T. Phenrat, N. Saleh, K. Sirk, R. D. Tilton and G. V. Lowry, Aggregation and sedimentation of aqueous nanoscale zerovalent iron dispersions, *Environ. Sci. Technol.* 41 (2007) 284-290.
- [46] A. Brunelli, G. Pojana, S. Callegaro and A. Marcomini, Agglomeration and sedimentation of titanium dioxide nanoparticles (n-TiO₂) in synthetic and real waters, *J. Nanopart. Res.* 15 (2013).
- [47] F. Gottschalk, T. Y. Sun and B. Nowack, Environmental concentrations of engineered nanomaterials: Review of modeling and analytical studies, *Environ. Pollut.* 181 (2013) 287-300.
- [48] S. Ottofuelling, F. Von der Kammer and T. Hofmann, Commercial Titanium Dioxide Nanoparticles in Both Natural and Synthetic Water: Comprehensive Multidimensional Testing and Prediction of Aggregation Behavior, *Environ. Sci. Technol.* 45 (2011) 10045-10052.

- [49] A. A. Keller, H. T. Wang, D. X. Zhou, H. S. Lenihan, G. Cherr, B. J. Cardinale, R. Miller and Z. X. Ji, Stability and Aggregation of Metal Oxide Nanoparticles in Natural Aqueous Matrices, *Environ. Sci. Technol.* 44 (2010) 1962-1967.
- [50] H. Xu, H. W. Paerl, B. Q. Qin, G. W. Zhu and G. Gao, Nitrogen and phosphorus inputs control phytoplankton growth in eutrophic Lake Taihu, China, *Limnol. Oceanogr.* 55 (2010) 420-432.
- [51] B. W. Ibelings and S. C. Maberly, Photoinhibition and the availability of inorganic carbon restrict photosynthesis by surface blooms of cyanobacteria, *Limnol. Oceanogr.* 43 (1998) 408-419.
- [52] H. L. Karlsson, J. Gustafsson, P. Cronholm and L. Moller, Size-dependent toxicity of metal oxide particles-A comparison between nano- and micrometer size, *Toxicol. Lett.* 188 (2009) 112-118.
- [53] H. Jensen, K. D. Joensen, J. E. Jorgensen, J. S. Pedersen and E. G. Sogaard, Characterization of nanosized partly crystalline photocatalysts, *J. Nanopart. Res.* 6 (2004) 519-526.

Appendix II

Publication II

Oxidative stress response of the aquatic macrophyte *Hydrilla verticillata* exposed to TiO₂ nanoparticles

Annette Okupnik, Stephan Pflugmacher

This is the peer reviewed version of the following article:

Okupnik, A., Pflugmacher, S., 2016. Oxidative stress response of the aquatic macrophyte *Hydrilla verticillata* exposed to TiO₂ nanoparticles. *Environmental Toxicology and Chemistry* 35(11), 2859-2866 which has been published in final form at <https://doi.org/10.1002/etc.3469>. This article may be used for non-commercial purposes in accordance with Wiley Terms and Conditions for Use of Self-Archived Versions.

Own contribution:

Literature review

Design of the experiments

Plant culture

Performance of all required laboratory studies including method optimization

Interpretation of the experimental results

Statistical analysis

Manuscript preparation

Revision of the manuscript according to the reviewers' comments

Abstract

The present study investigated the effects of titanium dioxide nanoparticles (TiO₂-NPs) on the oxidative stress response in *Hydrilla verticillata*. Macrophytes were exposed to different concentrations of TiO₂-NPs (0 mg/L, 0.01 mg/L, 0.1 mg/L, 1 mg/L, 10 mg/L) for 24 h, based on currently predicted levels of nano-TiO₂ in surface waters. Additionally, TiO₂-NPs with varying crystalline statuses were used to assess the potential influence of crystalline phases on oxidative stress responses. The level of hydrogen peroxide (H₂O₂), reduced and oxidized glutathione (GSH and GSSG) and activities of the antioxidative enzymes peroxidase (POD), catalase (CAT) and glutathione reductase (GR) were measured and compared to a bulk counterpart. Although, POD was not considered as active, the results imply an activation of the enzymatic defense system as increased CAT and GR activities were observed. Exposure to bulk TiO₂ revealed lower enzyme activities at all exposure concentrations, suggesting a nano-specific influence on the antioxidative defense mechanisms in *H. verticillata*. Moreover, all TiO₂-NP concentrations resulted in a decreased GSH/GSSG ratio, indicating a high GSH-dependent metabolic activity to protect against the destructive effects of reactive oxygen species (ROS) generated during nano-TiO₂ exposure. As the level of H₂O₂ was solely elevated after exposure to 10 mg/L of P25, it appears plausible that adaptive metabolic mechanisms of *H. verticillata* are able to cope with environmentally relevant concentrations of TiO₂-NPs.

Introduction

Nanotechnology is a rapidly growing industry with manufactured titanium dioxide nanoparticles (TiO₂-NPs) being one of the most commonly employed metal oxide NPs [1]. This naturally occurring mineral exists in three crystalline phases brookite, anatase and rutile, from which only the last two play a significant role in industrial applications [2]. Because of its optical properties TiO₂-NPs are increasingly incorporated into a variety of consumer and household products and are common additives in food [3]. Additionally, TiO₂ is considered an excellent band-gap semiconductor due to its wide energy gap ($E_g = 3.2$ eV). Thus, nano-TiO₂ is used for its photocatalytic properties in electronic products, self-cleaning coatings, cleaning products and hair styling devices. Furthermore, research interests regarding the catalytic and photocatalytic properties of nano-TiO₂ for applications in environmental remediation including the degradation or adsorption of contaminants from

water, groundwater and air has increased [4]. Due to increasing production volumes concerns about the fate and behavior of nano-TiO₂ in the aquatic environment have arisen, as water reservoirs will be the final destination of TiO₂-NPs [5]. Even though TiO₂, in its large-scale bulk form, is considered to be chemically inert, nano-TiO₂ may exhibit physical and chemical properties that differ from those of their bulk counterparts [6]. The risk assessment and management of NPs is difficult as long as immense knowledge gaps regarding their ecotoxicology exist [7]. Currently, there is emerging literature concerning the toxicity of TiO₂-NPs, especially towards freshwater algae and invertebrates. Nanotoxicity to different algal species has been assessed via growth inhibition tests [8-10], and revealed decreased algae growth but with in part variable values of EC₅₀ (half maximal effective concentration). The same applies for current toxicity data for freshwater invertebrates [11]. Only a few studies have investigated the ecotoxicity of nano-TiO₂ towards aquatic plants. Li et al. [12] did not observe adverse effects on the growth rate and chlorophyll content of the macrophyte *Lemna minor* L. at nano-TiO₂ concentration levels of 0.01 mg/L to 5 mg/L, but discussed a potential transfer of TiO₂-NPs in the aquatic food chain as their attachment to plant cell walls has been assessed. Growth inhibition of another *Lemna* species has been observed by Kim et al. [13], however, at a concentration above 250 mg/L TiO₂-NPs representing a much higher nano-TiO₂ concentration than currently expected to be present in aquatic ecosystems [14].

As it is already known that nano-TiO₂ is photoinducible and redox active, TiO₂-NPs are considered to be potential generators of reactive oxygen species (ROS) in aquatic organisms [11]. ROS are partially reduced forms of atmospheric oxygen like the superoxide radical (O₂⁻), hydrogen peroxide (H₂O₂) or the hydroxyl radical (OH⁻) and can be viewed as cellular indicators of oxidative stress in organisms [15]. This is a deleterious process that can be an important mediator of damage to cell structures, including lipids and membranes, proteins, and DNA [16]. Under physiological steady state conditions ROS are scavenged by different antioxidative defense mechanisms. Nonenzymatic antioxidants are major cellular redox buffers, for example ascorbate and reduced glutathione (GSH), whereas enzymatic ROS scavenging mechanisms include various antioxidant enzymes [17]. Superoxide dismutase (SOD) catalyzes the dismutation of two superoxide radicals to H₂O₂ and oxygen. The resulting H₂O₂ is reduced by enzymes such as catalase (CAT), peroxidases (POD) and ascorbate peroxidase (APx) [18]. In addition, glutathione reductase (GR) plays a pivotal role in the protection against oxidative cell damage as it catalyzes the reduction of the

oxidized glutathione (GSSG) back to GSH in a NADPH-dependent reaction [19]. Currently, only a few biochemical studies have investigated the effect of TiO₂-NPs on oxidative stress parameters in aquatic organisms. Experiments with the microalgae species *Nitzschia closterium* have revealed time-dependent changes in the activity pattern of SOD, CAT and POD, as the activities were first induced and subsequently inhibited after exposure to 5 mg/L TiO₂-NPs [20]. In a study with the planktonic crustacean *Daphnia magna*, nano-TiO₂ exhibited sublethal toxicity by elevating the levels of antioxidative enzymes such as CAT after exposure to 10 mg/L TiO₂-NPs [21]. Also, Federici et al. [22] have supposed an induction of the antioxidant defense system in rainbow trout (*Oncorhynchus mykiss*) exposed to TiO₂-NP concentrations up to 1 mg/L as a depletion of hepatic total GSH (tGSH) and an increased level of tGSH in the gills was observed. Study results evaluating the potential of TiO₂-NPs to affect ROS levels and antioxidant defense systems in aquatic plants are scarce, despite the fact that they modify aquatic environments through their development and metabolic activity and thus play an important role in aquatic ecosystems [23]. To the best of our knowledge, only one study has previously addressed oxidative stress parameters in a macrophyte after nano-TiO₂ exposure. Song et al. observed increased levels of antioxidative enzymes (CAT, POD and SOD) in *L. minor* after exposure to anatase TiO₂-NPs up to 200 mg/L as well as serious cell damage at a higher TiO₂-NP concentration of 500 mg/L [24]. Thus, as an induction of oxidative stress in macrophytes by TiO₂-NPs seems to be a possible mechanism of their ecotoxicity there is a need for further research on the sublethal toxicity of nano-TiO₂ towards aquatic plants, especially including lower and thus more realistic TiO₂-NP concentration levels. As currently low quantities of nano-TiO₂ in the range of approximately 10 to 10⁻³ µg/L are expected for surface waters [14] this approach would contribute to a proper risk assessment of TiO₂-NPs in the aquatic environment.

The present investigation was therefore designed to study effects of varying concentrations of nano-TiO₂ on the oxidative stress response of the aquatic macrophyte *Hydrilla verticillata* (L.f.) Royle. *H. verticillata* was selected as a model aquatic plant as it is a widely distributed submerged macrophyte which grows in a great variety of aquatic habitats [25]. *H. verticillata* was exposed to different concentrations of TiO₂-NPs (0 mg/L, 0.01 mg/L, 0.1 mg/L, 1 mg/L, 10 mg/L), and the experimental setup thus included currently predicted levels of nano-TiO₂ in surface waters. Additionally, the investigated TiO₂-NPs contributed varying crystalline status (anatase, rutile and anatase/rutile in mixture) to assess a potential

influence of the crystalline phase on their ecotoxicity. In this regard, we focused on H₂O₂ production, the level of GSH and GSSG as well as the activities of the antioxidative enzymes POD, CAT and GR as indicator so the oxidative stress status in the exposed plants. Oxidative stress parameters were assayed and compared to a bulk counterpart to evaluate nano-specific toxicity.

Material and Methods

Plant material

H. verticillata was provided by Extraplant (Extragroup GmbH). Macrophyte cultures were cultivated in a glass tank (60 cm × 60 cm × 60 cm) at 25 ± 1 °C in a 14:10-hour light-dark photoperiod under cool white fluorescent light (38 µE/m²/s). Macrophytes were cultured for 7 d before exposure to assure their acclimation to laboratory conditions. Plants were cultured in a modified 5% Hoagland's nutrient solution which was prepared according to Okupnik et. al. [26].

TiO₂-NPs

In order to propose a potential release into the aquatic environment, 3 commercially available titanium based NPs with different crystallinity status were used. TiO₂ particles used in the present study were from the same batch as those used in our previous study [26]. All TiO₂-NPs were provided as nanopowders. Anatase TiO₂ (100% anatase, < 25 nm, specific surface area 45- 50 m²/g) was purchased from Sigma Aldrich Co. Ltd.. Rutile TiO₂ (100% rutile, 10- 30 nm, specific surface area 50 m²/g) was obtained from Iolitec. The AEROXIDE® P25 TiO₂ nanoparticles (~ 20/80% rutile/anatase, 21 nm, specific surface area of 50 ± 15 m²/g) were provided by the manufacturer Evonik Degussa Corporation.

Preparation of the nanoparticle suspensions and characterization

TiO₂-NP stock solutions (100 mg/L) were prepared by weighing and direct transfer into the test medium. NP suspensions were sonicated in an ultrasonic bath (Allpax Palsson) at 40 kHz for 2 h, as this time proved to be sufficient to increase the dispersion stability of the NP stock solution. To evaluate the stability of such prepared NP suspensions a sedimentation analysis was performed after 24 h by measuring the absorption of light in an

UV/Vis-spectrophotometer (UVIKON 922, Kontron Instrument) at varying wavelengths (290 nm for P25, 320 nm for anatase TiO₂, 328 nm for rutile TiO₂). Therefore, the specific absorption maxima of the different NPs were analysed beforehand. The desired exposure concentrations (0.01 mg/L, 0.1 mg/L, 1 mg/L and 10 mg/L) were prepared by diluting the respective NP stock solution. A characterisation under experimental conditions for zeta potential and size was done in our previous study using a Zetasizer Nano ZS (Malvern Instruments). Before assessment of TiO₂-NP characteristics a zeta potential transfer standard (Malvern Instruments) and a size standard (Thermo Scientific) were analyzed to ensure analytical accuracy. Detailed information regarding the method and TiO₂-NP characteristics is given in our previous study [26].

Exposure scenario

A total biomass of 4.3 ± 0.2 g fresh weight (FW) from *H. verticillata* was exposed to 500 mL of the respective TiO₂-NP solution. Immediately before initiation of the exposure TiO₂-NP stock solutions were sonicated to minimize particle aggregation and sedimentation. To assess nano-specific toxicity a bulk sized counterpart ($< 5 \mu\text{m}$, rutile and small amount of anatase, Sigma Aldrich Co. Ltd.) was included in this investigation. The same preparation method as for the TiO₂-NPs was used for the bulk TiO₂. Additionally, control macrophytes were exposed to culture medium free of TiO₂-NPs in parallel. Due to the importance of the pH level on NPs stability and the biological response of macrophytes, pH values were measured (526 MultiCal, WTW) at the start and the end of the experiment. Controls, nano-TiO₂ and bulk TiO₂ treatments were conducted in quadruplicate. After 24 h of exposure, macrophytes were washed twice with 100 mL of deionized water, shock-frozen in liquid nitrogen and stored at -80°C . The frozen macrophytes were pulverized in liquid nitrogen using a mortar and pestle, and corresponding amounts of the tissue powder were homogenized with a mechanical TissueLyser LT (Quiagen) for 6 min at 50 oscillation/s using two 7 mm stainless steel beads.

Measurement of cell internal hydrogenperoxide

Levels of H₂O₂ were determined colorimetrically according to Jana and Choudhuri [27]. H₂O₂ was extracted by homogenizing 0.2 g of pulverized macrophyte tissue with 3 mL sodium phosphate buffer (50 mM, pH 7.0). The homogenate was centrifuged at 20,800 g

for 15 min at 4 °C and the supernatant was collected. Supernatant amounting to 600 µL was mixed with 200 µL of 0.1% (m/v) titanium chloride in 20% (v/v) H₂SO₄ and the red-orange coloration of titanium peroxide was detected at 410 nm. Three replicates of each sample were monitored in 3 individual measurements of the same sample. As the supernatants were not completely transparent the blank also included sample. H₂O₂ contents were calculated using the extinction coefficient 0.28 L/mmol cm and expressed as µmol/gFW.

Determination of reduced glutathione (GSH) and oxidized glutathione (GSSG)

In order to monitor the glutathione status of *H. verticillata* during exposure the level of GSSG and GSH was determined; the latter by measuring the amount of tGSH, representing GSH and GSSG. Concentrations of tGSH and GSSG were carried out using the GSH spectrophotometrically recycling method according to Aravind and Prasad [28] and Giustarini et al. [29] with modifications. In order to determine the level of GSSG, 0.2 g of pulverized macrophyte tissue was homogenized for 10 min in 0.72 mL of 50 mM Tris base buffer (Tris-(hydroxymethyl)-aminomethane) containing 31 mM of N-ethylmaleimide (NEM) which covalently reacts with GSH in the sample. After derivatization, sample aliquots were acidified with 80 µL of 60% (w/v) Tri-chloroacetic acid (TCA) and again thoroughly mixed for 10 min before centrifugation (Minispin centrifuge 5417 R, Eppendorf, Germany) at 20,800 g for 5 min at 4 °C. The acid de-proteinized supernatant amounting to 250 µL was thereafter extracted with 3 volumes of methylene chloride (Merck, purity ≥ 99.5%) and centrifugation at 20,800 g for 5 min at 4 °C followed to obtain supernatants for GSSG determination. To determine the amount of tGSH, pulverized macrophyte tissue (0.2 g) was homogenized in 0.8 mL 7.5% (w/v) Trichloroacetic acid (TCA) buffer containing 2.3 mM ethylenediaminetetraacetic acid tripotassium salt dihydrate (Tripotassium EDTA). After mixing for 10 min the solution was centrifuged at 20,800 g for 5 min at 4 °C. The concentration of tGSH was measured in the prepared supernatants. Levels of tGSH and GSSG were determined spectrophotometrically via analysis of the increase of absorbance at 412 nm based on the reduction of DTNB (5,5-dithio-bis(2-nitrobenzoic acid)) to TNB (2-nitro-5-thiobenzoic acid) in the presence of 10 U/mL glutathionereductase (GR) and 4.8 mM nicotinamide adenine dinucleotide phosphate (NADPH) in a 200 mM phosphate buffer at 4 °C. Standard curves containing known concentrations of purified solid GSH and GSSG (≥98%) were used for calculating the amount of tGSH and GSSG. The content of GSH was calculated by subtracting GSSG from tGSH.

Enzyme extraction and activity assays

Enzyme extraction was prepared according to Pflugmacher [30] with minor modifications. Pulverized macrophyte tissue (1.5 ± 0.1 g) was resuspended in 3 mL of sodium phosphate buffer (0.1 M, pH 6.5) containing 20% (v/v) glycerol, 1.4 mM dithioerythritol (DTE) and 1 mM ethylenediaminetetraacetic acid (EDTA). The homogenate was centrifuged at 5,400 g for 10 min in an ultracentrifuge (Optima MAX-XP, Beckman Coulter). The supernatant was again centrifuged at 86,900 g for 60 min to collect the microsomal protein fraction. The supernatant was precipitated twice with solid ammonium sulfate (0–35% and 35–80% saturation) with another centrifugation step at 21,700 g for 20 min in between. Solutions were centrifuged for 30 min at 48,900 g and pellets were resuspended in 1 mL of sodium phosphate buffer (20 mM, pH 7). All centrifugations were carried out at 4 °C. Solutions were desalted by gel filtration using sephadex columns (NAP-10, GE Healthcare, UK), immediately snap-frozen in liquid nitrogen and stored at -80 °C for enzyme activity assay. Protein concentrations were determined at 595 nm using the protein dye Bradford, according to the method of Bradford [31]. Bovine serum albumin (BSA) was used as protein standard to generate a calibration curve at 595 nm.

POD was measured using guajacol as substrate, according to Pütter [32] by measuring the POD-catalyzed oxidation of guajacol to tetraguajacol at 436 nm. CAT was measured according to Aebi [33] by monitoring the degradation of H_2O_2 at an absorbance of 240 nm. GR activity was measured according to Carlberg and Mannervik [34] by monitoring the consumption of NADPH during the regeneration of GSH from GSSG at an absorbance of 340 nm. Enzymatic activities were expressed $\mu\text{kat}/\text{mg}$ protein, with [kat] being the conversion rate of 1 mol of substrate per second. Protein concentrations and all enzymatic measurements were performed in triplicate for each replicate.

Statistical analysis

To all data sets, Shapiro-Wilks W test and Levene's test were applied to test normality and homogeneity of variances, respectively. For data sets not normally distributed, a logarithmic (Log10) or square root transformation was applied. If applicable, a one-way analysis of variance (ANOVA) followed by a post-hoc Dunnett test was performed to determine statistical significant differences between the exposure concentration groups and the respective controls. Additionally, changes in the enzyme activity were compared to the

respective bulk exposure scenario to assess nano-specific changes in enzyme activity pattern. Kruskal-Wallis one-way analysis of variance and Mann-Whitney U test were performed for data sets not fitting normal distribution and homogeneity of variances. All data are reported as means \pm standard deviation. Statistical analysis was carried out using commercial software SPSS 21.0 (SPSS Inc.). The comparisons were examined at a significance level of $p < 0.05$.

Results

Effects of nano-TiO₂ on the level of cell internal hydrogenperoxide

No significant alterations ($p > 0.05$) in the level of H₂O₂ were observed in plants treated with rutile and anatase TiO₂ with respect to the control treatments (Figure 1). Moreover, exposure to the bulk counterpart had no effects on H₂O₂ levels. In contrast, exposure to 10 mg/L of P25 caused a significant ($p = 0.017$) increased level of H₂O₂, which was elevated by 30% with respect to the control treatment.

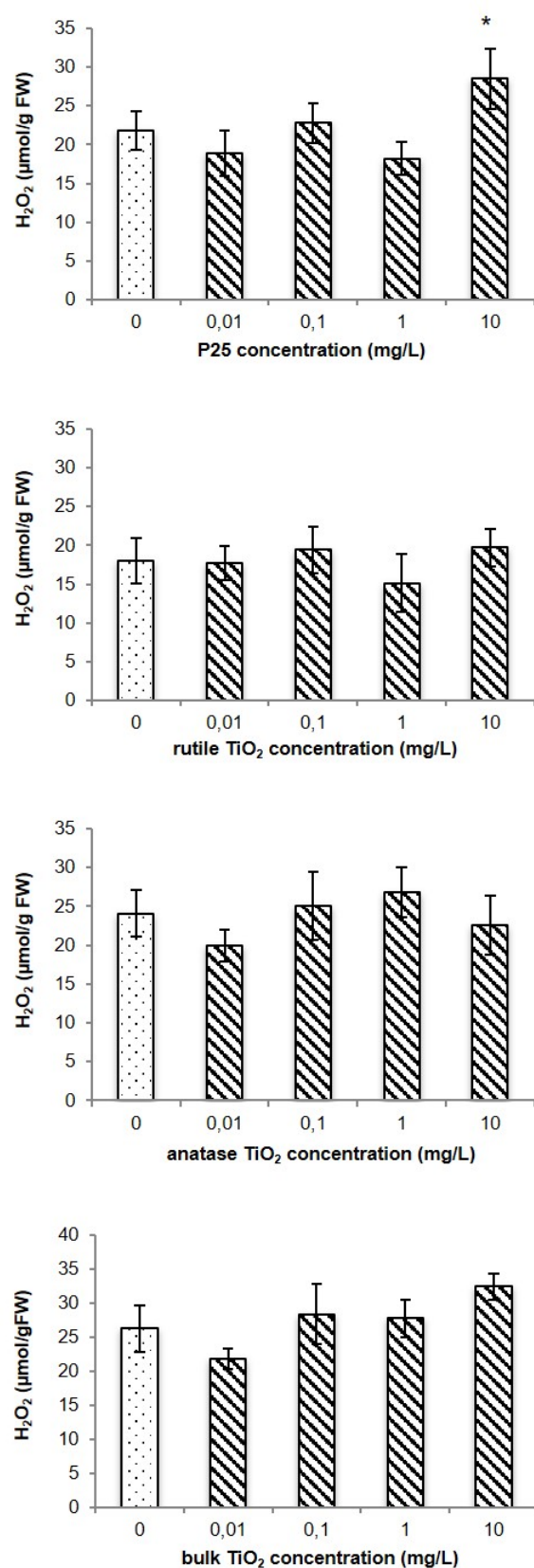


Figure 1. Concentration-dependent formation of hydrogen peroxide (H_2O_2) in *H. verticillata* after 24 h exposure to TiO_2 nanoparticles and bulk TiO_2 . Data are reported as means \pm standard deviation. * $p < 0.05$ versus respective control group

Effects on GSH and GSSG levels

Exposure of *H. verticillata* to nano-TiO₂ caused alterations in the contents of GSH and GSSG for all TiO₂-NPs investigated in the present study (Figure 2). Moreover, compared to the respective control treatments, the amount of GSH decreased at all concentration levels. With the exception of exposure to 1 mg/L rutile TiO₂, the lowered contents of GSH were statistically significant ($p < 0.05$) for all investigated TiO₂-NPs. Exposure to 10 mg/L anatase TiO₂, 0.1 mg/L P25 as well as rutile TiO₂ resulted in the highest decrease of GSH, amounting to 62%, 69% and 48%, respectively. In parallel, the amount of GSSG increased after exposure to TiO₂-NPs. In accordance with their GSH pattern, plants treated with 0.1 mg/L of P25 and rutile TiO₂ showed the highest increase of GSSG levels, surpassing more than 2-fold and 5-fold the respective control values. Plants treated with bulk TiO₂ did not reveal a clear tendency of decreased GSH or induced GSSG levels with respect to the nano-exposures. Exposure to 0.1 mg/L of bulk TiO₂ decreased the amount of GSH, however, this decrease was to a significantly ($p < 0.001$) lesser extent than for all of the investigated nano exposure treatments at this concentration level.

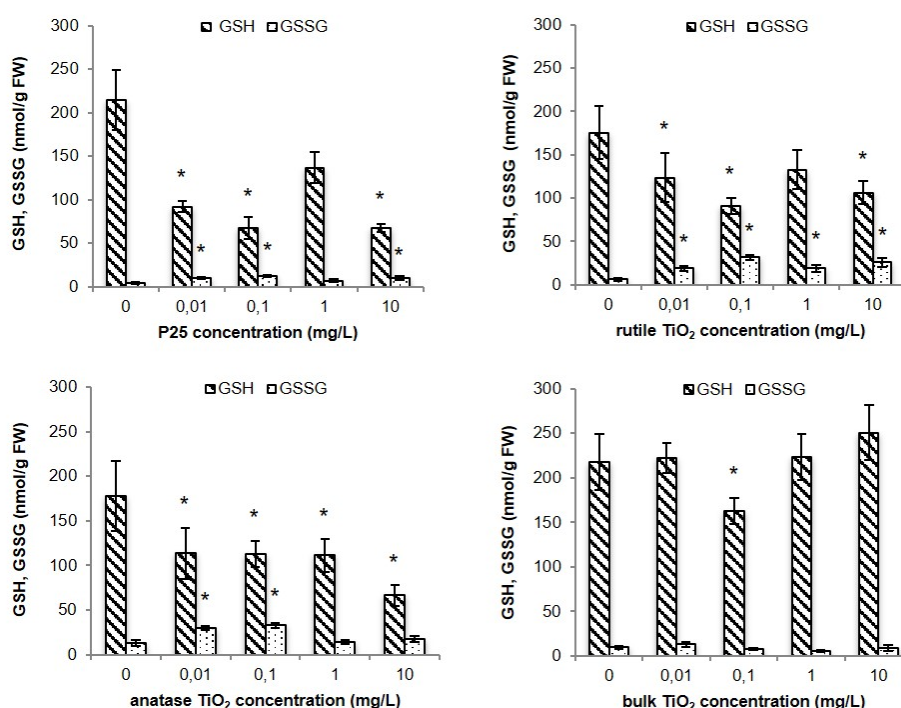


Figure 2. Content of reduced glutathione (GSH) and oxidized glutathione (GSSG) after 24 h exposure to TiO₂ nanoparticles and bulk TiO₂. Data are reported as means \pm standard deviation. * $p < 0.05$ versus respective control group

Effects on antioxidative enzyme activity

Analysis of the POD activity revealed no clear tendency of a changed enzyme activity pattern, neither for plants exposed to TiO₂-NP nor for the bulk TiO₂ exposure. Thus, from this point on, we will focus on how TiO₂-NP exposure affected GR and CAT activities. Compared to the respective control treatments, all TiO₂-NPs showed the tendency to increase the GR activity in a concentration-dependent manner, however, not statistically significant for the P25 exposure scenario. Anatase-TiO₂ showed significantly ($p < 0.001$) increased GR levels at the highest exposure concentration of 10 mg/L. In this case, the level of the GR activity was almost double as high as in plants not exposed to anatase TiO₂. The GR activity was significantly elevated after exposure to 10 mg/L ($p = 0.044$), 1 mg/L ($p = 0.002$) and 0.1 mg/L ($p = 0.02$) rutile TiO₂. Exposure to 1 mg/L of rutile TiO₂ had the highest impact on the GR activity of *H. verticillata*, which was elevated by 48% compared to the control treatment. In plants exposed to bulk TiO₂ the GR levels were not significantly altered, nonetheless, for the highest concentration a slightly elevated enzyme activity could be suggested. Compared to the GR levels of the respective bulk concentrations, all TiO₂-NPs induced higher GR activities over the entire particle concentration range. A significant ($p < 0.01$) enzyme activity elevation was detected after exposure to 1 mg/L of P25, 1 mg/L and 0.1 mg/L of rutile TiO₂ as well as 10 mg/L of anatase TiO₂ (Figure 3A).

Analysis of the CAT activity also revealed a promoted enzyme activity after nano-TiO₂ exposure, whereas in *H. verticillata* exposed to bulk TiO₂ the CAT activity pattern remained unchanged. Plants treated with anatase TiO₂ and P25 showed significantly ($p < 0.05$) increased CAT activities for the highest exposure concentrations with respect to the control group. In accordance to its GR activity pattern, rutile exposure revealed a significantly ($p < 0.05$) increased enzyme activity at a concentration of 0.1 mg/L and all higher concentration levels. Altogether, compared to non-exposed plants the CAT activity was increased by a factor of 2.1, 2.3 and 2.5 after exposure to 10 mg/L of P25, anatase TiO₂ and rutile TiO₂, respectively. Furthermore, all TiO₂-NP induced higher levels of CAT activity at varying particle concentrations compared to the bulk counterpart (Figure 3B). This increase in enzyme activity was significant ($p < 0.05$) for the exposure settings with 10 mg/L P25 as well as 10 mg/L and 0.1 mg/L of rutile TiO₂. Moreover, all concentrations of anatase-TiO₂ exhibited significantly ($p < 0.05$) higher levels of CAT activity compared to the respective bulk TiO₂ concentration.

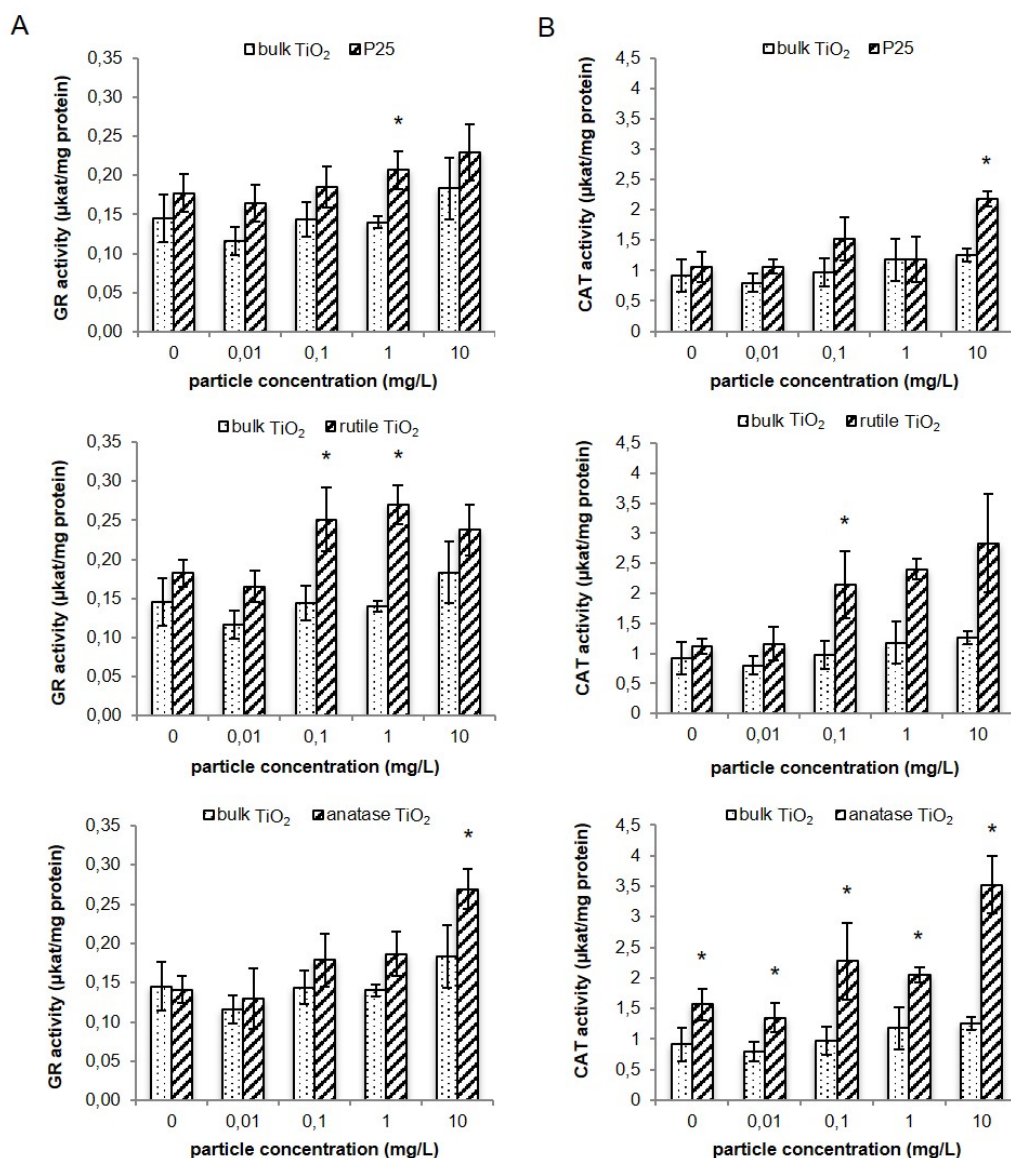


Figure 3. Activity of (A) glutathione reductase (GR) and (B) catalase (CAT) in *H. verticillata* after exposure to TiO₂ nanoparticles and bulk TiO₂. Data are reported as means \pm standard deviation. * $p < 0.05$ versus respective bulk TiO₂ concentration

Discussion

The production of ROS in plant cells plays an important role in the control of various processes like pathogen defense and programmed cell death as ROS act as important signalling molecules [17]. However, stress conditions can disrupt the cellular homeostasis and thus, enhance the production of normally low-level ROS. Therefore, the level of ROS

is kept under tight control and excess ROS can be combated by several antioxidant systems, including the antioxidants ascorbate and GSH as well as antioxidative enzymes [19]. Altogether, they play an important role in the adaptation and survival of plants under abiotic stress conditions, as they function to interrupt the cascades of uncontrolled oxidation [15, 35]. However, if the level of ROS exceeds the antioxidative capacity, the plant suffers so called oxidative stress; a mediator of damage to cell structures, including lipids and membranes, proteins, and DNA [16]. In the present study, oxidative stress effects provoked by TiO₂-NP exposure were investigated in *H. verticillata*, a widely distributed submerged macrophyte which grows in a great variety of aquatic habitats [25]. Analysis of the amount of H₂O₂ was performed, as it is the most representative and potent ROS [19]. The results obtained in the present study imply, that H₂O₂ levels were not influenced after 24 h of exposure to anatase and rutile TiO₂, whereas exposure to the highest exposure level of P25 elevated the production of H₂O₂ by 30%. As the pH rather stayed stable throughout exposure (pH 6.5 to 7.3), a pH-driven ROS formation appears unlikely. Nevertheless, exposure to all investigated TiO₂-NPs stimulated the antioxidative response in *H. verticillata*, as increased activities of the antioxidative enzymes CAT and GR were observed. As this change in the enzyme activity pattern did not occur after exposure to the bulk sized counterpart, a nano-specific influence on antioxidative defense mechanisms in *H. verticillata* can be suggested. The enzyme CAT participates in the main defense system against the accumulation and toxicity of H₂O₂, as it metabolizes the conversion of H₂O₂ into water and oxygen [19]. In the group of H₂O₂-degrading enzymes CATs are unique, as they do not require cellular reducing equivalents [15].

The promoted CAT activity after TiO₂-NPs exposure suggests an increased formation of its substrate H₂O₂, which acted as stimulus for the macrophyte defense system in all nano-TiO₂ treatments. The maintenance of appropriate H₂O₂ levels after anatase and rutile TiO₂ exposure implies that enhanced ROS formation did not exceeded the scavenging ability of CAT. Probably, higher concentrations of anatase and rutile TiO₂ or an extended exposure time might have caused increased H₂O₂ based on an overwhelmed antioxidative defence system in such exposed plants.

Interestingly, study results imply that POD was not considerably activated to counteract an increased level of H₂O₂. Thus, it can be suggested that POD is less sensitive to stress caused by short time and low level TiO₂-NP exposure. This assumption is supported by the study

of Song et al. [24], as significantly increased POD activities in *L. minor* have only been observed after increasing exposure to 100 mg/L anatase TiO₂ for 7 d. In contrast to our findings, exposure to 10 mg/L nano-TiO₂, the lowest exposure concentration in the present study, did not influence the CAT activity. As the characteristics of NPs affect their ecotoxicity, this could be attributed to the larger particle size Song et al. have revealed for comparable concentrations of nano-TiO₂ in their culture media (> 1500 nm vs. < 500 nm). Exposure with large particles, exhibiting a small surface-to-volume ratio, may have contributed to a lower interaction of anatase-TiO₂ with *L. minor*. Furthermore, it is known that macrophytes can display individual strategies against oxidative stress [36] and the present study investigated oxidative stress responses of *H. verticillata*, thus another plant species.

Consistent with increased CAT activities the observation of changes in the GR activity pattern imply an ongoing detoxification of ROS in *H. verticillata* after TiO₂-NP exposure for 24 h. Exposure to bulk TiO₂ did not reveal changes in the enzyme activity, hence, the study results once again indicate a nano-specific influence on the antioxidative system. GR catalyzes the NADPH-dependent reduction of GSSG to GSH and thus, plays a key role in sustaining the GSH pool [19]. GSH is one of the most important components of the antioxidative defence system in plants, as it participates in the ascorbate-GSH cycle and is the reducing equivalent for the enzyme glutathione peroxidase (GPx) which catalyzes the detoxification of H₂O₂ [15]. Moreover, GSH is not only important for H₂O₂ removal as it also acts as a co-substrate for the conjugation reaction with electrophilic xenobiotics catalyzed by glutathione S-transferases [19]. Both the depletion of intracellular GSH and the increased amount of GSSG evidenced the potential of TiO₂-NPs to influence the level of antioxidants even after a short exposure time of 24 h. In accordance, another study demonstrated that long-term exposure (14 d) with nano-TiO₂ can affect the glutathione status of aquatic organisms, as the level of tGSH in rainbow trout was elevated in gill and decreased in the liver after exposure to 1 mg/L and 0.5 mg/L of P25, respectively [22]. Referring to the observed changes in the contents of GSH and GSSG after nano-TiO₂ exposure, it can be proposed that the glutathione status in *H. verticillata* is a sensitive indicator for oxidative stress caused by TiO₂-NP, because already low level concentrations revealed a significant raise or decline of GSH and GSSG, respectively. This redox unbalance is an obvious sign of a high metabolic activity of GSH-dependent enzymes in the plant, which aimed at protecting against the destructive effects of ROS generated during nano-

TiO₂ exposure. Hence, a putative activation of the ascorbate-GSH cycle as well as GPx can be evidenced for *H. verticillata* exposed to nano-TiO₂. This assumption was confirmed by the elevation of the GR activity, which probably aimed to face the need for increased amounts of GSH. However, changes in GR activity pattern were not sufficient to maintain the GSH/GSSG ratio. Especially exposure to P25 revealed a large decrease in GSH, which was consistent with the lack of a significant increased GR activity when compared to the control treatment. Probably, a longer exposure scenario with further time-dependent GR activity increases would have revealed a normalization of the GSH content or at least would have brought the amount of GSH at a constant level, as it has been observed in a previous study with another macrophyte exposed to a cyanobacterial toxin [37]. Referring to the available data for a 24 h nano-TiO₂ exposure, a proper scavenging of ROS in exposed *H. verticillata* via GSH-dependent pathways can be questioned. Nevertheless, this emphasizes the important role of CAT for H₂O₂ metabolism in exposed *H. verticillata*, which does not depend on GSH and seemed to be sufficient to keep the amount of H₂O₂ constant for plants exposed to anatase TiO₂ and rutile TiO₂. In contrast, high concentrations of P25 probably increased H₂O₂ to a level overwhelming the capacity of CAT, which showed the lowest increase of its activity compared with all other TiO₂-NPs of the present study. Due to the drop of GSH other H₂O₂-degradating enzymes, such as GPx and APx, were not able to fill this role adequately.

In general, the results of the present study suggest NP-specific effects on the antioxidative system of *H. verticillata*, although TiO₂-NPs formed larger sized aggregates in the exposure media (438nm, -22mV for P25; 525nm, -26mV for rutile TiO₂, 489nm, -22mV for anatase TiO₂). Furthermore, the antioxidative defense system of macrophytes seems not to be predominantly affected by a specific crystalline phase of TiO₂, as all investigated TiO₂-NP revealed similar patterns of enzyme activation and GSH/GSSG ratio depletion, especially when compared to the bulk-sized counterpart. The investigated biomarkers chosen as oxidative stress related parameters were useful in assessing the health of the macrophytes. The results of the present study implied adaptations of these after TiO₂-NP exposure, however, it can be suggested that macrophytes are able to cope with currently predicted concentrations of TiO₂-NPs in the range of approximately 10 - 10⁻³ µg/L in surface waters [14]. This assumption is based on the fact that particularly higher exposure concentrations exhibited the potential to influence the antioxidative defense system and ROS status in *H. verticillata*. Moreover, activities of the enzymatic defense enzymes CAT and GR were

activated which is considered as an indication of low-level stress [24]. Nevertheless, short-term TiO₂-NP exposures caused adaptations of macrophytes antioxidative defense system, but any statement regarding the localisation of the ROS generation in *H. verticillata* can only be considered as an assumption. However, an intracellular formation of ROS is unlikely as the investigated TiO₂-NPs formed large sized aggregates. These aggregates would have been unable to penetrate through the cell wall and transport across the plasma membrane. Moreover, the significant differences between plants treated with TiO₂-NPs and bulk TiO₂ might be a result of an external localized cell wall damage followed by a ROS driven lipid peroxidation of the cell membrane. This assumption is in accordance with the study by Song et al. [24] as increased contents of Malondialdehyde, a decomposition product of polyunsaturated fatty acids of membranes, were observed after nano-TiO₂ exposure. The putative increased NP influx into plant cells might have caused intracellular ROS generation after interaction with oxidative organelles like chloroplasts and mitochondria.

As the concentration of TiO₂-NPs will probably elevate in the future due to rapidly increasing production volumes, the question remains as to whether higher exposure concentrations are able to cause severe damage to macrophytes due to oxidative stress effects. The present study mainly investigated adaptations of the antioxidative defense system after exposure to TiO₂-NPs exceeding the µg/L range and thus, assumptions regarding a worst-case scenario can be made. The antioxidant enzymatic and non-enzymatic response in such exposed macrophytes suggests, that even though plant stress became obvious the continued activity of the antioxidative enzymes was able to counteract the increased ROS production. Exposure solely to 10 mg/L of P25 caused elevated levels of H₂O₂. This represents a concentration 1,000 times higher than environmentally relevant and thus, it seems to be unlikely that an overproduction of ROS in plant cells is a mode of nano-toxicity after short-term exposure to high TiO₂-NP concentrations. Nevertheless, an ongoing sedimentation of NP aggregates in the respective suspensions became apparent by a decreased turbidity after 24 h of exposure. Moreover, suspension instability was proven by the sedimentation analysis of the NP stock solutions, which revealed a decreased optical absorbance around 78%, 65% and 51% for P25, rutile TiO₂ and anatase TiO₂, respectively. In relation to that, decreased TiO₂-NP concentrations in the water column with increased exposure time can be suggested due to aggregate formation, which will also be the likely natural fate and behavior of NPs in aquatic ecosystems [38]. However, even after

considering a decrease in the originally exposure concentration of 10 mg/L of P25 during exposure, it appears unlikely that the respective exposure concentrations reached the currently predicted environmental concentrations after 24 h. Moreover, it should be taken into account that effects on the antioxidative apparatus of *H. verticillata* were assessed after 24 h and thus, after a relatively short exposure time. Even if TiO₂-NPs will be removed out of the water column due to aggregation, macrophytes might suffer from long-term exposure to TiO₂-NPs. Assuming a continuous release of nano-TiO₂ into the aquatic environment TiO₂-NPs and therefore a chronic exposure of the inhabiting organisms to TiO₂-NPs, they may thus be considered as pseudo-persistent contaminants. Therefore, future research will focus on time-dependent alterations of ROS status and enzymatic defense in *H. verticillata* to get further insight into the antioxidative response of macrophytes after TiO₂-NP exposure.

Conclusion

In the present study, oxidative stress effects in *H. verticillata* caused by TiO₂-NPs of various crystallinity statuses were investigated. Exposure to each of the investigated TiO₂-NPs respectively, stimulated the antioxidative response in *H. verticillata*, as a concentration-dependent increase in activities of the antioxidative enzymes CAT and GR were observed. No significant changes in enzyme activities were observed for the treatments with a bulk sized counterpart and moreover, plants exposed to bulk-TiO₂ exhibited lower enzyme activities at all concentration steps. Thus, a nano-specific influence on antioxidative defense mechanisms can be suggested. Moreover, promoted CAT activities suggest an increased formation of its substrate, H₂O₂, which was solely elevated after exposure to 10 mg/L P25, suggesting that the prevalent ROS formation after exposure to anatase and rutile TiO₂ did not overwhelm the compensatory capacity of CAT. As POD was not considerably activated in the present study it could be suggested that it is less sensitive to oxidative stress caused by nano-TiO₂ and thus does not play a pivotal role to counteract excess H₂O₂ in plant cells after such exposures. However, a high metabolic activity of the H₂O₂-degradating enzymes APx and GPx, which require GSH as cellular reducing equivalent, could be suggested as a shift in the GSH/GSSG ratio was observed after exposure with all investigated TiO₂-NPs. Furthermore, the GSH status in *H. verticillata* appears to be a sensitive indicator for oxidative stress caused by TiO₂-NP exposure, because already low nano-TiO₂ concentrations decreased the amount of GSH and increased the level of GSSG. Although GR activity was elevated, the change in enzyme activity seemed not to be sufficient to

maintain the physiological GSH/GSSG ratio. Considering currently expected quantities of nano-TiO₂ in surface waters, it can be concluded that macrophytes are able to cope with environmentally relevant concentrations of TiO₂-NPs. Furthermore, the antioxidative defense system of macrophytes was not predominantly affected by a specific crystalline phase of TiO₂, and thus none of them should be excluded for future research approaches. To the best of our knowledge, this is the first study evaluating oxidative stress effects of TiO₂-NPs on an aquatic macrophyte, including different crystal structures of TiO₂ as well as currently predicted levels of nano-TiO₂ in surface waters. Together with future study results on time-dependent alterations of the ROS status and enzymatic defense in *H. verticillata* a further insight into the antioxidative response of macrophytes after TiO₂-NP exposure will be achieved.

Acknowledgement

The authors acknowledge V. Contardo-Jara for her support during the planning phase of the study as well as S. Kühn for her support and assistance in the laboratory. Moreover, we thank M. Esterhuizen-Londt for proof-reading of the manuscript.

Reference list

- [1] Shukla RK, Sharma V, Pandey AK, Singh S, Sultana S, Dhawan A. 2011. ROS-mediated genotoxicity induced by titanium dioxide nanoparticles in human epidermal cells. *Toxicol in Vitro* 25:231-241.
- [2] Diebold U. 2003. The surface science of titanium dioxide. *Surf Sci Rep* 48:53-229.
- [3] Weir A, Westerhoff P, Fabricius L, Hristovski K, von Goetz N. 2012. Titanium dioxide nanoparticles in food and personal care products. *Environ Sci Technol* 46:2242-2250.
- [4] Varner KE, Rindfusz K, Gaglione A, Viveiros E. 2010. Nano titanium dioxide environmental matters. EPA/600/R-10/089. State-Of-The-Science Review. US Environmental Protection Agency, Washington, DC.
- [5] Klaine SJ, Alvarez PJJ, Batley GE, Fernandes TF, Handy RD, Lyon DY, Mahendra S, McLaughlin MJ, Lead JR. 2008. Nanomaterials in the environment: Behavior, fate, bioavailability, and effects. *Environ Toxicol Chem* 27:1825-1851.
- [6] Skocaj M, Filipic M, Petkovic J, Novak S. 2011. Titanium dioxide in our everyday life; is it safe? *Radiol Oncol* 45:227-247.
- [7] Handy RD, Owen R, Valsami-Jones E. 2008. The ecotoxicology of nanoparticles and nanomaterials: current status, knowledge gaps, challenges, and future needs. *Ecotoxicology* 17:315-325.
- [8] Sadiq IM, Dalai S, Chandrasekaran N, Mukherjee A. 2011. Ecotoxicity study of titania (TiO₂) NPs on two microalgae species: *Scenedesmus* sp and *Chlorella* sp. *Ecotox Environ Safe* 74:1180-1187.
- [9] Aruoja V, Dubourguier HC, Kasemets K, Kahru A. 2009. Toxicity of nanoparticles of CuO, ZnO and TiO₂ to microalgae *Pseudokirchneriella subcapitata*. *Sci Total Environ* 407:1461-1468.
- [10] Wang JX, Zhang XZ, Chen YS, Sommerfeld M, Hu Q. 2008. Toxicity assessment of manufactured nanomaterials using the unicellular green alga *Chlamydomonas reinhardtii*. *Chemosphere* 73:1121-1128.
- [11] Menard A, Drobne D, Jemec A. 2011. Ecotoxicity of nanosized TiO₂. Review of in vivo data. *Environ Pollut* 159:677-684.
- [12] Li L, Sillanpaa M, Tuominen M, Lounatmaa K, Schultz E. 2013. Behavior of titanium dioxide nanoparticles in *Lemna minor* growth test conditions. *Ecotox Environ Safe* 88:89-94.

- [13] Kim E, Kim SH, Kim HC, Lee SG, Lee SJ, Jeong SW. 2011. Growth inhibition of aquatic plant caused by silver and titanium oxide nanoparticles. *Toxicology and Environmental Health Sciences* 3:1-6.
- [14] Gottschalk F, Sun T, Nowack B. 2013. Environmental concentrations of engineered nanomaterials: review of modeling and analytical studies. *Environ Pollut* 181:287-300.
- [15] Mittler R. 2002. Oxidative stress, antioxidants and stress tolerance. *Trends Plant Sci* 7:405-410.
- [16] Valko M, Leibfritz D, Moncol J, Cronin MTD, Mazur M, Telser J. 2007. Free radicals and antioxidants in normal physiological functions and human disease. *Int J Biochem Cell B* 39:44-84.
- [17] Apel K, Hirt H. 2004. Reactive oxygen species: Metabolism, oxidative stress, and signal transduction. *Annu Rev Plant Biol* 55:373-399.
- [18] Asada K. 1992. Ascorbate Peroxidase - a Hydrogen Peroxide-Scavenging Enzyme in Plants. *Physiol Plantarum* 85:235-241.
- [19] Gill SS, Tuteja N. 2010. Reactive oxygen species and antioxidant machinery in abiotic stress tolerance in crop plants. *Plant Physiol Biochem* 48:909-930.
- [20] Xia B, Chen BJ, Sun XM, Qu KM, Ma FF, Du MR. 2015. Interaction of TiO₂ nanoparticles with the marine microalga *Nitzschia closterium*: Growth inhibition, oxidative stress and internalization. *Sci Total Environ* 508:525-533.
- [21] Kim KT, Klaine SJ, Cho J, Kim SH, Kim SD. 2010. Oxidative stress responses of *Daphnia magna* exposed to TiO₂ nanoparticles according to size fraction. *Sci Total Environ* 408:2268-2272.
- [22] Federici G, Shaw BJ, Handy RD. 2007. Toxicity of titanium dioxide nanoparticles to rainbow trout (*Oncorhynchus mykiss*): Gill injury, oxidative stress, and other physiological effects. *Aquat Toxicol* 84:415-430.
- [23] Madsen JD, Chambers PA, James WF, Koch EW, Westlake DF. 2001. The interaction between water movement, sediment dynamics and submersed macrophytes. *Hydrobiologia* 444:71-84.
- [24] Song GL, Gao Y, Wu H, Hou WH, Zhang CY, Ma HQ. 2012. Physiological effect of anatase TiO₂ nanoparticles on *Lemna minor*. *Environ Toxicol Chem* 31:2147-2152.
- [25] Cook CDK, Luond R. 1982. A Revision of the genus *Hydrilla* (Hydrocharitaceae). *Aquat Bot* 13:485-504.

- [26] Okupnik A, Contardo-Jara V, Pflugmacher S. 2015. Potential role of engineered nanoparticles as contaminant carriers in aquatic ecosystems: Estimating sorption processes of the cyanobacterial toxin microcystin-LR by TiO₂ nanoparticles. *Colloid Surface A* 481:460-467.
- [27] Jana S, Choudhuri MA. 1982. Glycolate metabolism of 3 submersed aquatic angiosperms during aging. *Aquat Bot* 12:345-354.
- [28] Aravind P, Prasad MN. 2005. Cadmium-induced toxicity reversal by zinc in *Ceratophyllum demersum* L. (a free floating aquatic macrophyte) together with exogenous supplements of amino- and organic acids. *Chemosphere* 61:1720-1733.
- [29] Giustarini D, Dalle-Donne I, Colombo R, Milzani A, Rossi R. 2003. An improved HPLC measurement for GSH and GSSG in human blood. *Free Radical Bio Med* 35:1365-1372.
- [30] Pflugmacher S. 2004. Promotion of oxidative stress in the aquatic macrophyte *Ceratophyllum demersum* during biotransformation of the cyanobacterial toxin microcystin-LR. *Aquat Toxicol* 70:169-178.
- [31] Bradford MM. 1976. A rapid and sensitive method for the quantitation of microgram quantities of protein utilizing the principle of protein-dye binding. *Analytical biochemistry* 72:248-254.
- [32] Pütter J. 1974. Peroxidases. In Bergmeyer HU, eds, *Methods of Enzymatic Analysis*, Vol 2. Academic Press, New York, pp 685-690.
- [33] Aebi M. 1974. Catalase. In Bergmeyer HU, eds, *Methods of Enzymatic Analysis*, 2nd ed, Vol 2. Academic Press, New York, pp 673-684.
- [34] Carlberg I, Mannervik B. 1985. Glutathione reductase. *Method Enzymol* 113:484-490.
- [35] Noctor G, Foyer CH. 1998. Ascorbate and glutathione: Keeping active oxygen under control. *Annu Rev Plant Physiol Plant Mol Biol* 49:249-279.
- [36] Romero-Oliva CS, Contardo-Jara V, Pflugmacher S. 2015. Antioxidative response of the three macrophytes *Ceratophyllum demersum*, *Egeria densa*, and *Hydrilla verticillata* to a time dependent exposure of cell-free crude extracts containing three microcystins from cyanobacterial blooms of Lake Amatitlan, Guatemala. *Aquat Toxicol* 163:130-139.
- [37] Pflugmacher S. 2004. Promotion of oxidative stress in the aquatic macrophyte *Ceratophyllum demersum* during biotransformation of the cyanobacterial toxin microcystin-LR. *Aquat Toxicol* 70:169-178.

-
- [38] Handy RD, Cornelis G, Fernandes T, Tsyusko O, Decho A, Sabo-Attwood T, Metcalfe C, Steevens JA, Klaine SJ, Koelmans AA, Horne N. 2012. Ecotoxicity test methods for engineered nanomaterials: practical experiences and recommendations from the bench. *Environ Toxicol Chem* 31:15-31.

Appendix III

Publication III

Oxidative stress mediated toxicity of TiO₂ nanoparticles after a concentration and time dependent exposure of the aquatic macrophyte *Hydrilla verticillata*

Annette Spengler, Lena Wanninger, Stephan Pflugmacher

This work was published in Aquatic Toxicology (2017) 190, 32-39.

DOI: <http://dx.doi.org/10.1016/j.aquatox.2017.06.006>

Own contribution:

Literature review

Design of the experiments

Plant culture

Sedimentation analysis

Enzyme extraction and activity analysis

Interpretation of the experimental results

Statistical analysis

Manuscript preparation

Revision of the manuscript according to the reviewers' comments

Abstract

The present study focused on oxidative stress effects in the aquatic macrophyte *Hydrilla verticillata* after exposure to titanium dioxide nanoparticles (TiO₂-NPs). Experiments were conducted with different TiO₂-NPs and concentrations (0.1 mg/L and 10 mg/L) in a time-dependent manner (0 h, 24 h, 48 h, 96 h, 168 h). To assess various levels of the oxidative stress response in *H. verticillata*, the level of hydrogen peroxide (H₂O₂), the ratio of reduced to oxidized glutathione (GSH/GSSG), and activities of the antioxidative enzymes catalase (CAT) and glutathione reductase (GR) were evaluated. Study results imply oxidative stress effects after TiO₂-NP exposure as adaptations in plants metabolism became apparent to counteract increased ROS formation. All TiO₂-NPs caused elevated activities of the enzymes CAT and GR. Moreover, decreased ratios of GSH/GSSG indicated an activation of GSH dependent pathways counteracting ROS formation. Plants exposed to a bulk-sized control revealed a size-dependent influence on the antioxidative stress response. As H₂O₂ level increases were solely detected after exposure to 10 mg/L TiO₂-NPs and nano-exposed plants showed normalization in its antioxidative stress response after 168 h of exposure, it can be suggested that macrophytes are able to cope with currently predicted low-level exposures to TiO₂-NPs.

Introduction

Due to increasing production volumes, titanium dioxide nanoparticles (TiO₂-NPs) will inevitably reach water bodies through wastewater and urban runoff. Thus, concerns about the fate and behavior of nano-TiO₂ in the aquatic environment have arisen and suggest the need for increased research activities leading to a more thorough risk assessment and management of nano-TiO₂. TiO₂ is a naturally occurring mineral that can exist in three crystalline forms, known as rutile, anatase, and brookite. Regarding its ecotoxicity potential, TiO₂-NPs are an extensively studied class of metal oxide NPs. This large amount of toxicity data can probably be ascribed to the fact that TiO₂-NPs were the first NPs made commercially available to various industrial and research activities (Kim et al., 2011). Nano-exposure of the aquatic environment involves the risk that the normally balanced ecosystem may be disrupted, due to toxic effects towards aquatic organisms living in the aquatic environment. Emerging literature regarding the toxicity of TiO₂-NPs in aquatic ecosystems has primarily concentrated on the ecotoxicity of nano-TiO₂ towards freshwater algae

(Aruoja et al., 2009; Sadiq et al., 2011; Wang et al., 2008). Only few studies have investigated nano-toxicity towards aquatic plants, even though they modify aquatic environments through their development and metabolic activity and thus, play an important role in marine and freshwater systems (Madsen et al., 2001). Initially, research activities mainly focused on the effects of TiO₂-NPs on the growth rate and chlorophyll content of macrophytes (Kim et al., 2011; Li et al., 2013), not taking into account the microresponse after nano-TiO₂ exposure. This is a relevant mode of NP-driven toxicity as TiO₂-NPs are considered to be potential generators of reactive oxygen species (ROS) in aquatic organisms (Menard et al., 2011), which are partially reduced forms of atmospheric oxygen like the superoxide radical (O₂^{•-}), hydrogen peroxide (H₂O₂) or the hydroxyl radical (•OH). ROS represent cellular indicators of oxidative stress in organisms (Mittler, 2002), a deleterious process that can be an important mediator of damage to cell structures, including lipids and membranes, proteins, and DNA (Valko et al., 2007). Plants resistance to environmental stresses is linked with the capability of its antioxidative system implicating various antioxidant enzymes and antioxidants. Ascorbate and reduced glutathione (GSH) are major cellular redox buffers, which provide reducing equivalents for the ROS reduction. An efficient destruction of O₂^{•-} and H₂O₂ depends on the action of several antioxidant enzymes acting in synchrony (Noctor and Foyer, 1998). The superoxide dismutase (SOD) catalyzes the dismutation of two O₂^{•-} to H₂O₂ and oxygen. The resulting H₂O₂ is reduced by the enzymes catalase (CAT), peroxidases (POD), ascorbate peroxidase (APx) and glutathione peroxidase (GPx) (Asada, 1992). Both, APx and GPx, require GSH as a cellular reducing equivalent for H₂O₂ removal and moreover, GSH acts as a co-substrate for the conjugation reaction with electrophilic xenobiotics catalyzed by glutathione *S*-transferases. To counteract a depletion of intracellular GSH the enzyme glutathione reductase (GR) plays a pivotal role in the protection against oxidative cell damage as it catalyzes the reduction of the oxidized glutathione (GSSG) back to GSH in a NADPH-dependent reaction (Gill and Tuteja, 2010). There is evidence that TiO₂-NPs affect the antioxidative defense response of aquatic organisms like algae, planktonic crustacean and fish (Federici et al., 2007; Kim et al., 2010; Xia et al., 2015). Currently, ecotoxicity testing of the induction of oxidative stress parameters in aquatic plants are scarce. However, a study conducted with *Lemna minor* L. has observed increased levels of antioxidant defense enzymes (CAT, POD and SOD) after high-level TiO₂-NP exposure for 7 d (Song et al., 2012). Moreover, our previous study revealed that already concentrations of less than 10 mg/L of TiO₂-NPs are able to influence activities of antioxidant defense enzymes as well as the level of GSH after exposure of

Hydrilla verticillata (L.f.) Royle for 24 h. Furthermore, compared to a bulk sized counterpart the effects seemed to be related to the smaller size of the TiO₂-NP, even after forming large scale aggregates after dispersion in the exposure medium (Okupnik and Pflugmacher, 2016). Thus, TiO₂-NPs are able to induce oxidative stress in macrophytes and future research should devote more attention to this specific mode of nano-toxicity towards aquatic plants.

In the present study, experiments were conducted with TiO₂-NPs of varying crystalline statuses (anatase, rutile, P25-mixed phase). To elucidate the stability of the respective NP suspensions over time, a sedimentation analysis was performed by examining changes of the particle size and particle concentration *via* dynamic light scattering (DLS) and measurements of optical absorbance in an ultraviolet-visible (UV/Vis)-spectrophotometer, respectively. For ecotoxicity testing *H. verticillata* was exposed to TiO₂-NPs (0.1 mg/L; 10 mg/L) in a time-dependent manner (0h, 24h, 48h, 96h and 168h). *H. verticillata* is a widely distributed submerged macrophyte which grows in a great variety of aquatic habitats (Cook and Luond, 1982) and thus, was selected as model aquatic plant. As previous research almost exclusively focused on changes of physiological parameters after nano-TiO₂ exposure, the main objective of this study was to investigate alterations of various biochemical markers over time. Hence, the production of H₂O₂, the GSH status (content of GSH and GSSG) and antioxidative enzyme activities (CAT and GR) were studied as oxidative stress related parameters. To the best of our knowledge, this is the first study investigating time-dependent changes of oxidative stress related parameters in macrophytes after TiO₂-NP exposure.

Material and Methods

Plant material

H. verticillata was provided by Extraplant (Extragroup GmbH, Germany). Macrophyte cultures were cultivated in a glass tank (60 cm × 60 cm × 60 cm) at 25 ± 1 °C in a 14:10-hour light-dark photoperiod under cool white fluorescent light (38 µE/m²/s). To assure plants acclimation to laboratory conditions, macrophytes were cultured for 7 d before starting TiO₂-NP exposure. A 5% modified Hoagland's nutrient solution according to our

previous studies (Okupnik et al., 2015; Okupnik and Pflugmacher, 2016) was used as culture medium providing optimal conditions for macrophyte growth.

TiO₂-NPs

In order to propose a potential release into the aquatic environment, three titanium based NPs with different crystallinity statuses were used. All TiO₂-NPs were provided as water-insoluble nanopowders and were from the same batch as in our previous studies (Okupnik et al., 2015; Okupnik and Pflugmacher, 2016). Anatase TiO₂ (100% anatase, < 25 nm, specific surface area 45- 50 m²/g, purity 99.7%) was purchased from Sigma Aldrich Co. Ltd. (Germany). Rutile TiO₂ (100% rutile, 10- 30 nm, specific surface area 50 m²/g, purity 99.5%) was obtained from Iolitec (Germany). The AEROXIDE® P25 TiO₂ nanoparticles (~ 20/80% rutile/anatase, 21 nm, specific surface area of 50 ± 15 m²/g, purity 99.9%) were provided by the manufacturer Evonik Degussa Corporation (Germany).

Preparation of the nanoparticle suspensions

TiO₂-NP stock solutions (100 mg/L) were prepared by weighing and direct transfer into the test medium. NP suspensions were sonicated in an ultrasonic bath (Allpax Palsson, Germany) at 40 kHz. A sonication time of 2 h proved to be sufficient to increase the dispersion stability of the NP stock solution. Exposure concentrations of 0.1 mg/L and 10 mg/L were prepared by diluting the respective NP stock solution with the test medium.

Characterization and behavior of TiO₂-nanoparticles in the exposure medium

NPs morphology was verified *via* ultra-high resolution scanning electron microscope analysis in our previous study which further provides detailed information regarding the characterization methods (Okupnik et al., 2015). The characterization under experimental conditions for NP size was done using a Zetasizer Nano ZS (Malvern Instruments, Germany). To evaluate the stability of the three investigated TiO₂-NP suspensions throughout the entire exposure time, a settling experiment was conducted. As an earlier sedimentation analysis, solely performed after 24 h of sedimentation, indicated instability of the investigated TiO₂-NP suspensions (Okupnik and Pflugmacher, 2016) a comprehensive sedimentation study combined with a particle size analysis was performed over a time span of 168 h. Results of the sedimentation analysis provided the basis for

decisions regarding the exposure medium renewal during the experiments, aiming at a steadily exposure of the test organism. The respective TiO₂-NP stock solutions were prepared as explained previously and left for sedimentation. During a test period of 168 h, aliquots of the dispersion were carefully taken from the supernatant at a certain height to avoid disturbance of the sedimentation process. The states of sedimentation were observed after 1 h, 3 h, 6 h, 24 h, 48 h, and 168 h. Changes of the z-average hydrodynamic diameter were determined by dynamic light scattering (DLS) and were performed in triplicate with each measurement being an average of 5 runs of 10 seconds. Moreover, the absorption of light was measured in an UV/Vis-spectrophotometer (UVIKON 922, Kontron Instrument, Italy) at varying wavelengths (290 nm for P25, 320 nm for anatase TiO₂, 328 nm for rutile TiO₂). Therefore, the specific absorption maxima of the different NPs were analyzed beforehand. Each of the TiO₂-NP experiments were run in triplicate and the results presented are the average of the runs. The change of optical absorbance with time can be related to the normalized NP concentration C/C_0 where C represents the concentration in time, and C_0 is the initial concentration.

Exposure scenario

A total biomass of 3.5 ± 0.1 g fresh weight (FW) from *H. verticillata* was exposed to 500 ml of the respective TiO₂-NP solution (0.1 mg/L and 10 mg/L) under culture conditions described above. Immediately before initiation of the exposure, TiO₂-NP stock solutions were sonicated to minimize particle aggregation and sedimentation. To assess nano-specific toxicity, a bulk sized counterpart ($< 5 \mu\text{m}$, purity $\geq 99.9\%$, rutile and small amount of anatase, Sigma Aldrich Co. Ltd., Germany) was included in this investigation. The same preparation method as described above was used for bulk TiO₂. Additionally, control macrophytes were exposed to culture medium free of TiO₂-NP in parallel, to evaluate the effects of the experimental conditions. Controls, nano-TiO₂, and bulk TiO₂ treatments were independently replicated four times. To avoid progressing NP sedimentation during the experiment evidently leading to lowered exposure concentrations, the exposure medium was renewed every 24 h for all particle treatments as well as the control treatment. After 24 h, 48 h, 96 h, and 168 h of exposure, macrophytes were washed twice with 100 ml of deionized water, shock-frozen in liquid nitrogen and stored at -80°C . To assess the condition of macrophytes at the start of the experiment, 0 h-control macrophytes were directly taken from the tank. The frozen macrophytes were pulverized in liquid nitrogen using a mortar

and pestle and corresponding amounts of the tissue powder were homogenized with a mechanical TissueLyser LT (Quiagen, Germany) for 6 min at 50 oscillation/s using two 7 mm stainless steel beads.

Measurement of cell internal hydrogenperoxide

Levels of H₂O₂ were determined colorimetrically according to Jana and Choudhuri (1982). For detailed information regarding sample preparation we refer to our previous study (Okupnik and Pflugmacher, 2016). H₂O₂ contents were calculated using the extinction coefficient 0.28 L/ mmol cm and expressed as $\mu\text{mol g/FW}$.

Determination of reduced glutathione (GSH) and oxidized glutathione (GSSG)

In order to monitor the glutathione status of *H. verticillata* during exposure the level of GSSG and GSH was determined; the latter by measuring the amount of total glutathione (tGSH), representing GSH and GSSG. Concentrations of tGSH and GSSG were carried out using the GSH spectrophotometrically recycling method according to Aravind and Prasad (2005) and Giustarini et al. (2003) with modifications as described in our previous study (Okupnik and Pflugmacher, 2016).

Enzyme extraction and activity assays

Enzyme extraction was prepared according to Pflugmacher (2004) with minor modifications (Okupnik and Pflugmacher, 2016). Protein concentrations were determined at 595 nm using the protein dye Bradford, according to the method of Bradford (1976). Bovine serum albumin (BSA) was used as protein standard to generate a calibration curve at 595 nm. CAT activity was measured according to Aebi (1974) by monitoring the degradation of H₂O₂ at an absorbance of 240 nm. GR activity was measured according to Carlberg and Mannervik (1985) by monitoring the consumption of NADPH during the regeneration of GSH from GSSG at an absorbance of 340 nm. Enzymatic activities were expressed in $\mu\text{kat/mg protein}$ or nkat/mg protein , with [kat] being the conversion rate of 1 mol of substrate per second. Protein concentrations and all enzymatic measurements were performed in triplicate for each independent replicate.

Statistical analysis

To all data sets Shapiro-Wilks W test and Levene's test were applied to test normality and homogeneity of variances, respectively. For data sets not normally distributed, a logarithmic (Lg10) or square root transformation was applied. If applicable, a one-way analysis of variance (ANOVA) followed by a post-hoc Dunnett's test was performed to determine statistical significant differences between the TiO₂ exposure and the respective negative and bulk TiO₂ controls, the latter to assess nano-specific changes. Kruskal-Wallis one-way analysis of variance and Mann-Whitney U test were performed for data sets not fitting normal distribution and homogeneity of variances. All data are reported as means \pm standard deviation. Statistical analysis was carried out using commercial software SPSS 21.0 (SPSS Inc., Chicago, IL, USA). The comparisons were examined at a significance level of $p < 0.05$.

Results

Behavior of TiO₂-nanoparticles in the test medium

For all investigated TiO₂-NPs a negative zeta potential was determined in our previous study (Okupnik et al., 2015) which was in accordance with a test medium pH of 6.3 ± 0.8 during exposure and thus above the respective pI_{IEP} of the NPs ($-22 \text{ mV} \pm 0.25$, pI_{IEP} ~ 3.6 for P25; $-22 \text{ mV} \pm 0.34$, pI_{IEP} ~ 3.5 for anatase TiO₂; $-26 \text{ mV} \pm 0.45$, pI_{IEP} ~ 2.7 for rutile TiO₂). Polydispersity data of the NP suspensions revealed PDI values of 0.28 ± 0.04 , 0.28 ± 0.05 , and 0.37 ± 0.05 for rutile TiO₂, anatase TiO₂ and P25, respectively, with the tendency of slightly decreased values with time. According to these previous findings, analysis of the z-average hydrodynamic diameter revealed that all TiO₂-NPs tended to aggregate in the test medium (Fig 1A). Immediately after sonication, particle sizes of about 440 to 530 nm, and thus much larger than the vendor reported sizes, were observed. In the first hours of DLS analysis, anatase TiO₂ and rutile TiO₂ only showed minor changes in their aggregate sizes, whereas P25 aggregate size increased from $\sim 440 \text{ nm}$ to $>800 \text{ nm}$ within the first 6 h. After 24 h, all tested TiO₂-NPs displayed a rapid decrease of its z-average hydrodynamic diameters, which subsequently continued, however, to a lesser extent. The sedimentation of large scale NP aggregates was confirmed by optical absorbance analysis of the samples. It was found that a reduction of absorbance over time occurred for all tested TiO₂-NPs (Fig 1B). The lowered absorbance and thus an ongoing sedimentation

in the NP suspensions became obvious immediately after starting measurements. Already within 24 h, optical absorbance decreased by more than 50% for all investigated TiO₂-NPs. Again, P25 was apparent in its sedimentation behavior as aggregate settling occurred to a larger extent than for rutile TiO₂ and anatase TiO₂. Hence, after 168 h of absorbance analysis, only 6%, 20% and 23% of P25, rutile TiO₂ and anatase TiO₂, respectively, remained in solution.

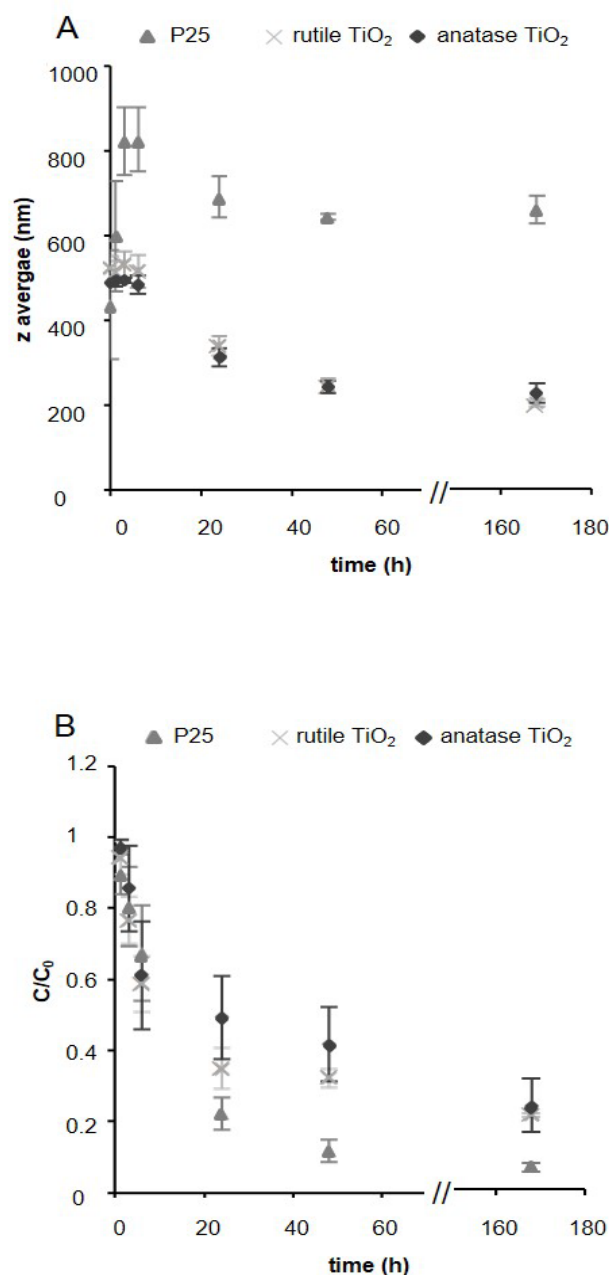


Figure 1. Size evolution (A) and sedimentation (B) of TiO₂ nanoparticles in 5% modified Hoagland's nutrient solution. Data are reported as means \pm standard deviation.

Effects of nano-TiO₂ on the level of cell internal H₂O₂

Figure 2 illustrates that the investigated TiO₂-NPs did not show a clear tendency of time-dependent alterations in the formation of H₂O₂. However, significant differences between nano-treated and control plants were observed after exposure to 10 mg/L P25, rutile TiO₂ and anatase TiO₂ after 96 h ($p = 0.004$; $p = 0.02$; $p < 0.001$, respectively). Moreover, *H. verticillata* exposed to bulk-TiO₂ did not show a changed H₂O₂ pattern with respect to the control treatments. Significant differences to the respective bulk TiO₂ exposures became apparent for both tested P25 concentrations ($p = 0.02$) already after 24 h of exposure. After elongation of exposure time, the highest P25 concentration still caused an elevated H₂O₂ level by 37% after 96 h and 31% after 168 h. Plants treated with 10 mg/L rutile TiO₂ showed higher H₂O₂ concentrations exceeding the exposure duration of 24 h, however, were only significantly increased by 33% after 96 h ($p < 0.001$) of exposure. In contrast, the lower rutile TiO₂ exposure setting revealed H₂O₂ levels comparable to the bulk TiO₂ treated plants. In accordance, low-level anatase TiO₂ treated plants showed an almost uninfluenced H₂O₂ status compared to bulk TiO₂ exposed plants, whereas a higher NP concentration seemed to influence H₂O₂ status after exposure exceeding 48 h, however, only statistically significant for the exposure time of 96 h ($p < 0.001$).

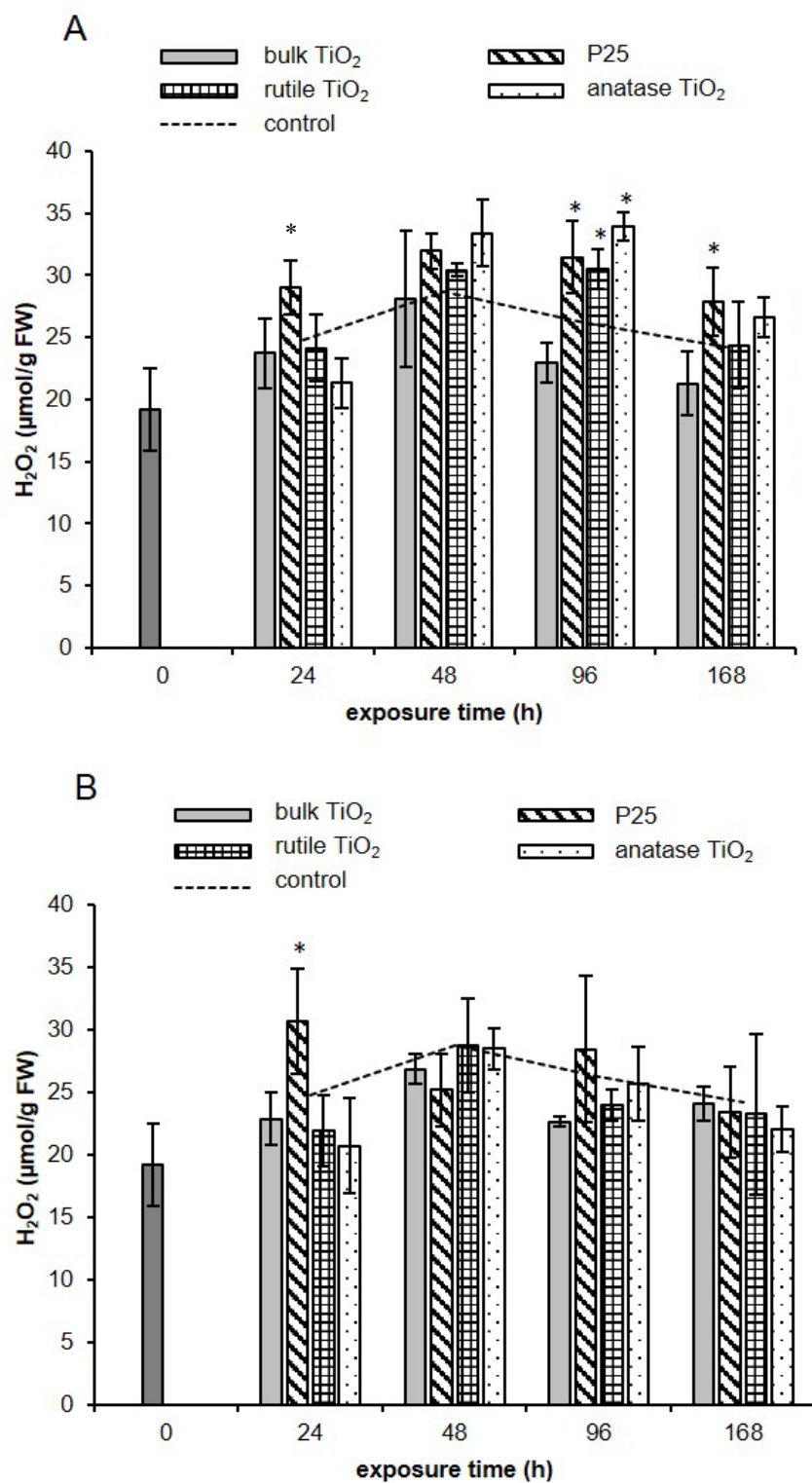


Figure 2. Formation of hydrogen peroxide (H₂O₂) in *H. verticillata* after exposure to 10 mg/L (A) and 0.1 mg/L (B) TiO₂ nanoparticles and bulk TiO₂. Data are reported as means ± standard deviation. * $p < 0.05$ versus respective bulk TiO₂ concentration

Effects on GSH and GSSG levels

Analysis of the GSH and GSSG contents revealed that NP exposures caused alterations of the GSH status in a time-dependent manner (Fig. 3). Compared to the respective control treatments all investigated TiO₂-NPs decreased the GSH/GSSG ratio for all investigated exposure times. Especially anatase TiO₂ and P25 induced significantly lowered GSH/GSSG ratios in *H. verticillata* for both concentration scenarios ($p < 0.05$) immediately after start of exposure. With the exception of plants exposed to rutile TiO₂ for 24 h, the oxidation of GSH progressed statistically significant ($p < 0.05$) for high-level exposures up to 96 h when compared to the control treatments. The highest drop of the ratio was detected after 96 h and was accounted for 69%, 76%, and 83% after exposure to 10 mg/L of P25, rutile TiO₂ and anatase TiO₂, respectively.

After prolonged exposure times, the GSH/GSSG ratios in NP treated plants showed a tendency to increase again, however, still with lower ratios than in control plants. In accordance, exposure to 0.1 mg/L revealed decreased ratios of GSH/GSSG compared to non-exposed plants but no significant difference became apparent after 96 h of exposure. In accordance to NP treated plants, exposure to bulk TiO₂ caused a 2.6 and 1.6 times decreased GSH/GSSG ratio over the complete exposure time for high and low concentration scenarios, respectively. However, the GSH status seemed to be less affected compared to NP exposures as broadly higher ratio values were measured for bulk exposure durations up to 96 h. The ratio was especially sensitive to exposures with P25 and pure anatase TiO₂ for both concentration scenarios as already the shortest exposure time in this study revealed statistically significant ($p < 0.05$) lower GSH/GSSG ratios. Such exposed plants showed a decrease by 72% and 43% as well as 67% and 65% compared to bulk exposed plants for the high and low level exposures to P25 and anatase TiO₂, respectively.

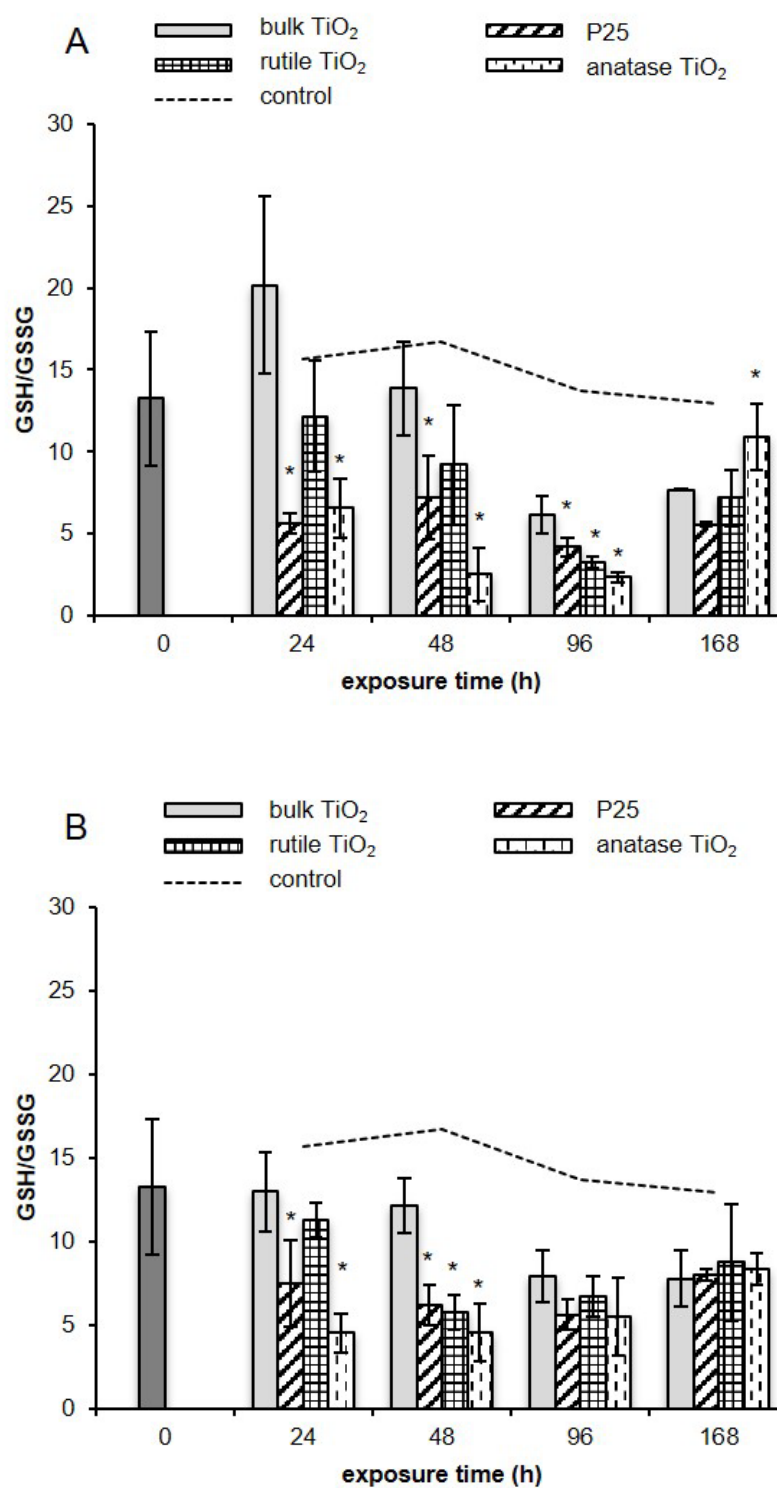


Figure 3. Ratio of reduced glutathione (GSH) and oxidized glutathione (GSSG) after exposure to 10 mg/L (A) and 0.1 mg/L (B) TiO₂ nanoparticles and bulk TiO₂. Data are reported as means \pm standard deviation. * *p* < 0.05 versus respective bulk TiO₂ concentration

Effects on antioxidative enzyme activity

Compared to the respective control treatments, all TiO₂-NPs showed the tendency to change activities of the antioxidative enzymes CAT and GR in *H. verticillata* during exposure (Fig. 4). However, differences between the tested TiO₂-NP crystal structures became obvious for both studied enzymes. Exposure of macrophytes to 10 mg/L of P25 and anatase TiO₂ provoked an almost similar response in CAT activity. The highest exposure concentration of 10 mg/L increased CAT activity significantly after 24 h ($p < 0.05$). This change in enzyme activity corresponds to a 2.24 and 1.95-fold higher activity compared to the respective control treatment for P25 and anatase TiO₂, respectively. Compared to bulk TiO₂ treated plants, a nano-specific influence on the CAT activity can be suggested as significant ($p < 0.05$) activity elevations by 81% and 58% became apparent for exposures to 10 mg/L of P25 and anatase TiO₂, respectively. After 48 h of exposure, CAT activities subsequently decreased and were equally 1.47-fold and 2.5-fold lower compared to the negative control and the bulk-sized control, respectively. Rutile TiO₂ exposure revealed contrary CAT activity changes as exposure to 10 mg/L exhibited higher enzyme activities not until 96 h of treatment. However, the 1.77-fold increased enzyme activity after 10 mg/L rutile TiO₂ exposure turned out to be statistically significant when compared to the respective control ($p < 0.01$). After 168 h of exposure with rutile TiO₂, a tendency of decreased CAT activities for both NP concentrations could be suggested, which turned out to be significant compared to the bulk-sized control for rutile TiO₂ treatments of 10 mg/L ($p < 0.01$) and 0.1 mg/L ($p < 0.05$). Macrophytes exposed to 10 mg/L of bulk TiO₂ showed concentration-dependent increased CAT activities which turned out to be significantly 1.7 times elevated after 168 h of exposure ($p < 0.05$). In contrast, the CAT activity remained at a level similar to the control group after a low-level exposure of 0.1 mg/L bulk TiO₂. Altogether, as in particular the high-level exposure scenario caused significantly changed CAT activities compared to control plants a concentration dependent influence can be suggested.

GR enzyme activity was affected by all three investigated TiO₂-NPs. Again, already short NP exposure of *H. verticillata* caused significantly influenced GR activities compared to control plants ($p < 0.05$): enzyme activities were 1.6-, 1.4-, and 1.3-fold higher than the in the negative control after high-level exposure to P25, anatase TiO₂, and rutile TiO₂, respectively. Moreover, compared to bulk TiO₂ treated plants, high-level NP exposure affected GR activity status, with a significantly elevated GR activity already after 24 h for

P25 and anatase TiO₂ ($p < 0.05$). In contrast to the results for the CAT activity, also low-level exposure with P25 caused elevated levels in enzyme activity after 24 h, however, only significant when compared to the respective bulk sized control ($p = 0.02$). Elongation of exposure revealed a subsequent decrease in GR activity for P25 treated plants, but both pure phase TiO₂-NPs still provoked an enhanced enzyme activity after 48 h differing significantly ($p < 0.05$) from non-exposed and bulk TiO₂ exposed macrophytes for both tested anatase concentrations and 0.1 mg/L rutile TiO₂. However, a concentration dependence in the antioxidative response can be suggested, as the GR activity surpassed by about 60% and 30% GR activity levels after bulk TiO₂ exposure for high- and low-level NP treatments after 48 h. Thereafter, GR activity was similar in nano-exposed and negative control as well as bulk sized control treated macrophytes for both pure phase NPs. Referring to the enzyme activity pattern after bulk TiO₂ exposure, no clear influence on GR enzyme activities became apparent when compared with control plants, indicating a nano-specific influence on GR activity.

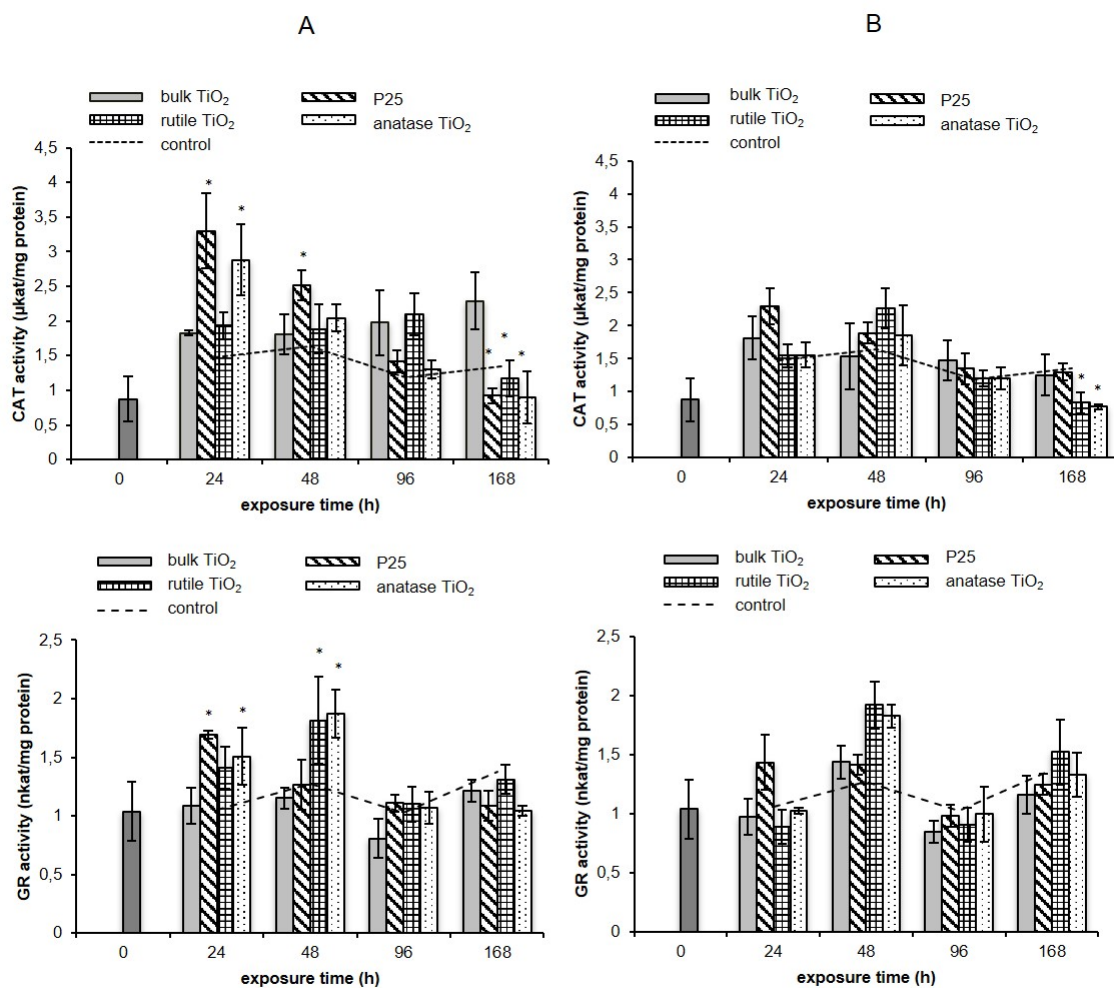


Figure 4. Activity of catalase (CAT) and glutathione reductase (GR) in *H. verticillata* after exposure to 10 mg/L (A) and 0.1 mg/L (B) TiO₂ nanoparticles and bulk TiO₂. Data are reported as means \pm standard deviation. * $p < 0.05$ versus respective bulk TiO₂ concentration

Discussion

Physicochemical processes like NP aggregation and sedimentation will significantly influence the fate of NPs in the aquatic environment and are the result of the combined effects of e.g. pH, ionic strength and composition, and the concentration of natural organic matter in the surrounding media (Keller et al., 2010). Thus, in ecotoxicity studies the characteristics of the exposure medium will have an effect on the NP suspension stability. Measurements of the optical absorbance *via* UV-Vis spectroscopy represent a convincing method for determining the sedimentation behavior of TiO₂-NP over time. Together with the DLS analysis of particle sizes at different stages of the sedimentation process an evaluation of NP suspension stabilities was enabled in this study. Based on the present results it can be concluded that the tested TiO₂-NP suspensions suffered from instability. Especially NP suspensions containing P25 were characterized by large particle aggregates which is consistent with study results by Ji et al. (2010). Furthermore, a comparatively rapid sedimentation of P25 aggregates indicated that the aggregate size significantly influenced the rate of sedimentation in NP suspensions. It can be suggested that the prevalent composition of the Hoagland's nutrient solution was unfavorable for obtaining a stable NP suspension as a rapid sedimentation of large scale particle aggregates due to gravitation occurred for all investigated TiO₂-NPs. Thus, a semi-static test system was used to avoid progressively decreased TiO₂-NP concentrations in the water column during exposure. Considering the environmental fate of TiO₂-NPs it can be suggested that they will suffer from aggregation after entering freshwater systems. However, we are aware of the fact that aquatic ecosystems are characterized by a more complex water chemistry than represented in our laboratory setting, possibly influencing TiO₂-NP characteristics and thus the sedimentation behavior in a different way than observed in the present sedimentation analysis. Available study results confirm this assumption as the magnitude of aggregation and sedimentation of TiO₂-NPs showed a strong dependence on the aqueous media they were suspended in (Brunelli et al., 2013; Keller et al., 2010). Nevertheless, after release in the aquatic environment NPs will aggregate to some degree (Handy et al., 2008), and these NP aggregates might not compulsorily be a toxicity risk for benthic organisms after rapid NP sedimentation. Instead, macrophytes and other aquatic organisms in the water column might suffer from long-term exposure to TiO₂-NPs in moving bodies of natural waters like streams and rivers due to mixing processes as well as if the NP loading is continuously or at least frequent. Thus, the results of the current study considering the time-dependent

antioxidative stress response of *H. verticillata* under semi-static test conditions can be considered as environmentally relevant. Interestingly, NPs interaction with the plant surface could be suggested even after aggregate formation in the test media as particle adhesion was observed during exposure. According to Tong et al. (2013), who investigated the phototoxicity of diversely shaped TiO₂-NPs towards bacteria, the spherical structure of the TiO₂-NPs might have contributed to the surface-particle interaction due to the formation of less compact aggregates allowing for a great degree of contact between macrophytes surface and the particles.

The present research attempts to fill the lack of available data concerning the nano-toxicity towards aquatic plants. For current research approaches, macrophytes seem to be an overlooked test species, ignoring their importance for aquatic ecosystems (Thomaz and Cunha, 2010). Hence, NP-driven toxicity towards macrophytes will also affect aquatic ecosystems as a whole. As the formation of ROS in aquatic organisms is a considered mode of nano-toxicity (Menard et al., 2011), our research activities particularly focused on the microresponse of macrophytes after TiO₂-NP treatment. An investigation of the antioxidative stress response in *H. verticillata* offers the possibility to understand early biological signals of plants stress after TiO₂-NP exposure before deleterious effects progress on the physiological, individual or population level (Bayne et al., 1985). Previous study results have indicated an activation of macrophytes defense system after 24 h of exposure to different concentrations of TiO₂-NPs probably aiming at the maintenance of physiological ROS levels in plant cells (Okupnik and Pflugmacher, 2016). There is no doubt that TiO₂-NPs will end up in relevant quantities in aquatic environments, and yet currently available data for nano-TiO₂ concentrations in surface waters reveal a broad spread in modelled and measured concentrations by a factor of 10⁴ underlying that there is still a lack in the quantitative knowledge. Despite this uncertainties, low concentrations of TiO₂-NP in the range of 10⁻³ to 10 µg/L are predicted for surface waters (Gottschalk et al., 2013). Thus, the investigated low-level concentration of 0.1 mg/L may currently be considered as worst-case scenario. However, keeping in mind the large scale production of TiO₂-NPs and further expanding production volumes in the coming years (Robichaud et al., 2009), TiO₂-NP concentrations in the low mg/L range may represent actual TiO₂-NP exposure levels of aquatic ecosystem in the near future.

As H_2O_2 is the most representative and potent ROS (Gill and Tuteja, 2010), analysis of the H_2O_2 level was performed. Study results did not reveal a clear time-dependent effect on H_2O_2 formation. Instead, a concentration dependent influence on the ROS status can be suggested as mainly high NP exposures raised H_2O_2 levels when compared to bulk exposed as well as control plants. However, after 168 h of exposure, a decline in H_2O_2 levels and thus, a normalization of ROS formation can be suggested. ROS like H_2O_2 can be removed by several antioxidant systems including low-molecular-weight enzymes that enable the detoxification of excess ROS (Mittler, 2002). In the group of H_2O_2 -degradating enzymes, CATs are unique as they are characterized by a very fast turnover rate and moreover, do not require reducing equivalents for H_2O_2 break down (Sharma et al., 2012). As TiO_2 -NP exposure induced changes in CAT activities in the present study, it also seems to participate in the defense against a nano-driven accumulation of H_2O_2 . In accordance to the observation of increased H_2O_2 levels for the high exposure scenario, exclusively exposures to 10 mg/L of TiO_2 -NPs caused significant increased CAT activities. Interestingly, CAT activity seemed to depend on the crystalline structure the plants were exposed to. *H. verticillata* treated with P25 (~ 80% anatase) and pure anatase TiO_2 showed the same pattern of CAT activity changes which differed from the CAT activity pattern in rutile exposed macrophytes. Referring to the results of the bulk TiO_2 treated plants, a nano-specific influence on CAT activity became obvious, especially after exposure to 10 mg/L of the respective particles. In contrast to rutile TiO_2 exposed macrophytes, H_2O_2 -degradation by CAT was sufficient to maintain H_2O_2 status for short exposure times to high-levels P25 and anatase TiO_2 . Further, the steadily decreased enzyme activity might explain increased ROS levels after 96 h. There is a consensus that the limitation of one component of the antioxidative stress response results in an up-regulation of other antioxidant processes to compensate (Foyer et al., 1997). Thus, other H_2O_2 -scavenging enzymes probably assumed the role of CAT and lead to decreased ROS levels after 168 h in nano-exposed plants. This appears likely, because CAT activities were decreased for both investigated concentrations and TiO_2 -NPs after 168 h. Among the antioxidant enzymes, POD probably took the task of H_2O_2 detoxification. Although our previous study results revealed that POD was not considerable affected by TiO_2 -NP exposure for 24 h (Okupnik and Pflugmacher, 2016), a shift in the POD activity after elongation of exposure time could explain the results of the present study. Referring to the study results revealed by Song et al. (2012), who investigated an increased POD activity after TiO_2 -NP exposure for 168 h, this appears to be a likely

explanation for the H_2O_2 decrease at an identical time level in the present study. Based on our study results, the apparent shift in the GSH/GSSG ratio for both tested concentrations indicated the involvement of H_2O_2 degrading pathways dependent on GSH which seemed to be enhanced during exposure. Hence, the putative activation of GPx as well as of the ascorbate-GSH cycle, also referred to as Halliwell-Asada pathway, is likely. Already short-time exposures revealed decreased GSH/GSSG ratios in TiO_2 -NP treated plants, thus indicating an immediate high GSH-dependent metabolism to counteract the ROS increase. Especially H_2O_2 breakdown by APX seems obvious as it is characterized by a higher affinity for H_2O_2 compared to CAT (Sharma et al., 2012). Hence, the ubiquitous ascorbate-GSH pathway probably contributed to H_2O_2 status normalization after longer exposure times to 10 mg/L TiO_2 -NPs and compensated for the loss in CAT activity. Inevitably, this would have caused enhanced oxidation of ascorbate and GSH to dehydroascorbate and GSSG, respectively, the latter proved by the present study results. In accordance to our previous concentration-dependent study, an investigation of the GSH status in *H. verticillata* revealed to be a sensitive indicator for oxidative stress caused by TiO_2 -NPs. All investigated nano-treatments caused the GSH/GSSG ratio to decrease and provide a clear sign for oxidative stress for such exposed plants. The observation of an increased GR activity can be interpreted as metabolic adaptation aiming to combat elevated GSH oxidation, which was observed for both tested TiO_2 -NP concentrations. Even though GR activity was increased already after 24 h of exposure, this metabolic adaptation was insufficient to maintain high ratios of GSH/GSSG. As GR catalyzes the rate limiting last step of the ascorbate-GSH pathway (Ahmad et al., 2008), its appropriate function can be questioned for prolonged exposure times, and might explain elevated H_2O_2 levels after 96 h of exposure to 10 mg/L of all investigated TiO_2 -NPs. Nevertheless, no significant difference between the GSH/GSSG ratio in nano-exposed and unexposed plants was detected after 168 h for both tested concentrations; thus, a metabolic stabilization is likely and in accordance with decreased H_2O_2 levels. From literature it is known that the gene expression in plant cells is sensitive to its redox state and especially the GSH status (Foyer et al., 1997; Noctor and Foyer, 1998). Thus, an up-regulation of GSH synthesis could be suggested due to elevated expressions of its catalyzing enzymes glutamylcysteine synthetase and glutathione synthetase leading to increased GSH levels after 168 h.

The parallel analysis of a bulk-sized control revealed a size-dependent influence on the antioxidative stress response, while nano-specific effects on enzyme activities as well as the GSH/GSSG ratio were observed for short-term exposures to 10 mg/L of all TiO₂-NPs. As bulk TiO₂ exposure did not lead to increased ROS levels for all investigated exposure times it can be assumed that *H. verticillata* had the ability to cope with such exposures due to metabolic adaptations. Furthermore, concerning the concentration dependence in the antioxidative response, the present study results for the CAT activity and the H₂O₂ status imply that in specific high exposure concentrations of TiO₂-NPs exhibit the potential to temporarily overwhelm the antioxidative capacity of *H. verticillata* as indicated by elevated H₂O₂ levels compared to the control. Instead, with the exception for P25 after 24 h of exposure, the putative induction of the ascorbate-GSH pathway in plants exposed to 0.1 mg/L of TiO₂-NPs seemed to be sufficient to maintain ROS status. Moreover, as no statistically relevant difference between unexposed and nano-exposed plants became apparent for the respective H₂O₂ levels, enzyme activities, as well as the GSH status after 168 h, oxidative stress effects induced in the high-level TiO₂-NPs exposure scenario seemed to be overcome and might be maintained with prolonged NP exposure. In accordance, investigations of the pigment status which were performed in the present study (data not shown) revealed no significant influence by TiO₂-NP exposure and contribute to the conclusion that such exposed plants did not suffer from high toxicity progressing through the physiological level. Thus, in respect to the currently predicted concentrations of TiO₂-NPs in the low µg/L range it can be suggested that oxidative stress effects after TiO₂ exposure may not cause severe damage to macrophytes at present. In general, the present results emphasize the importance to study the time-dependence of oxidative stress related effects, as it provides the opportunity to get an insight in the compensatory character of antioxidative stress responses after TiO₂-NP exposure of macrophytes.

Conclusion

Due to a lack of literature concerning oxidative stress related effects in macrophytes after TiO₂-NP exposure the present study aimed to make a contribution to a more proper assessment of TiO₂-NP risk for macrophytes. Moreover, as aquatic plants possess an important role in aquatic ecosystems and investigations of biochemical responses after TiO₂-NP exposure enable the assessment of early biological signals of plants stress this study was conducted. Different levels of the oxidative stress responses in *H. verticillata*

were assessed by investigations of the ROS evolution as well as the enzymatic and non-enzymatic antioxidative stress response for different times of exposure to nano-TiO₂. A characterization of TiO₂-NP suspensions under experimental conditions indicated a rapid sedimentation of large scale particle aggregates due to gravitation for all investigated TiO₂-NPs and contributed to adaptations in the experimental setup to maintain NP exposure. In general, study results imply oxidative stress effects after TiO₂-NP exposure as adaptations in plants metabolism became apparent to counteract increased ROS formation. All TiO₂-NP caused elevated activities of the enzymes CAT and GR and moreover, decreased ratios of GSH/GSSG indicate the activation of GPx as well as of the ascorbate-GSH cycle, both depending on GSH. Already short-time exposures to TiO₂-NPs revealed decreased GSH/GSSG ratios, thus, GSH-associated metabolism seemed to be a major mechanism for cellular protection against increased ROS levels. As H₂O₂ level increases were solely detected after exposure to 10 mg/L TiO₂-NPs a concentration dependent potential to overwhelm the antioxidative capacity could be derived. In accordance to H₂O₂ level increases, CAT activity decreased with prolonged exposure to high levels of TiO₂-NPs. However, other H₂O₂-scavenging enzymes probably assumed the role of CAT and lead to decreased ROS levels after 168 h in nano-exposed plants. The parallel analysis of a bulk-sized control in the present study revealed a size-dependent influence on the antioxidative stress response, while nano-specific effects on enzyme activities as well as the GSH/GSSG ratio were observed for short-term exposures to 10 mg/L of all TiO₂-NPs. Thus, results imply that one cannot equate the toxicity of bulk TiO₂ and TiO₂-NPs even after assuming the formation of large scale aggregates in the aquatic environment. However, as no statistically relevant difference between unexposed and nano-exposed plants became apparent for the respective H₂O₂ levels and the antioxidative response after 168 h, oxidative stress effects induced in the high-level TiO₂-NPs exposure scenario seemed to be overcome. This observation contributes to the conclusion that TiO₂ exposure may currently not cause severe oxidative damage to macrophytes especially not at the low µg/L range as currently predicted for the aquatic environment.

Acknowledgements

The authors acknowledge T. Bucheli (Agroscope Reckenholz- Tänikon Research Station) for providing laboratory equipment for particle characterization. Furthermore, the authors would like to thank V. Contardo Jara for her support in regard of study planning and results discussion as well as S. Kühn for her support and assistance in the laboratory. Moreover, we thank M. Esterhuizen-Londt for proof-reading the manuscript.

Funding

This research did not receive any specific grant from funding agencies in the public, commercial, or not for-profit sectors.

Reference list

- Aebi, M., 1974. Catalase, in: Bergmeyer, H.U. (Ed.), *Methods of Enzymatic Analysis*, 2nd ed. Academic Press, New York, pp. 673-684.
- Ahmad, P., John, R., Sarwat, M., Umar, S., 2008. Responses of proline, lipid peroxidation and antioxidative enzymes in two varieties of *Pisum sativum* L. under salt stress. *Int. J. Plant Prod.* 2, 353-365.
- Aravind, P., Prasad, M.N., 2005. Cadmium-induced toxicity reversal by zinc in *Ceratophyllum demersum* L. (a free floating aquatic macrophyte) together with exogenous supplements of amino- and organic acids. *Chemosphere* 61, 1720-1733.
- Aruoja, V., Dubourguier, H.C., Kasemets, K., Kahru, A., 2009. Toxicity of nanoparticles of CuO, ZnO and TiO₂ to microalgae *Pseudokirchneriella subcapitata*. *Sci. Total Environ.* 407, 1461-1468.
- Asada, K., 1992. Ascorbate peroxidase - a hydrogen peroxide-scavenging enzyme in plants. *Physiol. Plantarum* 85, 235-241.
- Bayne, B.L., Brown, D.A., Burns, K., Dixon, D.R., Ivanovici, A., Livingstone, D.A., Lowe, D.M., Moore, M.N., 1985. *The effects of stress and pollution on marine animals*. Praeger, New York, USA.
- Bradford, M.M., 1976. A rapid and sensitive method for the quantitation of microgram quantities of protein utilizing the principle of protein-dye binding. *Anal. Biochem.* 72, 248-254.
- Brunelli, A., Pojana, G., Callegaro, S., Marcomini, A., 2013. Agglomeration and sedimentation of titanium dioxide nanoparticles (n-TiO₂) in synthetic and real waters. *J. Nanopart. Res.* 15: 1684.
- Carlberg, I., Mannervik, B., 1985. Glutathione reductase. *Method Enzymol* 113, 484-490.
- Cook, C.D.K., Luond, R., 1982. A Revision of the genus *Hydrilla* (Hydrocharitaceae). *Aquat. Bot.* 13, 485-504.
- Federici, G., Shaw, B.J., Handy, R.D., 2007. Toxicity of titanium dioxide nanoparticles to rainbow trout (*Oncorhynchus mykiss*): Gill injury, oxidative stress, and other physiological effects. *Aquat. Toxicol.* 84, 415-430.
- Foyer, C.H., Lopez-Delgado, H., Dat, J.F., Scott, I.M., 1997. Hydrogen peroxide- and glutathione-associated mechanisms of acclimatory stress tolerance and signalling. *Physiol. Plantarum* 100, 241-254.

- Gill, S.S., Tuteja, N., 2010. Reactive oxygen species and antioxidant machinery in abiotic stress tolerance in crop plants. *Plant Physiol. Bioch.* 48, 909-930.
- Giustarini, D., Dalle-Donne, I., Colombo, R., Milzani, A., Rossi, R., 2003. An improved HPLC measurement for GSH and GSSG in human blood. *Free Radical Bio. Med.* 35, 1365-1372.
- Gottschalk, F., Sun, T., Nowack, B., 2013. Environmental concentrations of engineered nanomaterials: review of modeling and analytical studies. *Environ. Pollut.* 181, 287-300.
- Handy, R.D., Owen, R., Valsami-Jones, E., 2008. The ecotoxicology of nanoparticles and nanomaterials: current status, knowledge gaps, challenges, and future needs. *Ecotoxicology* 17, 315-325.
- Jana, S., Choudhuri, M.A., 1982. Glycolate metabolism of 3 submersed aquatic angiosperms during aging. *Aquat. Bot.* 12, 345-354.
- Ji, Z., Jin, X., George, S., Xia, T., Meng, H., Wang, X., Suarez, E., Zhang, H., Hoek, E.M., Godwin, H., Nel, A.E., Zink, J.I., 2010. Dispersion and stability optimization of TiO₂ nanoparticles in cell culture media. *Environ. Sci. Technol.* 44, 7309-7314.
- Keller, A.A., Wang, H., Zhou, D., Lenihan, H.S., Cherr, G., Cardinale, B.J., Miller, R., Ji, Z., 2010. Stability and aggregation of metal oxide nanoparticles in natural aqueous matrices. *Environ. Sci. Technol.* 44, 1962-1967.
- Kim, E., Kim, S.H., Kim, H.C., Lee, S.G., Lee, S.J., Jeong, S.W., 2011. Growth inhibition of aquatic plant caused by silver and titanium oxide nanoparticles. *J. Toxicol. Environ. Health Sci.* 3, 1-6.
- Kim, K.T., Klaine, S.J., Cho, J., Kim, S.H., Kim, S.D., 2010. Oxidative stress responses of *Daphnia magna* exposed to TiO₂ nanoparticles according to size fraction. *Sci. Total Environ.* 408, 2268-2272.
- Li, L., Sillanpaa, M., Tuominen, M., Lounatmaa, K., Schultz, E., 2013. Behavior of titanium dioxide nanoparticles in *Lemna minor* growth test conditions. *Ecotox. Environ. Safe.* 88, 89-94.
- Madsen, J.D., Chambers, P.A., James, W.F., Koch, E.W., Westlake, D.F., 2001. The interaction between water movement, sediment dynamics and submersed macrophytes. *Hydrobiologia* 444, 71-84.
- Menard, A., Drobne, D., Jemec, A., 2011. Ecotoxicity of nanosized TiO₂. Review of in vivo data. *Environ. Pollut.* 159, 677-684.
- Mittler, R., 2002. Oxidative stress, antioxidants and stress tolerance. *Trends Plant. Sci.* 7, 405-410.

- Noctor, G., Foyer, C.H., 1998. Ascorbate and glutathione: Keeping active oxygen under control. *Annu. Rev. Plant Phys.* 49, 249-279.
- Okupnik, A., Contardo-Jara, V., Pflugmacher, S., 2015. Potential role of engineered nanoparticles as contaminant carriers in aquatic ecosystems: Estimating sorption processes of the cyanobacterial toxin microcystin-LR by TiO₂ nanoparticles. *Colloids Surf. A* 481, 460-467.
- Okupnik, A., Pflugmacher, S., 2016. Oxidative stress response of the aquatic macrophyte *Hydrilla verticillata* exposed to TiO₂ nanoparticles. *Environ. Toxicol. Chem.* 35(11), 2859-2866.
- Pflugmacher, S., 2004. Promotion of oxidative stress in the aquatic macrophyte *Ceratophyllum demersum* during biotransformation of the cyanobacterial toxin microcystin-LR. *Aquat. Toxicol.* 70, 169-178.
- Robichaud, C.O., Uyar, A.E., Darby, M.R., Zucker, L.G., Wiesner, M.R., 2009. Estimates of upper bounds and trends in nano-TiO₂ production as a basis for exposure assessment. *Environ. Sci. Technol.* 43, 4227-4233.
- Sadiq, I.M., Dalai, S., Chandrasekaran, N., Mukherjee, A., 2011. Ecotoxicity study of titania (TiO₂) NPs on two microalgae species: *Scenedesmus* sp. and *Chlorella* sp. *Ecotox. Environ. Safe.* 74, 1180-1187.
- Sharma, P., Jha, A.B., Dubey, R.S., Pessarakli, M., 2012. Reactive oxygen species, oxidative damage, and antioxidative defense mechanism in plants under stressfull conditions. *J. Bot.* 2012, 1-26.
- Song, G.L., Gao, Y., Wu, H., Hou, W.H., Zhang, C.Y., Ma, H.Q., 2012. Physiological effect of anatase TiO₂ nanoparticles on *Lemna minor*. *Environ. Toxicol. Chem.* 31, 2147-2152.
- Thomaz, S.M., Cunha, E.R., 2010. The role of macrophytes in habitat structuring in aquatic ecosystems: methods of measurement, causes and consequences on animal assemblages' composition and biodiversity. *Acta. Limnol. Bras.* 22, 218-236.
- Valko, M., Leibfritz, D., Moncol, J., Cronin, M.T.D., Mazur, M., Telser, J., 2007. Free radicals and antioxidants in normal physiological functions and human disease. *Int. J. Biochem. Cell B.* 39, 44-84.
- Wang, J.X., Zhang, X.Z., Chen, Y.S., Sommerfeld, M., Hu, Q., 2008. Toxicity assessment of manufactured nanomaterials using the unicellular green alga *Chlamydomonas reinhardtii*. *Chemosphere* 73, 1121-1128.

Xia, B., Chen, B.J., Sun, X.M., Qu, K.M., Ma, F.F., Du, M.R., 2015. Interaction of TiO₂ nanoparticles with the marine microalga *Nitzschia closterium*: Growth inhibition, oxidative stress and internalization. Sci. Total. Environ. 508, 525-533.